Missouri S&T Library and Learning Resources

Scholars' Mine

Doctoral Dissertations | Student Theses and Dissertations

1970

Electrode reactions in zinc electrolysis

Ernest R. Cole

Follow this and additional works at: https://scholarsmine.mst.edu/doctoral_dissertations

 Part of the Metallurgy Commons

Department: Materials Science and Engineering

Recommended Citation

Cole, Ernest R., "Electrode reactions in zinc electrolysis" (1970). *Doctoral Dissertations*. 2036.
https://scholarsmine.mst.edu/doctoral_dissertations/2036

This thesis is brought to you by Scholars' Mine, a service of the Missouri S&T Library and Learning Resources. This work is protected by U. S. Copyright Law. Unauthorized use including reproduction for redistribution requires the permission of the copyright holder. For more information, please contact scholarsmine@mst.edu.

ELECTRODE REACTIONS IN ZINC ELECTROLYSIS

BY

ERNEST RAY COLE, JR., 1932-

A DISSERTATION

Presented to the Faculty of the Graduate School of the

UNIVERSITY OF MISSOURI - ROLLA

In Partial Fulfillment of the Requirements for the Degree

DOCTOR OF PHILOSOPHY

in

METALLURGICAL ENGINEERING

1970

T2399
155 pages
c.I

T. J. O'Keefe
Advisor

H. P. Leigh, Jr.

W. J. James

J. B. Clark

M. E. Straumanis

Fred Kisslinger

ABSTRACT

The effects of temperatures from 0°C to 50°C and current densities from 10 asf to 200 asf on the current efficiency in the electrolysis of pure zinc sulfate solutions (65 gpl Zn^{++} - 200 gpl H_2SO_4) were determined.

Pure platinum and platinum coated titanium anodes were used with an aluminum cathode. Platinum anodes were not inert at certain combinations of temperature and current density, and platinum acted as a low overvoltage impurity causing resolution of the cathode deposit.

Orientation of the zinc deposits was found to vary with temperature and to have a distinct relationship to current efficiency.

Preconditioning of lead and lead alloy anodes was investigated as a possible means of producing a stable anode. Electrodes were conditioned in fluoride solutions and compared to anodes conditioned in H_2SO_4 solutions under similar circumstances. The scanning electron microscope was utilized to study the morphology of the anodic coating. X-ray and potential decay data were employed to determine the phases present on the electrode surface.

ACKNOWLEDGEMENTS

The author wishes to express his sincere appreciation to all the members of his committee, but above all to his advisor, Dr. Thomas J. O'Keefe, for his guidance and assistance throughout this work.

Special acknowledgement is made to NSF for grant GK-2677 which made possible the purchase of the scanning electron microscope. Without the SEM, this project and work similar to it, would not have been possible.

He also wishes to thank the U.S. Bureau of Mines staff, Rolla, Missouri, for their many contributions.

Further, he acknowledges a debt of gratitude to Dr. H.W. Weart, Chairman of the Department of Metallurgical and Nuclear Engineering, Dr. W.J. James, Director of the Graduate Center for Materials Research, and the American Zinc Company, for the financial assistance necessary for this study. Special thanks are also due Dr. James for his helpful discussions and constructive criticism that did so much in helping to complete this work.

Last, but most important, the author recognizes that without the devotion, patience and many sacrifices of his wife, Peggy, and daughters, Sue, Pat and Kathy, this research endeavor would not have been possible.

TABLE OF CONTENTS

Table of Contents Continued Page

Table of Contents Continued Page

LIST OF FIGURES

FIGURE PAGE

FIGURE PAGE

FIGURE PAGE

LIST OF TABLES

I. INTRODUCTION

The commercial production of zinc by electrolysis is not new. Its recorded beginning dates back to 1881 following a patent by Letrange of France. The process has come down to the present day remaining essentially unchanged and consists of three basic steps:

1) Leaching of roasted zinc concentrates in dilute sulfuric acid, i.e., $ZnO + H_2SO_4 = ZnSO_4 + H_2O$.
2) Purification of the resulting zinc sulfate solution.
3) Electrolysis to recover the metallic zinc as a high purity product.

Only the high hydrogen overvoltage on zinc permits the deposition of zinc at the cathode since thermodynamics favors decomposition of water and evolution of hydrogen.

The literature written on zinc electrolysis is voluminous, but due to the interaction of many variables inherent in the process, the problem is exceedingly complex and studies of zinc electrolysis have not lost their essentiality.

The problem has been divided into two parts in this investigation; one encompassing cathode reactions, the second, anode reactions.

Scanning electron microscopy (SEM) was utilized in both phases of this work to examine the structure of the electrodes.

A. Cathode Reactions

An attempt was made to reduce the number of variables in the electrolysis to a minimum so that an accurate impression of the results of variations in temperature and current density on current efficiency and deposit morphology could be obtained.

To this end, very pure solutions were prepared to eliminate impurity interactions and platinum anodes were used to negate the effects of lead and manganese that are of necessity present when lead-silver anodes are employed in zinc electrolysis.

Deposit morphology was considered, along with current efficiency, as one of the major criterion for evaluating results since a porous or pitted structure with a large amount of surface area available for oxidation will result in a marked decrease in melting efficiency.

B. Anode Reactions

A dense, hard, fully adherent coating of lead oxide on lead-silver anodes, commonly used in commercial zinc electrolysis, is necessary to keep lead in the cathode deposit to a minimum. It is usually only after weeks in service that the anode attains these optimum properties. In recent years, preconditioning treatments have been developed that shorten the long conditioning time to a few days. The mechanism of the preconditioning process necessary to produce a satisfactory anode as well as the

physical characteristics of the resulting structure are not fully understood.

In this phase of the research, methods of preconditioning several lead alloy anodes in various solutions, particularly fluoride solutions, were investigated to determine as much as possible about the reactions taking place at the anode during electrolysis.

Potential decay curves, hardness measurements, x-ray diffraction and scanning electron microscopy were used to determine the phases present on the conditioned anode.

II. LITERATURE REVIEW

One of the first significant milestones in electrolytic zinc production from the time of its conception in 1881, other than improvements in the roasting process to avoid the formation of insoluble zinc ferrites ($ZnO \cdot Fe_2O_3$), was the development of lead-silver anodes by Tainton, Hanley and others.

Pure lead anodes had been used for years as the best material available; however, they dissolved to a considerable extent at the current densities and temperatures encountered in zinc electrolysis, ultimately contaminating the zinc deposit and the valuable manganese dioxide by-product which was recovered from the bottom of the cells.

Tainton, et. al.,[1] investigated binary alloys of lead, alloyed with arsenic, antimony, barium, bismuth, calcium, cerium, copper, mercury, silver, thallium and tin under conditions of commercial zinc electrolysis, i.e., aluminum cathodes, C.D. - 100 asf, 220 - 300 gpl H_2SO_4 and 5 gpl manganese added as manganous sulfate.

The lead-silver anodes were far superior in performance to any of the other binary alloys investigated and the optimum concentration of silver, based on performance and economy appeared to be 1.0%. Concentrations of silver above the eutectic at 2.6% resulted in lower efficiency of the zinc deposit and sometimes severe resolution, due to

free silver from the anode dissolving in the electrolyte and depositing with the zinc, probably reacting as a local cell.

Hanley, Clayton and Walsh[2,3] studied the effects of various alloying elements on anode potential and found that, other than lead-silver, a lead-thallium (5.0%) alloy anode was very passive, but thallium had little effect on reducing the anode potential over a pure lead anode. However, their investigations indicated a ternary alloy of lead-calcium (0.1%) - thallium (4.0%) not only was more stable than pure lead anodes, but also resulted in lower lead content of the zinc deposit and a reduction of the anode potential by 40%.

Kiryakov and Stender[4,5,6] after reviewing the results of work done on alloys of lead, deduced that no alloys had been found for zinc electrolysis superior to lead with 1% silver. They surmised that a more uniform distribution of silver in the lead, and a greater effectiveness of the protective action of silver would result if a third component were introduced into the system that would form solid solutions with lead and silver. To test the above hypothesis, they added thallium, bismuth, mercury, tin, gold, platinum, cobalt, arsenic, selenium, calcium, barium, and strontium to a lead-silver alloy. Since cobalt would not alloy directly with the lead-silver, it was necessary to first alloy the cobalt with a third element and then with the lead-silver.

It was indicated that electropositive (noble) elements lowered rather than increased stability and the protective action of calcium was only temporary. Further, they found the quaternary lead-silver (1.0%)-tin (0.3%)-cobalt (0.02%) alloy had a more uniform distribution of silver in the alloy, was more stable than all of those tested and gave particularly low values of anode potential, i.e., 1.91V at 25°C in 2N H_2SO_4 at 100 asf. They also found that cobalt, whether in solution or alloyed, had the same effect on lowering anode potential.

A protective film was obtained on the quaternary lead-silver-tin-cobalt alloy upon anodizing in 2N H_2SO_4, which was particularly massive and compact, and no ions of cobalt could be detected in the solution around the anode in accordance with their supposition that the protective action of cobalt was developed inside the protective film.

They concluded that the occurrence of the alternating process of oxidation of divalent cobalt ions ($Co^{++}=Co^{+++}+e^{-}$) and the catalytic reduction of oxidized ions going on at different points on the inhomogeneous surface of the anode can explain the observation of lowering of anode potential and elevation of the stability of the electrode.

Koenig, MacEwan and Larsen[7] looked at the effect of adding magnesium, sodium, chromium, manganese, nickel, iron and cobalt as sulfates to an electrolyte of 40 gpl Zn^{++}-105 gpl H_2SO_4, on pure lead anodes. Cobalt, present in the

electrolyte at 20 mg/l, was the only one of the above impurities to have a significant effect on anode potential (less noble by 0.117V) and the lead in the zinc deposit was only 0.002%. However, cobalt resulted in a rapid resolution of the zinc deposit.

They also investigated binary alloys of lead with bismuth, magnesium, arsenic, cadmium, antimony, tin and silver added as the second constituent. They observed that some of the metals alloyed with the lead dissolved during electrolysis. Magnesium had no effect on the zinc deposit, arsenic and antimony caused rapid resolution, cadmium and tin gave smooth bright deposits, bismuth a spongy deposit and silver a fine crystalline deposit with some resolution from the back of the cathode. All of the above alloys resulted in a lowering of the anode potential, but only lead-silver resulted in low lead content in the cathode deposit.

To study the method of lead transfer to the cathode, they put a pure lead anode inside a canvas bag and electrolysis was carried on for several hours. At the end of this time a large amount of PbO_2 was found in the bag but analysis of the cathode revealed only a trace of lead.

Koch[8] found no effect of cobalt on lead anodes in 2N H_2SO_4 during the initial sulphation of lead and noted that cobalt only became effective when the potential had risen to a value where oxidation of Co^{++} to Co^{+++} could occur. He concluded that cobalt reduces the oxygen overpotential thus

facilitating the evolution of oxygen with the possible result that once a conducting path of PbO_2 is formed, a significant proportion of the current may be used for oxygen evolution in preference to the oxidation of lead sulfate.

Lander[9] postulated an identical series of reactions to explain the depolarizing effects of silver and cobalt as follows:

1. $PbSO_4 + 2H_2O = PbO_2 + SO_4^{=} + 4H^+ + 2e$ + 1.685V
2. $Co^{++} = Co^{+++} + e$ + 1.820V
3. $Ag^+ = Ag^{++} + e$ + 1.980V

Reaction 1 takes place at the positive plate of the lead-acid cell. On charge, as the reaction nears completion, the evolution of oxygen commences and at the same time the positive plate potential becomes more positive to an extent, sufficient for reactions 2 or 3 to occur when Co^{++} or Ag^+ is present in the electrolyte. If these reactions occur, Co^{+++} and Ag^{++} can oxidize water to H_2O_2 as in reactions 4 and 5,

4. $2\ H_2O + 2\ Co^{+++} = H_2O_2 + 2\ Co^{++} + 2H^+$ $\Delta F° = -1.5$ kcal
5. $2\ H_2O + 2\ Ag^{++} = H_2O_2 + 2\ Ag^+ + 2H^+$ $\Delta F° = -9.5$ kcal

and H_2O_2 decomposes in acid solution to give oxygen,

$$2\ H_2O_2 = O_2 + 2\ H_2O \qquad \Delta F° = -50.4 \text{ kcal}$$

Lander feels that the effect of silver and cobalt is to supply an alternate path for the evolution of oxygen;

therefore, their presence should result in a decreased oxygen overvoltage and a reduction in anode corrosion under constant current conditions.

Fink and Dornblatt[10] some years earlier studied the effect of silver (0.05 - 0.15%) on properties and performance of antimonial lead storage battery grids and decided that silver had a two-fold result, in that the oxygen overvoltage was reduced, and a more impervious and tenacious peroxide film was built up on the surface of the anode.

Wark[11] made a detailed study of the electrolysis of very highly purified zinc sulfate solutions using pure lead anodes and aluminum cathode. The significant data obtained with pure solutions indicated that current efficiency (C.E.):

1. is almost independent of temperature in the range 30 to 40°C.
2. is constant with time over a considerable period; and reduction in C.E. with time can be attributed to residual impurities.
3. may be slightly lowered by unnecessary additions of gluc or other colloids.
4. is not materially influenced over the range of interest in practice by current density. At very low current densities "resolution" becomes important.

5. is determined by the ratio of acid to zinc concentration rather than by concentration alone, i.e., the current deposits zinc and hydrogen in proportion to their concentration in solution. The ideal molecular ratio for maximum C.E. is

$$\frac{ZnSO_4}{H_2SO_4} = 2 \text{ to } 5 \ .$$

Wark found that 100 mg/l of cobalt added to pure zinc sulfate solutions caused a drastic reduction in current efficiency as temperature increased from 20 to 50°C and current density decreased from 60 to 30 asf. At 20°C, C.E. was greater than 80% after 24 hours, but at 45°C, the C.E. was reduced to 40% after only 8 hours, both measurements being made at the same current density. He deduced that cobalt deposited with the zinc and presented a surface of lower overvoltage for hydrogen deposition so as to set up a local couple. As zinc dissolved more cobalt was uncovered and the resolution proceeded at even faster rates. Ultimately, the zinc dissolved off of the aluminum cathode.

Tromshina and Stender[12] examined the influence of zinc ion concentration (30 - 90 gpl), H_2SO_4 concentration (100 - 200 gpl) and also temperature (30 -70°C) on zinc cathode potential and zinc yield using current densities as high as 10,000 A/m^2 and very pure solutions.

They found that with increasing electrolyte temperature, the zinc current yield decreased significantly at low current

densities. At high current densities an increase in temperature resulted in an increased yield of zinc, especially in high acid ($\geq$ 2N H_2SO_4) electrolytes. This indicated that the overvoltage for discharging hydrogen ions on zinc increases more rapidly than the overvoltage for discharging zinc ions with increases in cathode current density. Since at low current density and with increased sulfuric acid concentration in the electrolyte, the hydrogen current yield exceeded 100% , they concluded that hydrogen was being produced by a secondary dissolving of zinc through the action of microcells on the cathode surface. The effect of the microcells was smothered at very high current densities as a result of the "anode protective" effect.

Pecherskaya and Stender[13] also discovered that the yields of hydrogen per unit current decrease in proportion to the increase in current density. They claimed that due to the presence of impurities deposited on the zinc cathode during electrolysis, new sources are formed for the liberation of hydrogen - short circuited glavanic cells, which promote the dissolution of zinc and the proportionate liberation of hydrogen.

They also investigated the effects of impurities that increase the hydrogen overvoltage and found increases in zinc yield with impurities of high hydrogen overvoltage.

Turomshina and Stender[14] looked at the results of adding ions of metals more electropositive than zinc to pure

zinc sulfate solutions and explained the increase in hydrogen efficiency as being due to local short-circuited galvanic cells on the surface of the zinc cathode.

Application of external cathodic current density to the system of local cells results in polarization of the local cathodes (the impurities) up to a point at which their negative potential becomes equal to the negative potential of the local anode. The emf of the microelements then approaches zero, and corrosion of the metal (zinc) electrode ceases.

Similar results[15] were obtained for ions of metals more electronegative than zinc. That is, either the elements or compounds of the elements formed short-circuited galvanic cells on the cathode surface which reduced the current efficiency for the zinc deposition.

Salin, et. al.,[16] examined the effects of electrolyte temperature on zinc electrolysis. Their results indicate that at 40 asf with pretreated (PbO_2 coated) lead-silver (1%) anodes in pure solutions of 50 gpl Zn - 120 gpl H_2SO_4, the zinc current efficiency has only a very slight relationship to the temperature. However, with factory electrolyte an increase in the temperature above 50 - 55°C will lead to a sharp reduction in current efficiency, due to impurities in the solution precipitating out on the cathode deposit. The number of such impurities depositing on the cathode per unit of time ($\frac{dm}{dt}$) may be calculated by the formula:

$$\frac{dm}{dt} = C_o \cdot \frac{D}{X}$$

where D is the diffusion coefficient, C_o the impurity concentration in the electrolyte, and X the thickness of the diffusion layer.

An increase in temperature, when there are impurities in the electrolyte, leads to an increase in the diffusion coefficient D and results in an increase in the number of microcells contributing to the corrosion of zinc.

Tainton[17] commented in his work on the effects of impurities in zinc electrolysis that a crystal or segregation of molecules must reach at least a certain size before becoming effective in increasing hydrogen evolution which would account for the fact that there seems to be a certain critical concentration for each impurity above which it becomes dangerous.

Farmer[18] studied the preconditioning of lead-silver (0.75%) anodes in various solutions prior to electrolysis in Trail's electrolytic cells. Theorizing that the protective PbO_2 coating on lead-silver anodes resulted from extended periods of oxidation, he attempted to reduce the conditioning time by oxidizing in an appropriate solution.

Solutions tried were H_2SO_4, H_3PO_4, NaOH, $PbNO_3$, $MnSO_4$, NaF and KF. The fluoride-H_2SO_4 solutions resulted in an anode of markedly improved response, i.e., .0012% lead in the zinc deposit after 20 weeks of testing versus .0052%

for anodes treated in the absence of fluoride. No satisfactory explanation could be offered for the remarkable effect of the fluoride ion in stabilizing the anode surface.

Burbank[19,20] attempted to identify the compounds formed on polarizing pure lead anodes above the $PbSO_4/PbO_2$ potential in 1.21 specific gravity H_2SO_4 by potential decay curves and x-ray diffraction. She established the existence of PbO_2, PbO_t, $Pb(OH)_2$, $PbO \cdot PbSO_4$ and $PbSO_4$ in this potential region and in addition found an unidentified material believed to be a form of lead monoxide, which she later identified as αPbO_2.

Anodization of lead in acid at potentials immediately below the reversible $\beta PbO_2/PbSO_4$ potential produced a deposit of PbO_t while anodization at potentials above the $PbO_2/PbSO_4$ potential resulted in a deposit of αPbO_2. The αPbO_2, while attached to the metal surface, appeared to be deformed into the tetragonal lattice. Burbank theorized that the stresses exerted by such a deformed lattice might be the primary cause of growth of pure lead grids in cells.

In a later series of investigations, Burbank[21,22] noted a difference in morphology of the PbO_2 deposits in the positive plates of good and bad lead acid cells. Plates with pebble-like nodular PbO_2 particles were found to soften and fail while plates made up of prismatic needles of PbO_2 particles maintained capacity and retained a firm texture.

She found that anodization of large prismatic crystals of $4PbO \cdot PbSO_4$ converted them to βPbO_2 and the prismatic

form of the basic sulfate was retained by the PbO_2 after anodization. This strengthened the PbO_2 deposit due to the interlocking of the large crystals.

Ruetschi and Cahan[23] have shown that the oxygen overvoltage on βPbO_2 is much higher than on αPbO_2 and the disparity increases with increases in current density. The Tafel slope for αPbO_2 is .051, indicating two electronic charges are involved in the rate determining step, while βPbO_2 has a Tafel slope of 0.121 indicating only one electronic charge is involved in the reaction.

Anodic corrosion in the potential region where oxygen is evolved increases strongly with the electrode potential. Therefore, electrodes with a low oxygen overvoltage should withstand corrosion better under constant current conditions. Certain additives, such as Co^{++} and Ag^{+}, can reduce the oxygen overvoltage and anodic corrosion.

Ruetschi and Angstadt[24] state that the following occurs upon anodization of lead in sulfuric acid. $PbSO_4$ forms an initial layer and thickens so that $SO_4^{=}$ and H^{+} ions are no longer able to readily penetrate. Any depletion of $SO_4^{=}$ ions is accompanied by an equivalent depletion of H^{+} ions and vice versa because of the tendency of the electrolyte to maintain electrical neutrality. The very high electric field established in the dense $PbSO_4$ layer, manifested by the large ohmic drop, will tend to repel positive H^{+} ions from the microcavities of the inner part of the film and

attract SO_4= ions and OH^- ions generated by dissociation of H_2O molecules. This latter effect tends to enhance the alkalinity in the interior of the corrosion film and to stabilize the high local pH. The pH gradient in the corrosion film, due to inhibited ionic diffusion, results in the formation of PbO, basic lead sulfates and αPbO_2 in acid media.

Abdul Azim and Anwar[25] during a study of anodic potential time curves in various media at 300 ua/cm^2 noted the arrests corresponding to the following equilibrium systems: $PbO_2/PbSO_4$, PbO_2/PbO, PbO/Pb and $PbSO_4$/Pb. The potential plateau for the PbO/Pb couple was well defined and was maintained for many hours before the voltage decayed further to the sulfate potential at -.33V.

Pavlov[26,27,28] has investigated the anodic oxidation of lead in N H_2SO_4 by potentiostatic methods with the results as listed below (potentials are vs. the Hg/Hg_2SO_4 reference electrode +0.667V).

up to -300mv	$PbSO_4$
-300mv to +900mv	$PbO \cdot PbSO_4$, $3PbO \cdot PbSO_4 \cdot H_2O$, $5PbO \cdot 2H_2O$, $4PbO \cdot PbSO_4$, PbO_t
>900mv	αPbO_2
>1200mv	βPbO_2

The mechanism for the above reactions was outlined by Pavlov as follows: Pb^{++} ions from the dissolution of the

metal react with SO_4= ions and are precipitated as $PbSO_4$ on the lead surface. During growth, the lead sulfate crystals obstruct the major part of the metal surface. At the $Pb/PbSO_4$ interface, the electrochemical process will stop since $PbSO_4$ is a dielectric, thus the only active electrochemical surface remaining is the metal surface between the $PbSO_4$ crystals. The flow of Pb^{++} ions, the amount depending on overvoltage of anodic dissolution, moves between the crystals toward the bulk of the solution while SO_4= ions, the amount depending on concentration, move in the opposite direction. Consequently, the components of the chemical reaction Pb^{++} and SO_4= are separated by a porous dielectric layer of $PbSO_4$ and the reaction between them will proceed in the region where the two flows meet each other. If the number of Pb^{++} ions in the flow exceeds the equivalent number of SO_4= ions in the opposite flow, then the zone at which precipitation takes place will be located at a certain distance from the metal surface. In order for the solution to remain electroneutral, the charge of Pb^{++} ions must be compensated. This is realized by disassociation of H_2O. Since the mobility of H^+ ions is several times higher than that of Pb^{++} ions, it follows that H^+ ions will have to migrate from the inner zone toward the bulk of the solution. Thus, charges of Pb^{++} are compensated by the OH^- obtained from the disassociation of water. This in turn increases the pH of the solution and thus enables the

formation of PbO_t, basic lead sulfates and αPbO_2 in acid media.

Simon, et. al.,[29] in examining the discharge and recharge of the PbO_2 electrode with optical microscopy, discovered that discharge begins with nucleation of $PbSO_4$ at selected sites on the surface of the PbO_2. Growth then depends on the continued dissolution of the PbO_2 and reaction between the Pb^{++} and $SO_4^=$ ions which deposit as $PbSO_4$ upon the surface of the lead sulfate already present. As $PbSO_4$ content increased, the amount of PbO_2 decreased, until all the PbO_2 remaining was encapsulated in the $PbSO_4$.

During recharge, the PbO_2 particles within the $PbSO_4$ crystals offered a conductive path through the highly resistive lead sulfate, and the reformation of PbO_2 began within the encapsulating $PbSO_4$ crystals at the surface of the residual PbO_2 particles. The lead dioxide thus formed grew rapidly toward the surface of the $PbSO_4$ crystals. Upon reaching the surface of the crystals, it appeared to spread and surround them, encapsulating them in turn and leaving hollow shells as the $PbSO_4$ crystals dissolved.

III. EXPERIMENTAL PROCEDURE

A. Cathode Reactions

1. Materials and Equipment. All electrolyses were performed galvanostatically using a Sorenson QRC40-15A D.C. power supply.

Neutral zinc sulfate solutions were prepared by dissolving stoichiometric amounts of lead-free photoconductive zinc oxide in Fisher's A300C reagent grade sulfuric acid and distilled H_2O, followed by a two step purification, consisting of oxidation with potassium permanganate and then treatment with zinc dust. For complete details of solution preparation, see Appendix A. The desired solution concentration of 65 gpl Zn^{++} and 200 gpl H_2SO_4 was then obtained from the neutral solution by either adding concentrated sulfuric acid directly or building up acid in the cell during deposition of zinc at the cathode, i.e., approximately 1.5g of H_2SO_4 is produced for each gram of zinc deposited.

A constant zinc ion, sulfuric acid concentration was maintained in the electrolytic cell by dripping in neutral solution with a CRC Vibrostaltic Pulsation Pump. The solution was fed in at the back of the anode to take advantage of the stirring effect from the oxygen evolution.

The cell itself was made from a pyrex 1000ml beaker with the spout heated and drawn down so that solution

overflowed during operation, maintaining the volume in the cell at precisely one liter. Prior to use for the first time, the glass cell was cleaned, as was all other glassware, by first soaking in NaOH to remove silicates, then washing with sodium dichromate-sulfuric acid cleaning solution and rinsing with hot tap water and copious amounts of distilled water.

During electrolysis, the cell was immersed in a water bath and fitted inside a plexiglass support that had been machined to hold the beaker atop a small CRC air driven magnetic stirrer. Temperature was controlled at $\pm$ 1.5°C by a hot plate in the early phases of the investigation, and later somewhat closer ($\pm$ 0.5°C) control was obtained using a Precision Lo-Temp Circulating System.

A 0.125" thick plexiglass top was used to hold and space the electrodes and to reduce the amount of solution evaporation. The top was approximately 5.0" in diameter, with an 0.032" slot cut so that the cathode could be slid in from one edge and be centered in the cell. Precisely 1.5" on each side of the center slot and parallel to it, two openings were cut 0.125" x 1.5" long for inserting the anodes. Later, the plexiglass lid was modified by drilling two 0.75" diameter holes strategically placed for admission and placement of a Luggin capillary to measure anode and cathode potentials.

Various metals were tried as anodes and cathodes but

the majority of the experiments was performed with platinum-coated titanium anodes (Platanodes) and pure (4-9's) aluminum cathodes.

The anodes were cut 1.5" wide x 5.0" long x various thicknesses and were bolted to an elliptical shaped, pure aluminum ring that held them 3.0" apart and parallel to each other. A banana plug was mounted in the center of one end for the electrical connection and the whole was wrapped tightly with teflon tape to prevent accidental contamination of the solution by corrosion products from the aluminum, or bolts holding the anodes, inadvertently getting back into the cell.

The cathodes were tee shaped, 1.25" wide x 4.25" long x 0.032" thick, with a 0.25" x 3.0" bar on top. The actual working area gave approximately 10 amps per square foot (asf) for each 0.5 amps of current. The cathodes were inserted into the slot in the plexiglass top and the arms of the tee were bent in opposite directions to hold them in place. A banana plug was attached to one arm of the tee for the electrical hook up, and the brass end of the plug was wrapped in teflon tape, as was mentioned before, to eliminate a source of solution contamination.

Teflon strips, 0.25" wide x 0.125" thick with a 0.032" slot in the center, were placed on the edges of the cathode and at the bottom to minimize current concentration in these areas and the resulting dendritic growth.

The cathodes were first sanded with 600 grit emery paper, to remove the rolled surface, then washed and blotted dry before being placed in the cell.

A salt bridge, with a Luggin capillary for contact at the electrode surfaces, and a Kiethley 610 C Electrometer were utilized to measure cathodic and anodic polarization potentials versus a Hg/Hg_2SO_4 (1N H_2SO_4) reference electrode. Potentials were recorded on an Esterline Angus chart recorder and all values are reported with reference to the standard hydrogen electrode (SHE) at 25°C.

Figure 1 depicts the experimental arrangement described above.

2. Operation of the Electrolytic Cell. The cleaned and dried cell was filled to one liter, with either neutral solution or solution already mixed to give 65 gpl Zn^{++}, 200 gpl H_2SO_4, placed in the water bath and allowed to stabilize at the desired temperature.

The magnetic stirrer was activated at this point for those experiments where stirring was desired by running compressed air through Tygon tubing connected to the intake and discharge apertures to spin a glass covered magnet inside the cell.

The cathode, with the teflon strips in place, was inserted into the slot in the plexiglass top and slid into the center. The anodes were then placed through the slots on both sides of the cathode and the whole assembly was

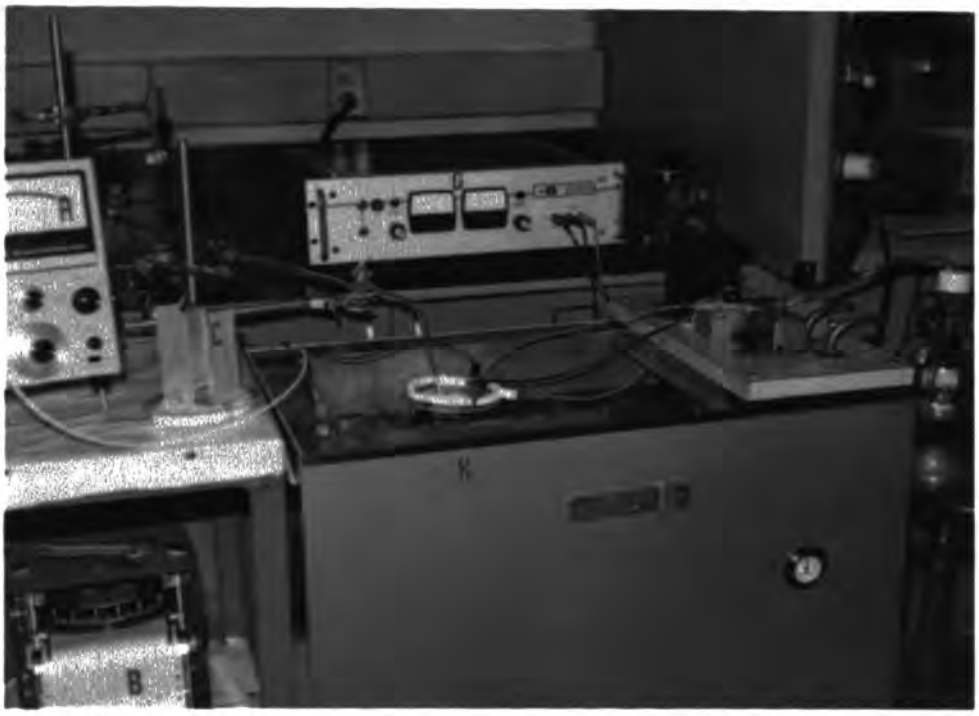

A. Keithley 610 C Electrometer

B. Esterline Angus Chart Recorder

C. Assembled Electrodes - ready for insertion in cell

D. Hg/Hg_2SO_4 (1N H_2SO_4) Reference Electrode

E. Salt Bridge

F. Electrodes and Top of Cell - immersed in water bath

G. Sorenson QRC 40-15a D.C. Power Supply

H. CRC "Vibrostaltic" Pump

I. Powerstat to Control Pumping Rate

J. Jug of Neutral Solution

FIGURE 1. EXPERIMENTAL APPARATUS

flushed with distilled H_2O and blotted dry. Leads from the power supply were attached, the electrodes were placed into the cell, and the power supply was immediately turned to the desired current setting.

As soon as the power was on, the polyethylene tube from the vibrostaltic pump was fitted into a small hole in back of one of the anodes and the variable autotransformer, used to control the pumping rate, was adjusted to give the desired number of drops of neutral solution per minute to maintain the required concentration of zinc ion and sulfuric acid. Periodically, an aliquot portion of electrolyte was withdrawn by pipet and titrated against 1N NaOH to determine H_2SO_4 concentration and the pumping rate was adjusted accordingly.

Disassembly of the cell at the completion of electrolysis was in the reverse order to the above. The cathode was removed as rapidly as possible, flushed with large amounts of distilled H_2O and blotted dry with tissue to prevent discoloration by corrosion. Once the deposit was completely dry, it was stripped from the aluminum by flexing. With some deposits that were strongly adherent, a knife or razor blade was inserted under one edge to pry them loose.

The weight of the zinc deposit was obtained to four decimal places on a Sartorius 2400 Digital Analytical Balance and compared to the theoretical to calculate current efficiencies. Selected deposits were examined on the

scanning electron microscope and photographs were taken of typical structures.

B. Anode Reactions

1. Materials and Equipment. The equipment used was the same as described under cathode reactions except the cell was a one liter polyethylene beaker to accommodate the NaF and KF solutions due to the corrosive nature of fluorides on glass.

All solutions were mixed from reagent grade chemicals and distilled water. Disposable plastic gloves, protective clothing and safety glasses were worn at all times when handling the fluoride solutions, due to the hazardous nature of the fluoride ion.

The electrodes were the same dimensions as before. Polarity was reversed and the anode was now in the center of the cell between two cathodes. Various metals were used as cathodes: aluminum, lead-silver, platinum-coated titanium and pure platinum. However, for the majority of the experiments, either lead-silver or platinum cathodes were employed.

Anodes were made from lead or lead alloys, cold rolled from various thicknesses to 0.032" and cut tee shaped to the same dimensions as the cathodes in part A. The rolled surface was removed by wire brushing and the anodes were carefully weighed before electrolysis. Specimens of the

various materials employed as anodes were cut, mounted, polished and etched as outlined in Appendix B and photomicrographs of typical structures were obtained and are included in Figure 2.

A Siemens Crystalloflex IV Diffractometer with copper K-alpha radiation, 0.1 mm slit, Ni filter and a counting rate of 4×10^4 imp/min was used to determine the phases present on the anode after electrolysis. A variable aperture was used to adjust peak height.

2. Operation of the Electrolytic Cell. Operation of the cell was essentially the same as described previously except for reversal of the anode and cathode positions and the extra safety precautions necessary for handling the fluoride solutions. One liter of solution sufficed for several experiments as depletion of the active species was minimal. Periodically, it was necessary to replace some distilled water lost by evaporation.

The majority of the anodes was conditioned for 12 hours and then they were removed from the cell, washed in distilled water, blotted dry and weighed again to determine the increase in weight during electrolysis.

The deposit was examined visually and with the light microscope and scanning electron microscope to determine surface morphology. Photographs were taken of typical structures revealed by SEM.

The relative hardness of the samples was determined

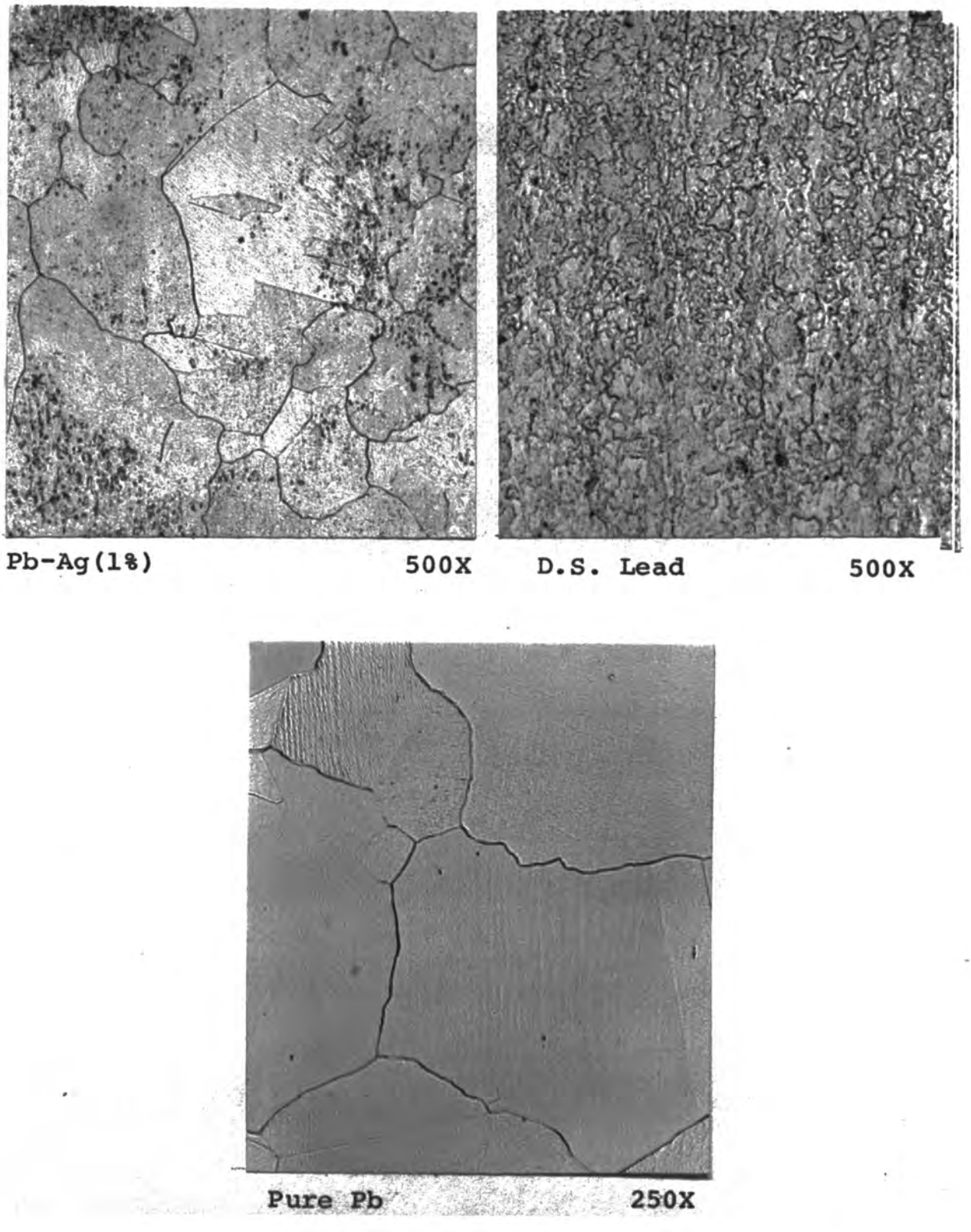

FIGURE 2. MICROSTRUCTURES OF THE AS ROLLED SURFACE OF LEAD AND LEAD ALLOYS USED IN THIS WORK.

by running a hard pencil lead or fingernail over the surface, or by using a Bierbaum Microcharacter in conjunction with a metallurgical microscope and measuring the width of a scratch produced by a ground diamond point that was mechanically drawn across the surface.

3. Measuring Potentials. The electrometer was warmed up for several hours and set to a predetermined value of range and polarity. The meter pointer was brought to zero with the medium and fine zero adjust knobs. The recorder was turned on and adjusted so that the pen was recording zero on the strip chart, corresponding to the zero of the electrometer. If a change in range or polarity was required, it was necessary to rezero the electrometer and the recorder.

The potential of the Hg/Hg_2SO_4 (1N H_2SO_4) reference electrode was measured against a saturated calomel electrode (0.242V) before and after each experiment. The equilibrium value recorded for the reference electrode was 0.671V $\pm$ 1mv (SHE).

The salt bridge was filled with 1N H_2SO_4, then placed in the cell through the opening in the plexiglass top and clamped in place with Luggin tip in contact with the anode surface. The electrical connections were made, and the power supply and the electrometer were turned on simultaneously. At completion of polarization, the power supply was turned off, the leads were disconnected from the cathodes and the anode, and the decay potential was recorded.

Values were extracted from the chart at the end of the measurements. Polarization and decay potentials versus time curves were plotted. Potential values were calculated using the equation $\pm E_{meter}$ (sign from polarity switch) = $E_{+lead} - E_{-lead}$.

IV. RESULTS AND DISCUSSION

A. Cathode Reactions

The results and discussion are divided into sections for clarity. In a few sections further amplification of experimental procedure was deemed advisable because, due to the specific nature of the procedure, it was not possible to include a complete discussion in the section on Experimental Procedure. Further, including the additional information at this point eliminates the need for continual referral to the previous section when trying to relate a particular procedure with the corresponding results and discussion.

1. Built Up Cell Acid Versus Added Acid. There are two ways to get the desired acid-zinc ratio from neutral solution. One is to remove zinc by electrolysis while simultaneously increasing the H_2SO_4 concentration, and the other method is to add the appropriate amount of acid to the solution. This experiment was initiated to determine which of these two methods of solution preparation would be the most desirable for subsequent investigations.

Neutral zinc sulfate solution prepared by procedures outlined in Appendix A was electrolyzed at 40°C for 20 hours at 40 asf (2 amps), followed by 20 hours at 60 asf (3 amps) to adjust the acid-zinc concentration to 200 gpl H_2SO_4, 65 gpl Zn^{++}. Deposits were stripped every four hours; accurate weights were obtained and current efficiencies

were calculated. Also, an aliquot portion of electrolyte was withdrawn from the cell and titrated against N NaOH to a methyl orange endpoint (pink to orange) to directly determine the H_2SO_4 concentration and indirectly determine the zinc concentration.

The 1100 aluminum alloy cathode and the platinum coated titanium anodes (platanodes) were washed and blotted dry between each run.

When the desired solution concentration was attained, an additional four hour deposit was made at 60 asf, holding the acid-zinc concentration constant by dripping in neutral solution. A comparison was then made between this deposit and another deposit made under identical conditions except the acid-zinc concentration was obtained by mixing reagent grade H_2SO_4 and neutral solution.

A macrophotograph, typical of a deposit obtained during acid build up and one obtained from mixed acid, along with an SEM photograph of the structure, representative of both deposits, are included in Figure 3.

Visually the deposits produced during acid build up were pitted and extremely porous, with the amount of pitting gradually increasing after the first four hours and then decreasing after 24 hours, as the acid concentration increased. Corresponding to the change in the number of holes with time was a change in the color of the solution. The clear solution turned faintly pink during the

first four hours of deposition indicating the presence of permanganate introduced during solution purification. The pink color gradually increased in intensity with subsequent deposits and then decreased until the solution was again clear after 24 hours. The presence of permanganate should indicate a very pure solution since it would appear there were no impurities present to reduce the Mn^{+7}. By the same token, the presence of enough manganese to color the solution may have been in part responsible for the large amount of pitting in the deposits. Also, some impurity that may have been previously oxidized by the permanganate could have been reduced and deposited at the cathode causing the pitting through the action of local cells.

Whatever the case, it would appear that a pure solution is not necessarily a deterrent to poor cathode morphology.

Current efficiencies were very high (∿100%) for all deposits throughout the first 30 hours of electrolysis, gradually tapering off to 97% for the last four hour deposit.

In the final four hour run at constant conditions and with a current efficiency of 95%, the deposit exhibited holes or pits all over the surface. However, the deposit made under identical conditions, but from a mixed electrolyte, had a uniform crystalline structure with no pits

(Figure 3) and the current efficiency was slightly higher.

The structure of good deposits and pitted deposits were the same (Figure 3) and consisted of stacks of hexagonal platelets predominantly oriented with the basal plane parallel to the plane of the aluminum cathode. X-ray analysis confirmed the apparent preferred orientation as the most prominant peak corresponded to reflections from (002) planes at right angles to the x-ray beam.

It was felt prior to these experiments that building up acid in the cell would result in a purer solution and consequently a better deposit, since all chemicals added would have gone through the two step purification (Appendix A). However, the above results do not bear out this premise and it was decided to prepare electrolyte by adding reagent grade H_2SO_4 to neutral solution to obtain the desired concentration. This, of course, was much quicker as acid build up in the cell is a time consuming process, made even more so due to the necessity of running at a relatively low current density to maintain the total cell voltage below 5 volts which appeared to exceed the critical cathode potential for dendritic initiation and growth.

2. Lead-Silver, Pure Lead and D.S. Lead Anodes. Zinc deposits of 4 hours, 12 hours, 24 hours and 4 hours were made in succession in mixed electrolyte, using anodes made from each of the materials listed above, and an 1100

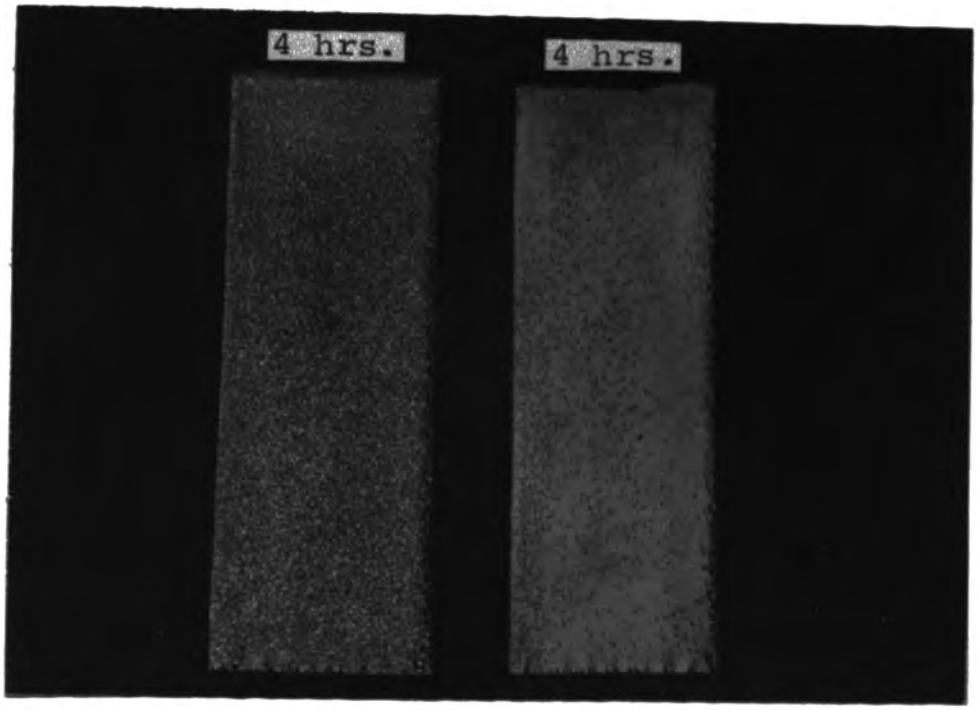

60 asf 0.89X

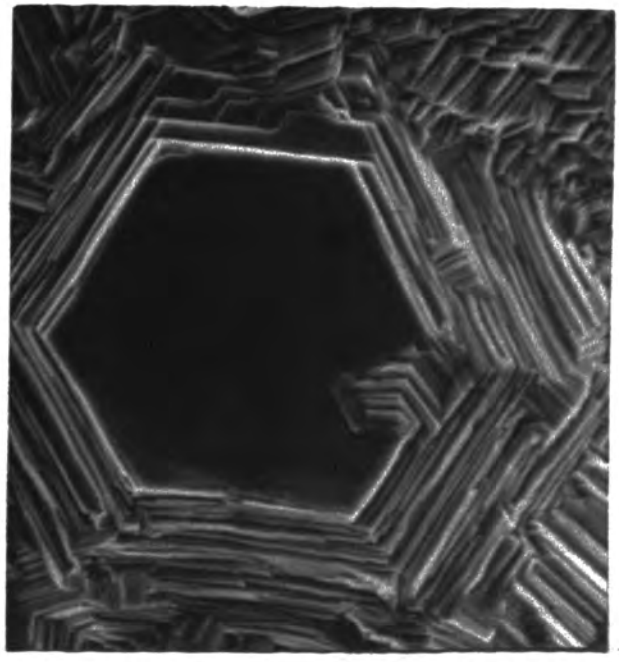

60 asf 1000X

FIGURE 3. TYPICAL STRUCTURE OF A GOOD DEPOSIT AND A PITTED DEPOSIT (upper) PRODUCED AT 40°C AND THE SCANNING ELECTRON MICROGRAPH OF THE STRUCTURE (lower) REPRESENTATIVE OF EACH.

aluminum alloy cathode at 40°C and at a current density of approximately 80 asf. The total cell voltage varied from 3.3 - 3.4 V for the lead-silver; 3.5 - 3.6 V for the dispersioned strengthened lead (D.S.); and 3.7 - 3.8 V for the pure lead anodes, over the 40 hours of electrolysis.

The lead-silver anodes were fashioned from an electrode supplied by the American Zinc Plant at Sauget, Illinois, of the same type used in their electrolytic cells. The anode, as received from American Zinc, was 0.25" thick with 1.0" diameter holes spaced 2.0" apart (center to center). It was necessary to cold roll the material from 0.250" to 0.160" (4 equal passes) to get 1.5" of solid metal for the experimental electrodes between the holes. Prior to electrolysis, the area of the working surface was reduced ∿50% by drilling 59, 0.25" diameter, equally spaced holes. The rolled surface of the electrode was then removed by wire brushing and the area inside the holes was reamed with a small file.

The D.S. lead and the pure (4 - 9's) lead anodes were prepared as above from lead sheet already on hand.

During zinc deposition the solution gradually turned from milky white to pink in the first four hours with the lead-silver anodes, and from milky white to blackish purple with the pure lead and the D.S. lead anodes. The solutions retained the colors noted above through the remaining 12 hour, 24 hour and 4 hour runs. Also, a brown residue

began to accumulate in the bottom of the cell which gradually increased throughout the electrolysis. At the end of the 40 hours of deposition, the solutions were decanted, the residue was collected, washed, dryed and analyzed by x-ray diffraction.

The anodes were stored in distilled water, rinsed and blotted dry between runs. The bottom of the distilled water beaker and the anodes were covered with a silvery white precipitate after more than a few hours storage. Samples of this white residue were also collected for identification by x-ray diffraction.

Typical structures and the scanning electron micrographs of the last four hour runs made with each set of anodes are included in Figure 4.

The surfaces of the deposits were pitted and had a silvery colored metallic sheen. The surface of the zinc deposit made with the pure lead anodes gradually darkened and became black with time while the deposits made with lead-silver and D.S. lead remained shiny and metallic looking after several months (see Figure 4).

The amount of residue in the bottom of the cells varied with each set of anodes used. The least amount resulted from the use of the lead-silver and the most from the D.S. lead. The large amount of lead in solution is what imparted a blackish color to the D.S. and pure lead cell while the small amount of lead present in the lead-

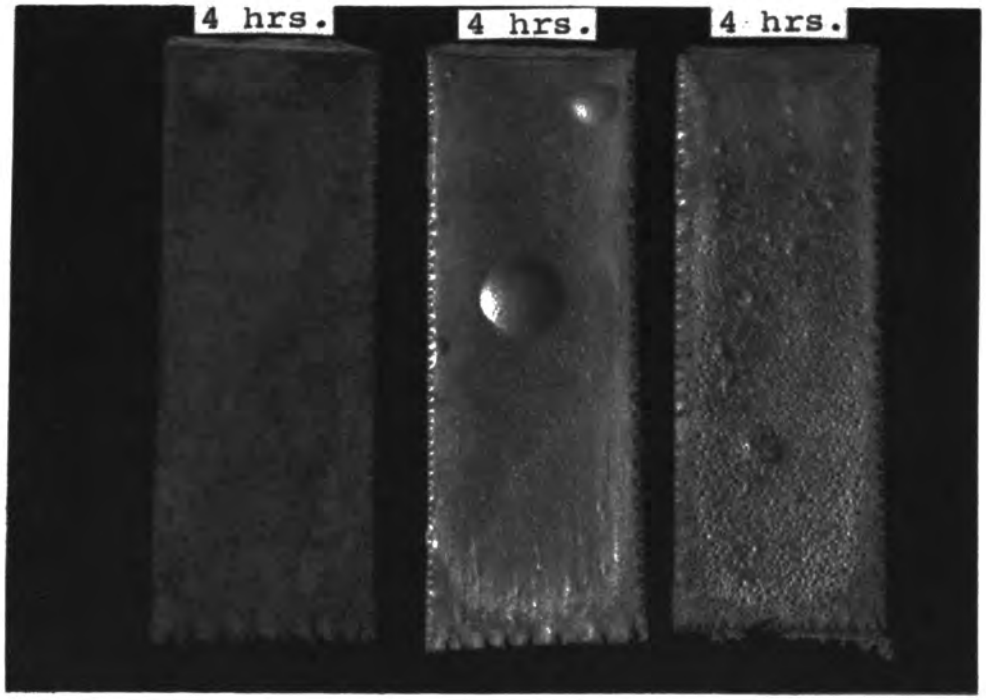

80 asf 0.89X

80 asf 1000X

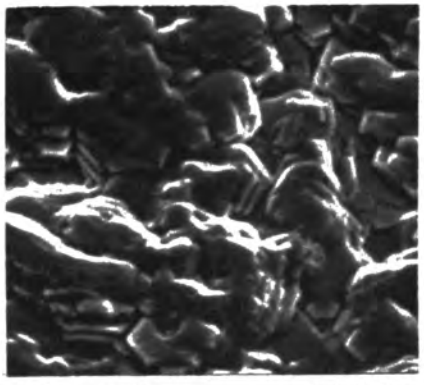

80 asf 1000X

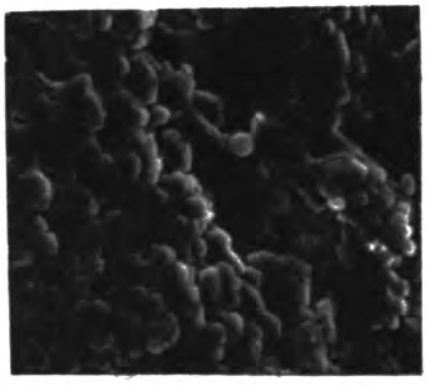

80 asf 1000X

FIGURE 4. DEPOSITS (upper) PRODUCED AT 40°C AND THE SCANNING ELECTRON MICROGRAPHS (lower) OF THE DEPOSITS MADE WITH PURE Pb, Pb-Ag(1%) AND D.S. Pb ANODES (left to right).

silver cell was not great enough to overcome the familiar pink color of permanganate.

SEM photos of the final four hour deposits were different for each set of anodes used (Figure 4), and this difference too could probably be attributed to the differing amounts of lead in solution.

The deposits were not analyzed for purity, but it is quite probable they were contaminated with a considerable quantity of lead, either occluded or electrochemically deposited on the cathode.

The residues from the bottom of the cells and the distilled water soak were identified as follows:

Lead-Silver	Mixture of β PbO_2 and $PbSO_4$
Pure Lead	α PbO_2
D.S. Lead	α PbO_2
White ppt.	Hydrocerussite (lead carbonate hydroxide) $Pb_3(CO_3)_2(OH)_2$

Both α PbO_2 patterns had a peak at 3.5 angstroms, which corresponds to the line of maximum intensity for β PbO_2.

It is obvious from the above data and from confirming reports in the literature[1,2,3,7] that lead-silver anodes are superior to pure lead and other alloys of lead for zinc electrolysis, in that they lower the potential and reduce the amount of lead in the zinc deposit.

3. Pitting of the Zinc Deposits. Prior to the experiments outlined in 1 and 2 above, seventeen runs (88 hours of electrolysis) were made, using platanodes and an 1100 aluminum alloy cathode for orientation purposes, and to establish and polish the techniques to be used for subsequent investigations. Current density and time of deposits varied from 10 to 200 asf and 4 to 24 hours, respectively. The electrolyte temperature was maintained at 40°C throughout.

The early deposits were very good with a flashy crystalline appearance but as electrolysis continued, increasing amounts of pits developed and the last four deposits all had pits scattered throughout the surface. A photograph of typical good and pitted deposits is included in Figure 3. The solution was set aside while experiments 1 and 2 above were performed and then taken up again and four more deposits were made, all of which had pitted surfaces. A new solution was prepared but pitting of the deposits occurred again after a few hours.

Every conceivable source of solution contamination was investigated in an attempt to locate the source of the pitting. The delivery tubing used to feed neutral solution into the cell was replaced, distilled water from a different source was tried, a new set of platanodes was used, and pure platinum anodes were substituted for the platanodes, but all for naught. The deposits continued

to be pitted after a few hours of electrolysis in a new solution.

Finally, everything was prepared as for the first experiments. New platanodes, a new aluminum cathode, and a new solution were used and the deposits again came out as in the early runs, being very flashy and crystalline in appearance with no pits or holes.

Close observation of the cell during electrolysis revealed that the solution was very opaque and milky white in color, with good deposits, but as pits developed, the solution cleared and it was possible to see through to the cathode and observe bubbles clinging to the surface of the deposit. Concurrently, with the clearing of the solution and the formation of holes, a deposit of salt was observed to build up on top of the cathode, which amounted to one or two grams from a 24 hour deposit at 80 asf. If a cathode was used for many runs, as it was in the first series of experiments, this salt deposit not only built up on the cathode outside the top, but also built up on the cathode between the solution level and the top. Some of this salt was invariably carried back into the solution by condensate or by jiggling the cathode during disassembly of the cell.

The solution and the aluminum cathode used to make the first zinc deposits were put back in the cell and two successive 24 hour deposits (Figure 5) at 80 asf were

made. All the salt built up on the cathode was gathered for analysis to investigate the effect of the salt on the zinc deposit.

Approximately 2 grams of salt removed from the cathode were added to a new solution and a 4 hour and 8 hour deposit was made at 80 asf. Also, in another experiment an 1100 alloy aluminum strip was placed in the bottom of the electrolytic cell and allowed to dissolve during electrolysis at 100 asf for four hours.

In a third experiment, 1 gram of one micron alumina powder was added to the cell to study the effects of aluminum oxide on the cathode deposit. Further, some salt from the top of an aluminum cathode from the Sauget Plant electrolytic cell was obtained and 12 grams were added to a new zinc sulfate solution and runs of 3 hours and 12 hours were made at 80 asf. Finally, the aluminum cathode was replaced with a zinc cathode and a titanium cathode.

The first deposits produced from a new solution at 40°C were very good, with a flashy, crystalline appearance, but when the total time of the electrolysis reached 24 to 30 hours, whether in one run or many, pitting began to show up on the zinc. A solution that produced a pitted deposit gradually became worse with subsequent deposits until it was almost impossible to produce any deposit at all (see Figure 5).

Simultaneously, with the appearance of the pitting,

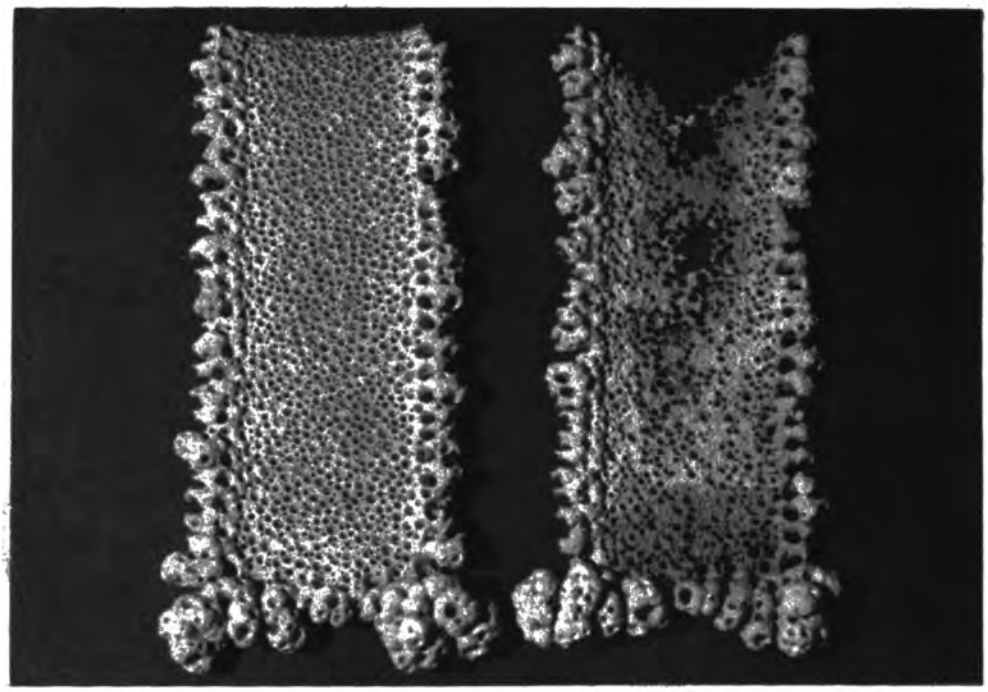

80 asf 0.89X

FIGURE 5. SUCCESSIVE 24 HOUR DEPOSITS PRODUCED AT 40°C IN "BAD SOLUTION."

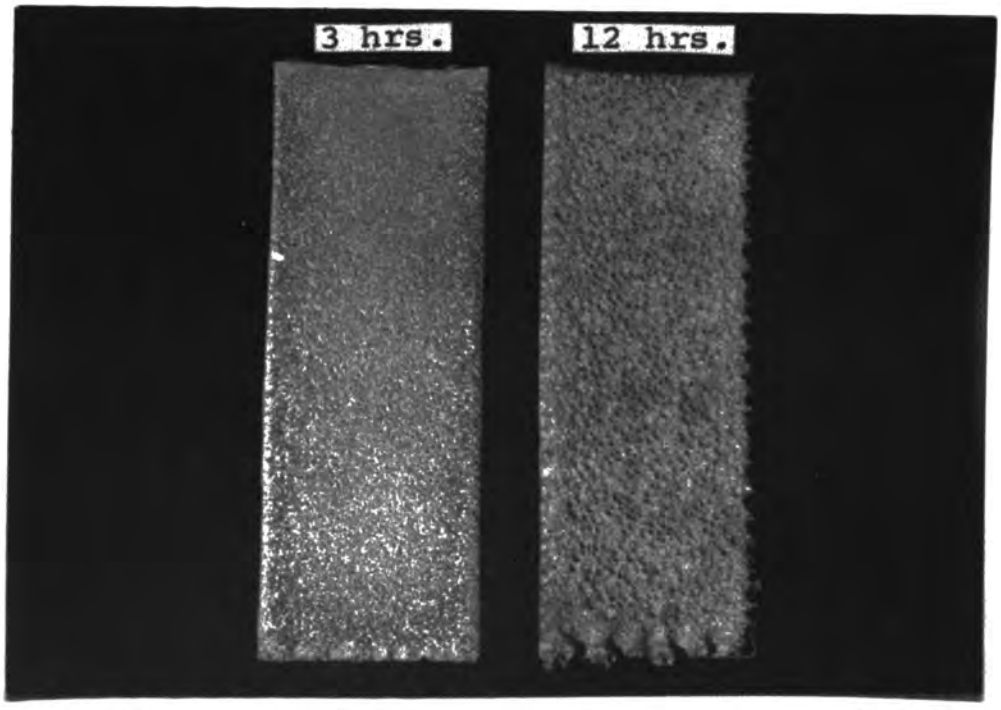

80 asf 0.89X

FIGURE 6. DEPOSITS PRODUCED AT 40°C AFTER 3 AND 12 HOURS WITH SALT FROM PLANT ADDED TO THE ELECTROLYTE.

the solution changed from dense, milky white to translucent; bubbles could be seen clinging to the cathode and a corrosive salt deposit began to build up on the exposed aluminum surface. The salt was identified by x-ray analysis as a hydrated zinc sulfate. However, some of the 1100 aluminum alloy must have been present, though in too small an amount to detect as the cathode was etched and corroded beneath the salt layer. Also, analysis of the solution by atomic absorption revealed, in addition to zinc, 6-10 ppm (mg/l) of aluminum that for the most part had dissolved from the cathode at or above the solution line during the first 24 hours of electrolysis. An additional 100 hours of electrolysis did not result in any increase in the amount of aluminum in the cell, probably because the solution was constantly being changed with time as neutral solution was pumped in and spent electrolyte overflowed.

All of the deposits made in new solutions with the hydrated zinc sulfate and alumina powder, and the deposit made with the aluminum strip in the bottom of the cell exhibited a flashy, crystalline structure, with no pits or holes and with good current efficiency; typical of deposits made in a good solution (see Figures 3 and 10).

Although the addition of aluminum to the electrolyte by the methods outlined above did not appear to be detrimental, the remainder of these experiments was carried out with aluminum cathodes of 4 - 9's purity in order to

minimize the possibility of solution contamination from alloying elements such as iron, silicon and manganese in the 1100 aluminum alloy cathodes.

The 3 hour and 12 hour deposits at 80 asf and 40°C, made in new solution, to which the salt from the plant electrode had been added, were heavily pitted; however, the pits in the 12 hour deposit were more prominent (Figure 6). During electrolysis, the solution was very deep purple in color, indicating the presence of more manganese than that added as permanganate during purification. Spectographic analysis of the salt confirmed the presence of manganese along with minor amounts of aluminum, iron, magnesium and zinc, as well as trace amounts of silver, calcium, chromium, copper, sodium, lead and silicon. Any of the above mentioned elements could have been responsible for the pitting, not to mention the infinite number of possibilities for synergistic effects.

The use of pure (4-9's) zinc cathodes did not eliminate the pitting and in addition the zinc had a tendency to dissolve at the solution line. If anything, a new solution seemed to "go bad" quicker with zinc cathodes than with aluminum.

It appears evident from the above that aluminum per se, in amounts that might normally be expected in the electrolyte, due to the use of aluminum cathodes, has no effect on the cathode deposit at least as far as contributing to the pitting or holes. However, the possibility

still exists that the aluminum might be causing the pitting due to some reaction at the cathode that cannot be duplicated by the direct addition of aluminum to the cell.

Two attempts were made to deposit zinc on titanium cathodes at 100 asf. The zinc quickly covered the cathode surface, but almost immediately began to go back into solution accompanied by evolution of large amounts of hydrogen. It would appear that the hydrogen overvoltage on titanium is too low to cathodically deposit zinc from zinc sulfate solutions. Or possibly, the titanium that dissolves from the cathode, co-deposits with the zinc, causing dissolution of the deposit due to the action of local cells. Perhaps special treatments of the surface of the titanium, prior to electrolysis, such as chemical etching, might be beneficial in making the titanium suitable for use as cathode material for zinc electrowinning.

Pure platinum foil was substituted for the platanodes to investigate the possibility that some titanium from the anodes might be the cause of pitting in the zinc deposits. The first run was made with only one anode at 40 asf for four hours. The aluminum cathode was completely covered with zinc, on the side away from the single anode, by a deposit of approximately one-third of the total weight, indicating the solution had good throwing power. A second platinum foil anode was obtained and a series of runs was made and compared to runs made under the same

conditions with platanodes. The deposits were comparable in every respect and it was decided to use platanodes for the remainder of this work due to their better structural properties and ease of handling as compared to the platinum foil.

Because of an error in calculations, the solution prepared for the first series of experiments had only 160 gpl H_2SO_4 and it was necessary to build up acid in the cell to adjust the concentration to the desired 200 gpl H_2SO_4, 65 gpl Zn. It was noted that deposits made in this solution were more flashy and crystalline in appearance, albeit, the current efficiencies were equal, to deposits made under comparable conditions in 200 gpl H_2SO_4, 65 gpl Zn solution.

It was decided to use the above method of solution preparation of partially mixing and building up acid for the remainder of these investigations. Building up 40 gpl acid in the cell served two purposes. It produced a more uniform and crystalline deposit, but most important, it served as a conditioning period for the cathode which was necessary for reasons to be explained later.

4. Current Density and Temperature. At this point all of the procedures used during zinc deposition were unvarying, except for the treatment of the cathode after the zinc deposit was stripped away. In an attempt to stabilize this last variable, prior to the current density-temperature investigations, various methods of preparing

the cathode surface for electrolysis were attempted, such as sanding, soaking in distilled water, dipping in NaOH or cell solution, etc. Evaluation was made and the best method chosen on the basis of constancy and reproducibility of results.

The effects of current density and temperature on current efficiency and deposit morphology at 0°C to 50°C were investigated by making a series of runs from 10 asf to 200 asf for 2, 4, 8, 12 and 24 hours at each selected current density and temperature.

Representative sections of the surfaces of the deposits produced with the above variables were examined by x-ray diffraction to determine crystal orientation.

The electrolyte was prepared by mixing and partially building up acid as outlined before. A pure (4-9's) aluminum cathode was used with two platinum coated titanium anodes.

The cathode and anode potentials at various current densities and temperatures were measured by techniques described previously and are included in Figures 7 and 8.

It was obvious at the beginning of the current density studies that treatment of the cathode between experiments had considerable effect on deposit morphology. At first, the cathode was sanded between each run for the sake of uniformity but the deposits began to pit far sooner than could be expected for a new solution. Also,

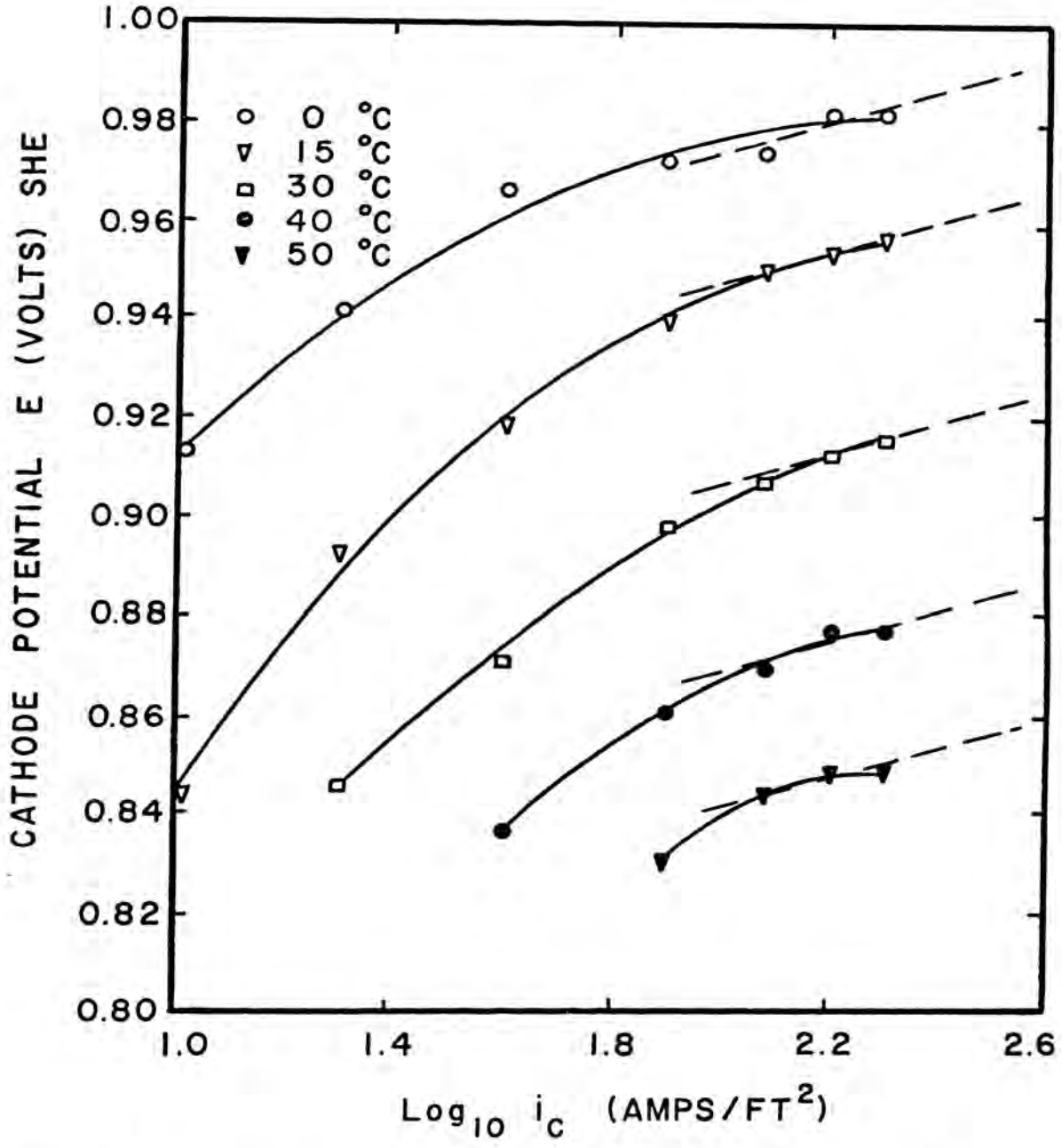

FIGURE 7. CATHODE POTENTIALS AT VARIOUS CURRENT DENSITIES AND TEMPERATURES.

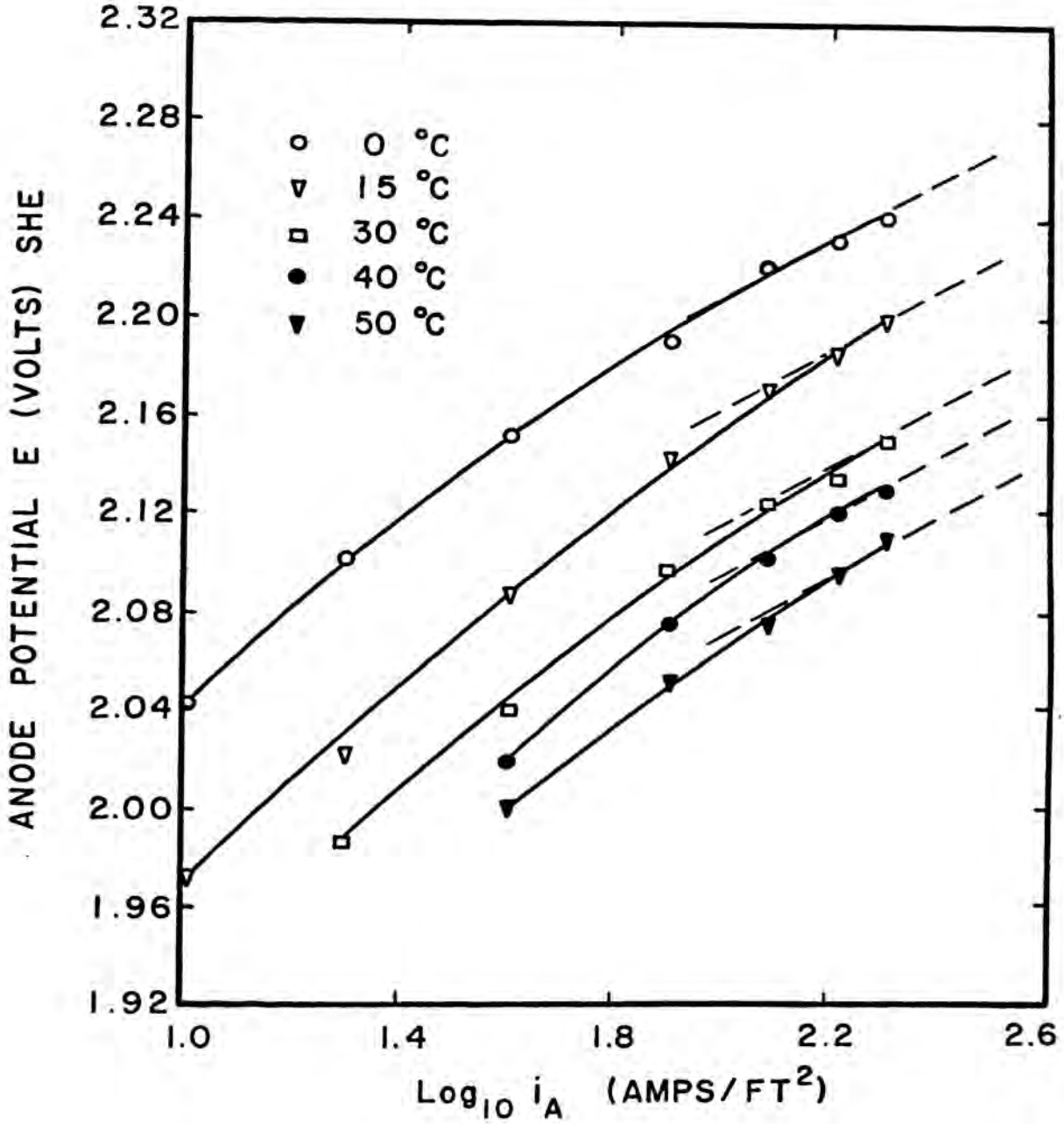

FIGURE 8. ANODE POTENTIALS AT VARIOUS CURRENT DENSITIES AND TEMPERATURES.

dipping the cathode in NaOH or cell solution prior to a run usually resulted in a pitted deposit. The most striking example of the effects of cathode pretreatment were produced by soaking a cathode in distilled water for 24 hours, followed by a 15 minute dip in cell solution. The deposit produced at 40°C and 40 asf was pitted and would not adhere to the cathode and the current efficiency was only 62% instead of the normal 95%.

A new aluminum cathode that had been prepared for electrolysis by sanding with 600 grit emery paper exhibited a uniform gray color after the first zinc deposit had been made and stripped off. An electron microprobe scan of the cathode surface revealed spots of zinc uniformly distributed on the aluminum. As soon as this surface layer was removed or altered, either mechanically or chemically, the deposit would usually show some degree of pitting.

Ultimately, the best procedure seemed to be to sand the surface of the aluminum cathode with 600 grit emery paper, wash, dry, build up acid and strip the deposit, leaving the smooth, gray zinc-aluminum surface. Then all runs were made at a particular current density and temperature without any further treatment of the cathode, except to strip, wash and dry between deposits.

a. Bath temperature 40°C. The first series of current density experiments was made at 40°C for various times at 40, 60, 80, 100 and 200 asf. Attempts to make

deposits at 10, 20 and 30 asf were unsuccessful. The zinc would deposit and then go back into solution with time until eventually only hydrogen was evolved at the cathode.

The deposits produced were very good, being flashy and crystalline in appearance and the current efficiency for each, regardless of current density and time, was relatively constant at 95% (Figure 9). Photos of a typical set of deposits (80 asf) are included in Figure 10, along with the corresponding scanning electron micrographs. The structure is representative of many of the zinc deposits made at 40°C during the course of these investigations, and consisted of stacks of hexagonal zinc crystals predominantly oriented with the basal plan (002) parallel to the surface of the cathode.

b. Bath temperature 0°C. Contrasting to the uniformity of the deposits made at 40°C and various current densities, the deposits made at 0°C varied markedly in several ways. One of the most notable results of deposition at this reduced temperature was the ability to make deposits at a current density as low as 10 asf without any loss of efficiency with time. Also, the microsctructure and the apparent orientation of the zinc crystals were different at different current densities.

The deposits made at the lower current densities (10 and 20 asf) were bright, flashy and crystalline as before, while those made at 80 and 200 asf were dull gray

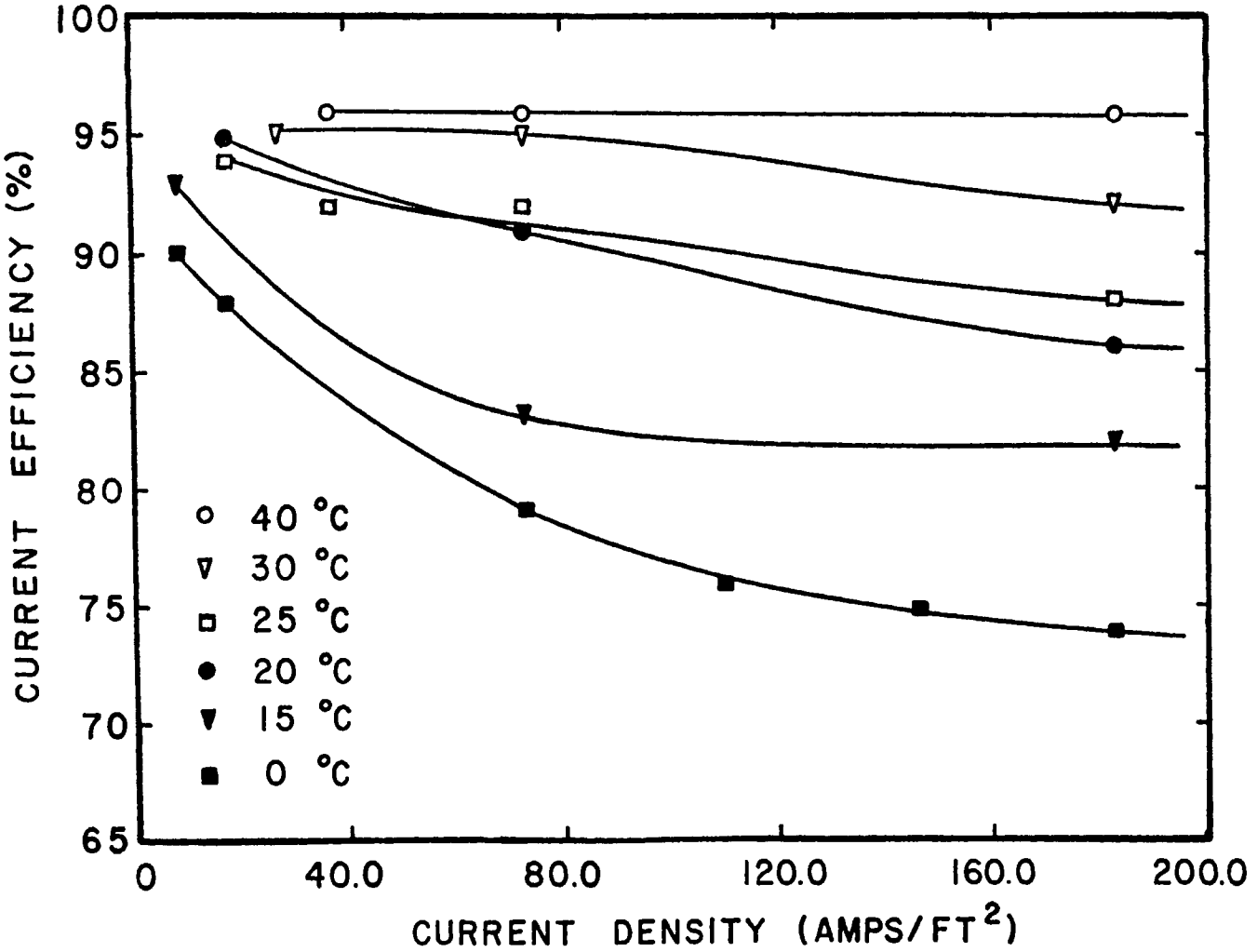

FIGURE 9. THE EFFECT OF TEMPERATURE AND CURRENT DENSITY ON TIME INDEPENDENT CURRENT EFFICIENCY.

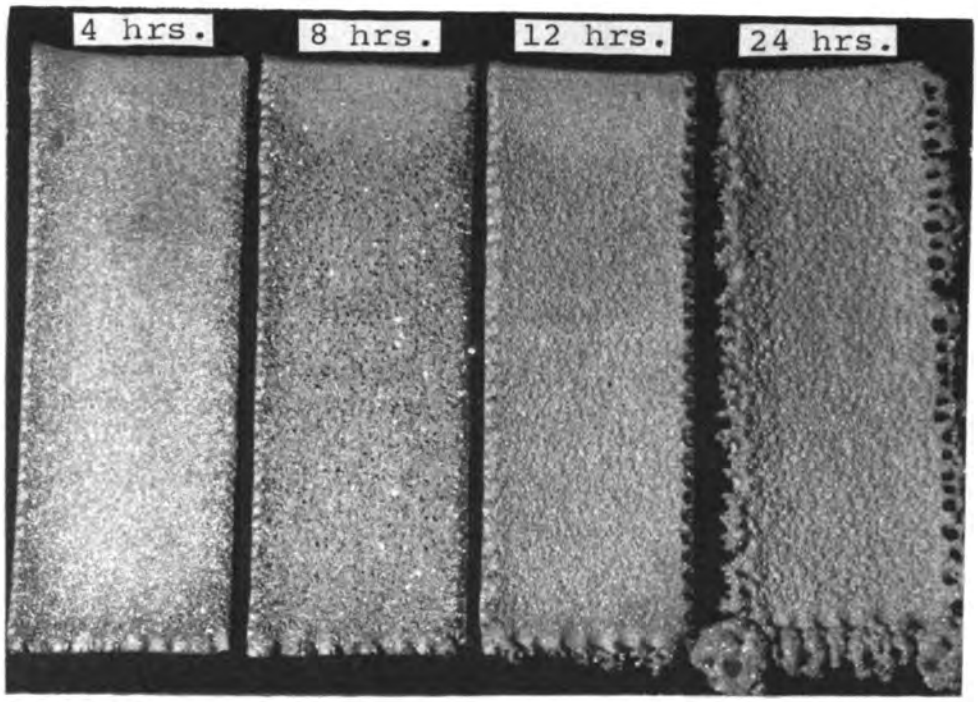

80 asf 0.89X

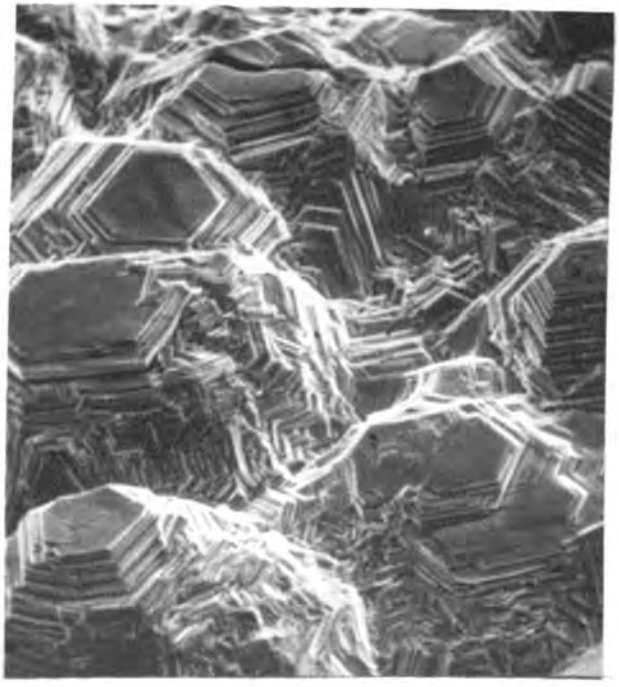

4 hr. deposit 300X

FIGURE 10. TYPICAL DEPOSITS (upper) PRODUCED AT 40°C AND 80 asf AND THE SCANNING ELECTRON MICROGRAPH OF THE STRUCTURE (lower) REPRESENTATIVE OF EACH.

in color and appeared to be extremely fine grained (Figure 11).

One 6 hour deposit at 80 asf exhibited a mixed structure, being very bright and crystalline in the center at the points of lowest current density and very smooth and gray on the edges and the bottom at the points of highest current density.

Photographs of the structures obtained on the SEM were quite different than those made at 40°C. The predominant morphology of the 10 asf deposits consisted of very thin, elongated hexagonal crystallites of different orientation which when extended laterally by growth intersected at approximately right angles. The orientation, as determined by x-ray diffraction, was equally mixed (101), (102) and (103). The structure of the dull gray material produced at 80 and 200 asf was fiberous and irregular in appearance due to only the very thin edge of the crystals being exposed, as the basal plane is in many cases almost perpendicular to the substrate. The principal orientation of the dull gray deposits tends toward (101) and (110).

The current efficiency dropped off quite rapdily with current density although the efficiency was relatively constant with time at a particular current density. Current efficiency varied from a high of approximately 90% at 10 asf to a low of 74% at 200 asf (Figure 9). Mechanical

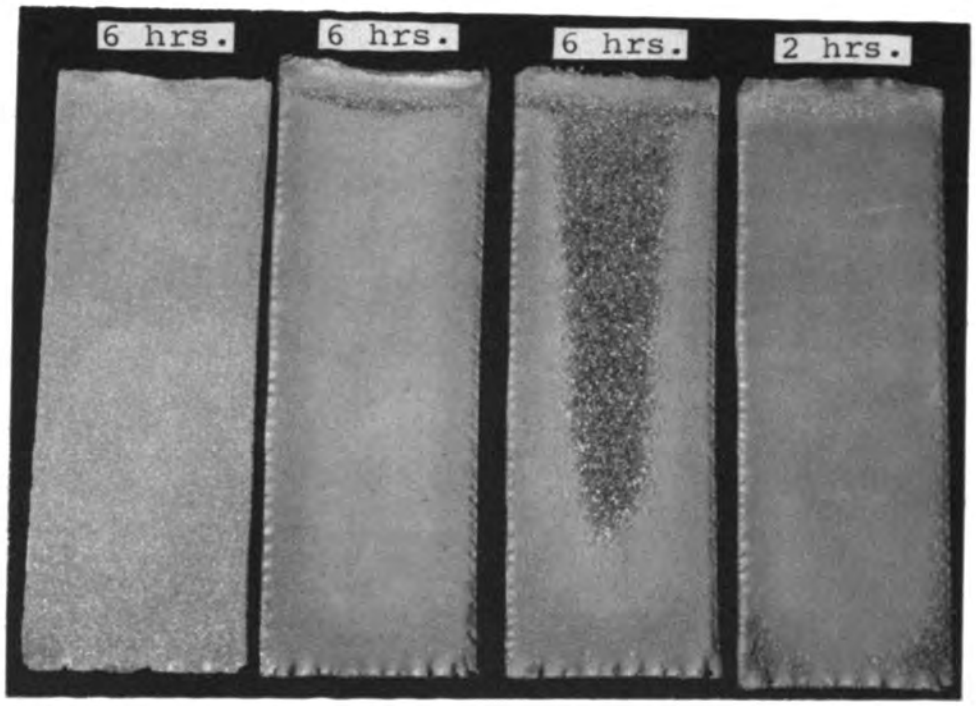

10 asf 80 asf 80 asf 200 asf

0.89X

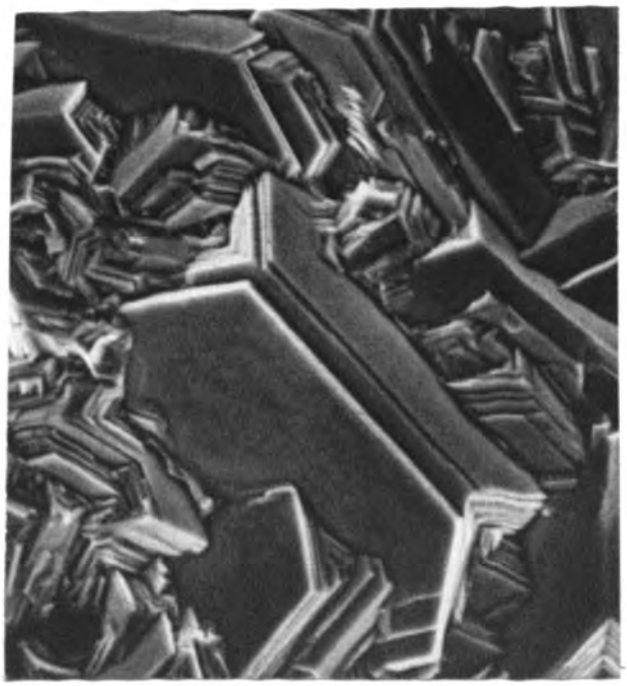

10 asf 1000X

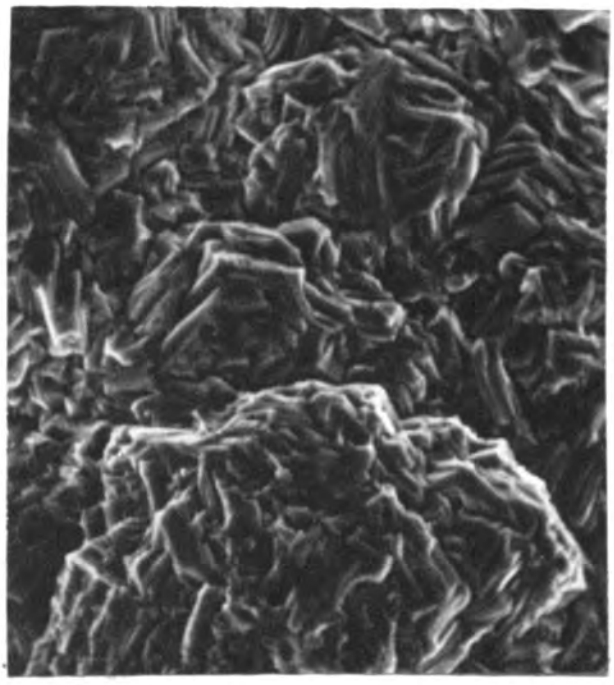

80 asf 1000X

FIGURE 11. DEPOSITS (upper) PRODUCED AT 0°C AT VARIOUS CURRENT DENSITIES AND THE SCANNING ELECTRON MICROGRAPHS (lower) OF REPRESENTATIVE STRUCTURES.

stirring of the solution had little, if any, effect on current efficiency which appears to rule out concentration polarization as a contributing factor to the decreased zinc yield.

c. Bath temperature 15°C. Runs made at 15°C were similar to the runs made at 0°C. The macrostructure was the same except the 80 asf deposits were now all flashy and crystalline in appearance instead of dull gray. The SEM photo of the 10 asf deposit was similar to the one for 0°C except the angular structure formed by intersecting basal planes of different crystals had almost disappeared (Figure 12). Likewise, the 80 asf deposit was also changed, as the fiberous structure produced by the prominence of the thin plate edges was replaced by stacks of more symmetrical hexagonal crystals inclined at a somewhat lesser angle to the cathode surface. However, the 200 asf deposit retained the fiberous nature of the 0°C deposit. The predominant orientation of all deposits produced at 15°C was basically (101) with some strong indications of (102) and (103) orientations at the higher current densities.

The current efficiency followed the same general range as the 0° deposits, only somewhat higher at all current densities, being approximately 93% at 10 asf and gradually decreasing to 82% at 200 asf (see Figure 9).

d. Bath temperature 20°C. The deposits at 20°C were the same in outward appearance as those produced at

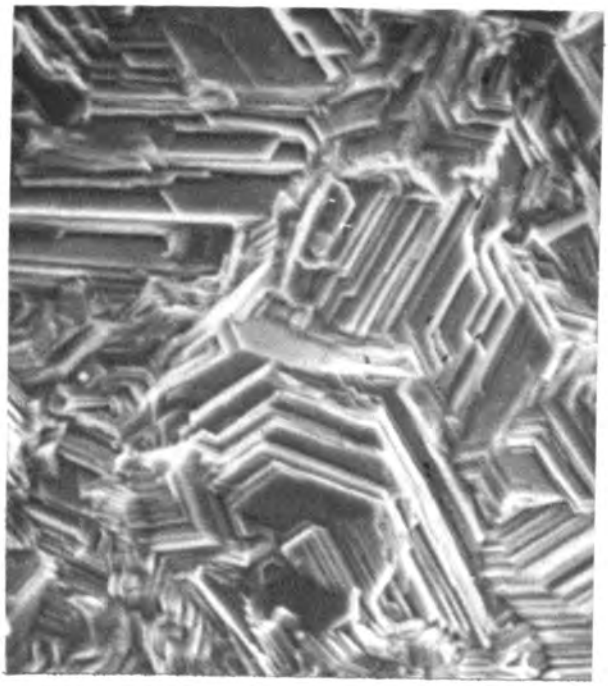

10 asf 1000X

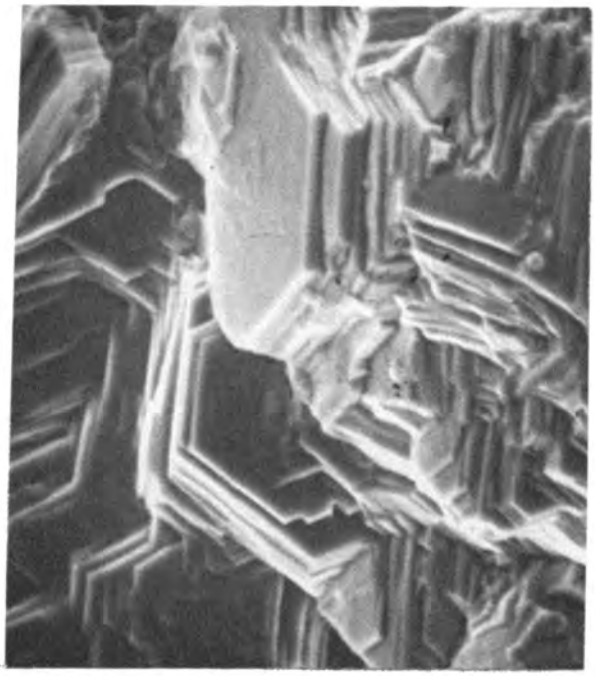

80 asf 1000X

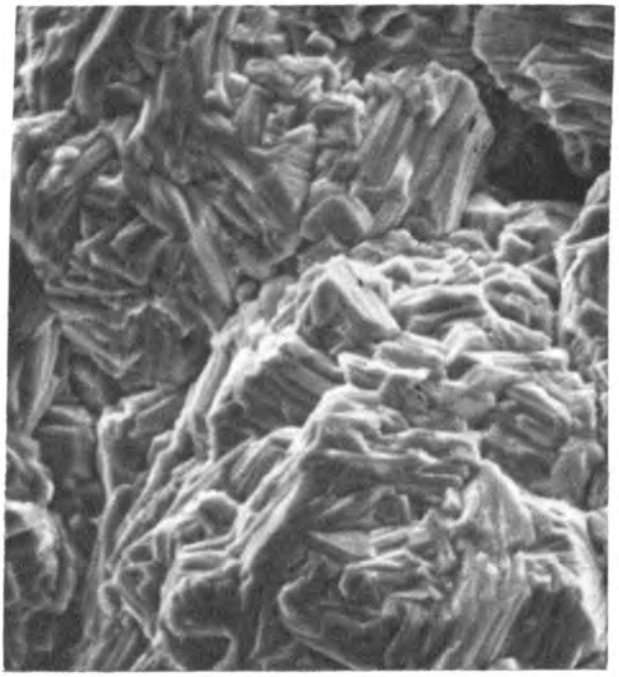

200 asf 1000X

FIGURE 12. SCANNING ELECTRON MICROGRAPHS OF DEPOSITS PRODUCED AT 15°C AND AT VARIOUS CURRENT DENSITIES.

15°C, except the 200 asf runs were now making the transition from gray to flashy and crystalline, having the former appearance on the edges and bottom and the latter in the center. The structure of the low current density deposits began to show more hexagonal platelets with the basal plane parallel to the cathode surface. The visual observation was confirmed by the strong (002) orientation revealed by x-ray diffraction. The structures of the 80 and 200 asf deposits were quite similar and appeared to be the same as the 80 asf deposit produced at 15°C (Figure 12). The crystals still maintained a strong (101) orientation at the elevated current densities.

More important, 20°C seemed to be the limiting temperature for 10 asf deposits, as the current efficiency dropped off markedly with time, reaching a low of 61% after 12 hours (Figure 13).

The current efficiency showed the same inverse relationship to current density as above even though the particular values were greater at the individual current densities investigated.

e. Bath temperature 25°C. The deposits made at this temperature were almost completely flashy and crystalline. Both the 80 asf and 200 asf deposits displayed the familiar microstructure of stacks of hexagonal platelets which were inclined at an angle to the substrate, similar to the 80 asf deposit produced at 15°C (Figure 12).

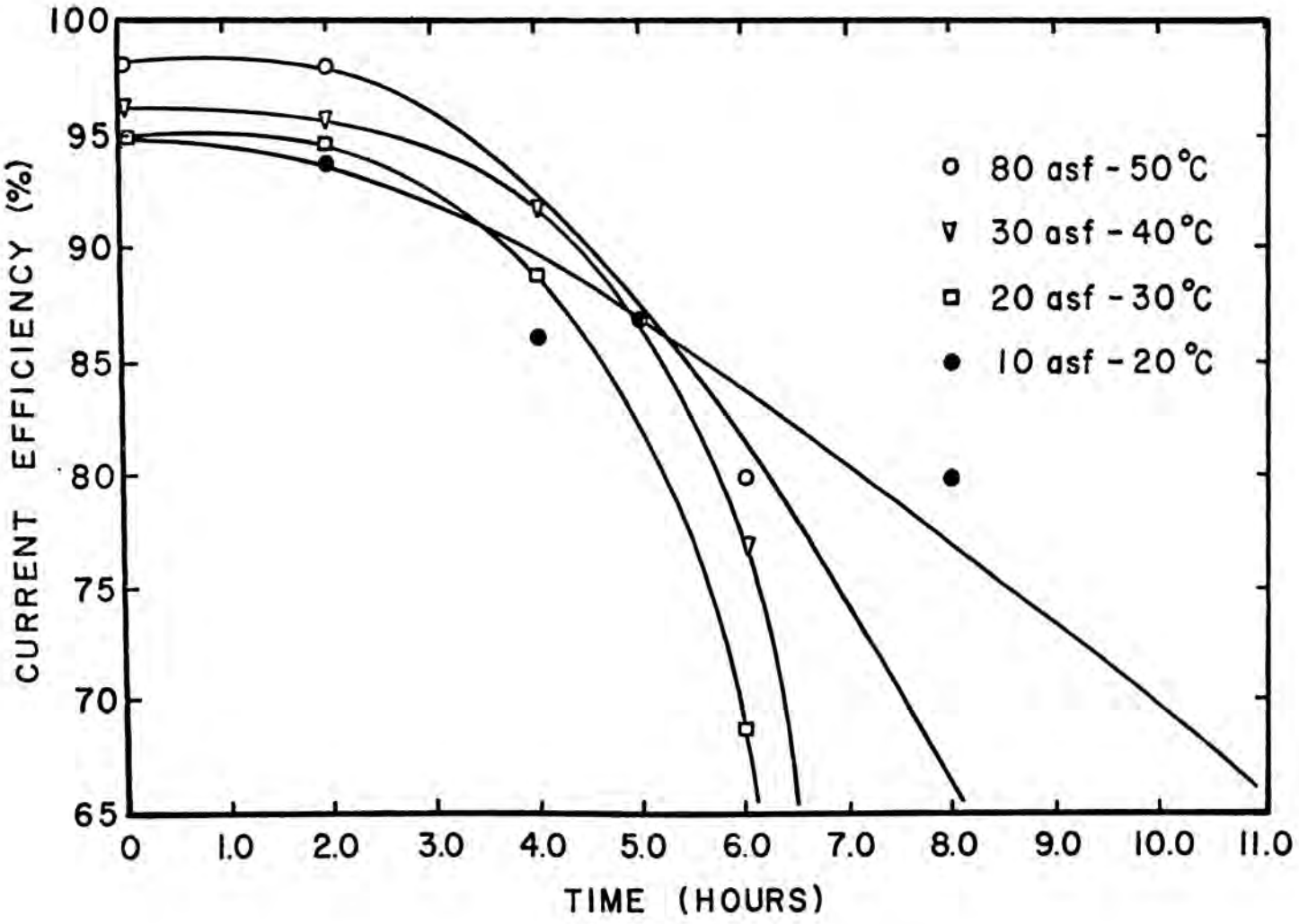

FIGURE 13. THE EFFECT OF TEMPERATURE AND CURRENT DENSITY ON TIME DEPENDENT CURRENT EFFICIENCY.

However, the crystallite size of the 80 asf deposit produced at 25°C was approximately three times larger than the crystallite size of the 80 asf deposit produced at 15°C. The orientation was still primarily (101) at the higher current densities.

It was no longer possible to make a lengthy deposit at 10 asf due to resolution. Deposits made at 20 asf were all good, but the 24 hour deposit exhibited a slight decrease in current efficiency (95% to 92%) indicating the beginning of resolution.

f. Bath temperature 30°C. With an increase to 30°C, resolution was now just beginning after 24 hours at 30 asf as indicated by a reduction in current efficiency from 95% to 93% and a dark black area at the top of the cathode.

The deposits were almost identical in outward appearance to those produced at 40°C (Figure 10).

The low current density deposits were exclusively (002) orientated, while the 80 asf and 200 asf deposits still showed a primary orientation in the (101) direction.

Contrasted to the conditions at 40°C where pitting of the deposits occurred after the total time of electrolysis in a new solution exceeded 24 to 30 hours, the solutions used at 30°C and below could be run indefinitely without any apparent deterioration in the quality of the cathode deposits, providing the current density was above

the critical current density for resolution. However, for the sake of uniformity a new solution was used for each temperature investigated.

g. Bath temperature 45°C. At this temperature the critical current density for the loss of efficiency was 40 asf. After two hours resolution had already begun although the current efficiency was relatively high (92%). After four hours the structure of the deposit was pitted and resolution had progressed to the point that current efficiency was only 71%.

h. Bath temperature 50°C. The most drastic change in deposit morphology resulted when the temperature was increased to 50°C. A two hour deposit at 80 asf in a new solution was very good, flashy and crystalline in appearance and the current efficiency was exceptionally high at 98%. However, after four more hours, pitting began to occur at the top of the deposit and with an additional six hours the entire surface was covered with pits (Figure 14) concentrated mostly in areas of high current density. Also, the black hemispherical discoloration, so commonly an indicator of resolution, began to appear across the top of the deposit. An additional six hour deposit was pitted badly and resolution was extensive as the current efficiency was reduced to 80%. A drop in the electrolyte temperature to 35°C gave a beautiful, flashy crystalline deposit (Figure 14) with no evidence of pitting

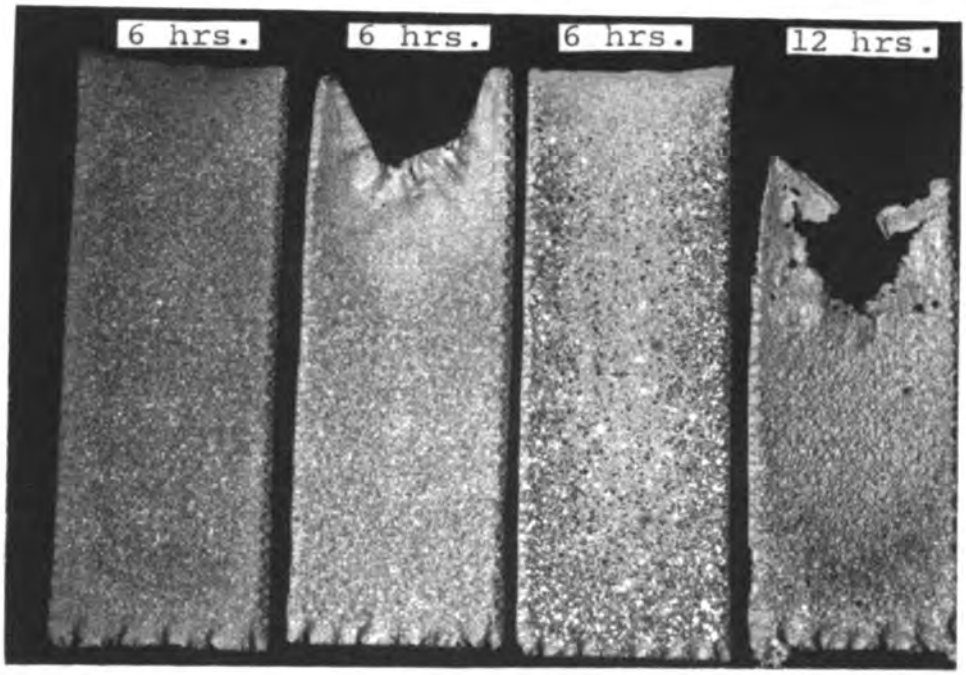

50°C 50°C 35°C 50°C

0.89X

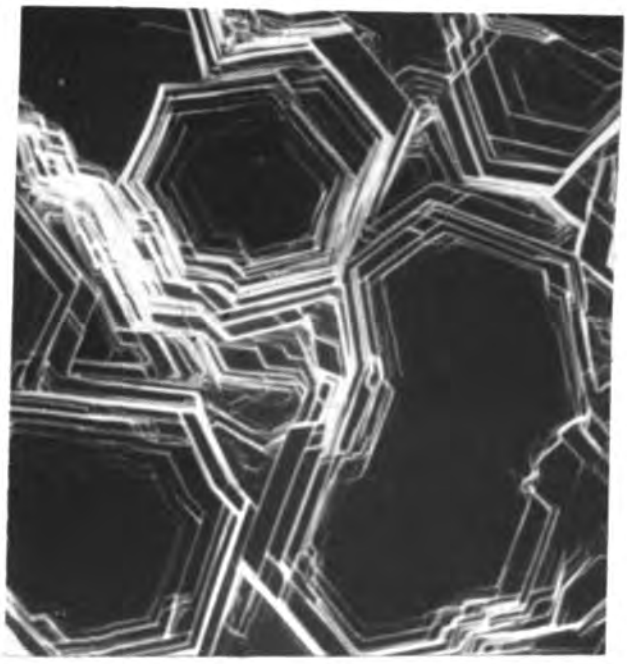

80 asf 300X

FIGURE 14. DEPOSITS (upper) PRODUCED AT 50°C AND 35°C BOTH AT 80 asf SHOWING THE EFFECT OF TIME AND TEMPERATURE. SCANNING ELECTRON MICROGRAPH (lower) IS OF A 50°C DEPOSIT.

or resolution after six hours at 80 asf. The solution temperature was again raised to 50°C and a 12 hour run was made at 80 asf. Resolution and pitting was almost catastrophic and only 35% of the deposit remained at the end of 12 hours.

5. Resolution. Current efficiency was constant with time at each particular current density and temperature investigated, except where resolution of the deposit occurred. At 0°C it was possible to make lengthy deposits at current densities as low as 10 asf, but as temperature increased, higher and higher current densities were required to avoid resolution and the accompanying loss in current efficiencies until, as can be seen in Figure 13, 80 asf was not sufficient to avoid cathode decomposition at 50°C.

During decomposition, zinc would deposit on the cathode by first covering the edges and bottom at the areas of high current density and then the remaining vee shaped area in the center would fill in.

Resolution occurred in reverse to deposition and first appeared as a black, crescent shapped area at the top of the cathode. As resolution progressed, it was accompanied by evolution of hydrogen which increased in inverse proportion to the amount of zinc deposited until no zinc remained on the aluminum cathode and only hydrogen was evolved.

During one run at 10 asf and 25°C that had almost completely redissolved, the current was turned off for a few seconds and the deposit was removed from the electrolyte to check the progress of resolution. The deposit was then quickly reimmersed, the current turned back on and zinc immediately redeposited over the whole surface of the cathode.

This initiated a series of experiments of current interruption for short times which was completely unsuccessful in retarding or reversing the progress of resolution.

In another experiment it was noted that if the cathode was tapped during the course of resolution, zinc redeposited at the top, on the bare aluminum, just below the solution line. As soon as tapping ceased, the very fine deposit of zinc redissolved.

An attempt was made then to make a deposit under resolution conditions using a mechanical vibrator to agitate the cell during deposition. Mechanical vibration only served to accelerate the process of resolution.

Two deposits that were made at 10 asf and 20°C that had low current efficiency (80%, Figure 15 and 61%, Figure 16) due to resolution were closely examined at high magnification using the scanning electron microscope. The representative structure of the deposits from the center of the cathodes was composed of a great deal of basal planes with (002) orientation (Figure 15, top lt.), but

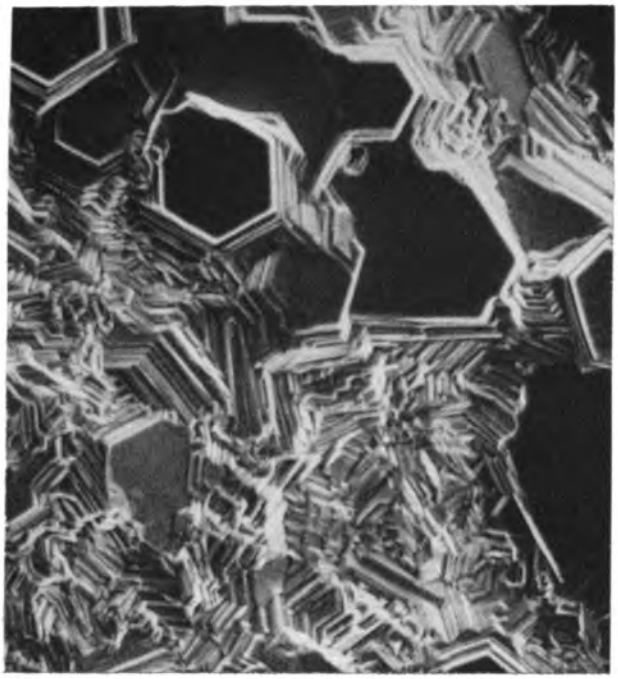

10 asf 500X
(unaffected area-middle)

10 asf 500X
(resolution area-top)

10 asf 500X
(demarcation zone)

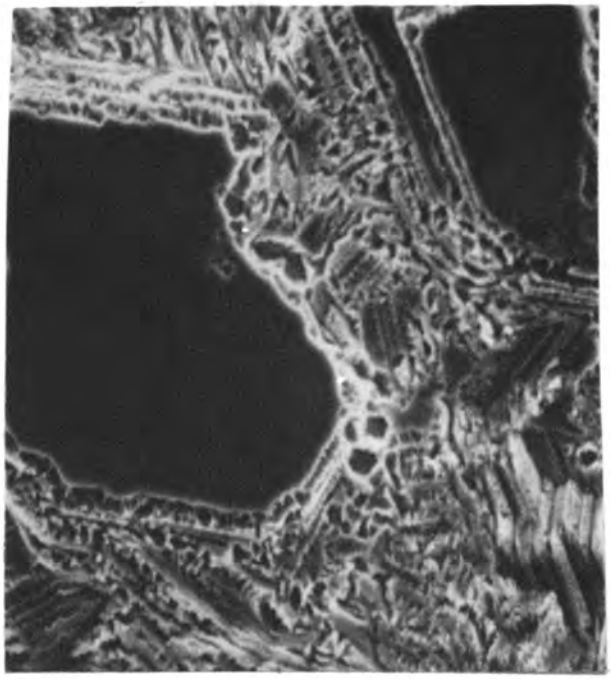

10 asf 1000X
(dipped in cell solution)

FIGURE 15. SCANNING ELECTRON MICROGRAPHS OF A DEPOSIT PRODUCED AT 20°C WITH 80% CURRENT EFFICIENCY.

10 asf 1000X
(resolution area-top)

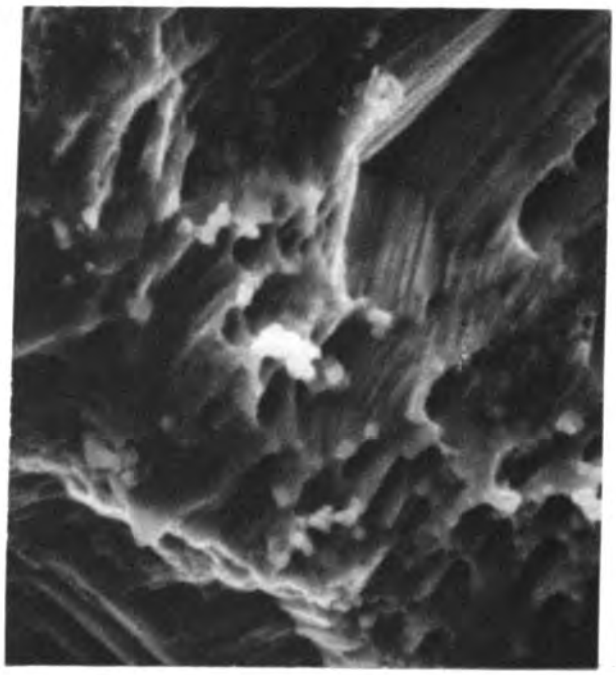

10 asf 3000X
(same area as at left)

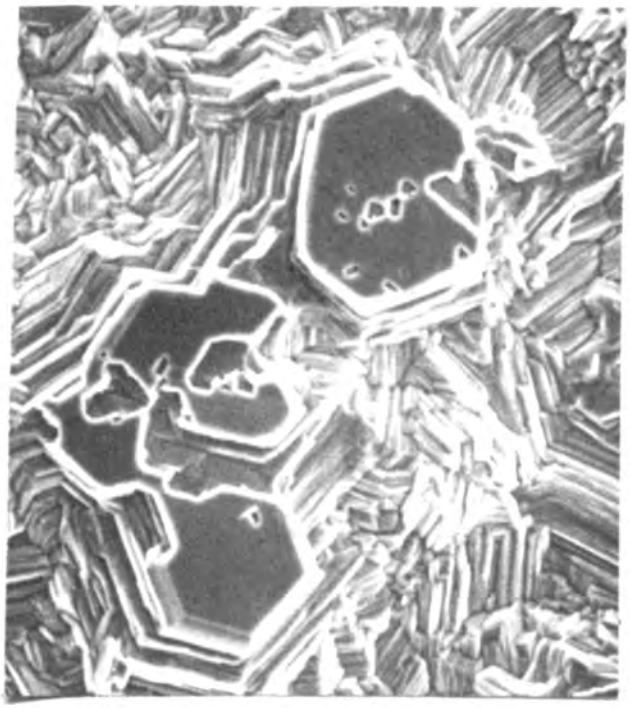

10 asf 600X
(demarcation zone)

10 asf 1800X
(same area as at left)

FIGURE 16. SCANNING ELECTRON MICROGRAPHS OF A DEPOSIT PRODUCED AT 20°C WITH 61% CURRENT EFFICIENCY.

there were no basal planes visible in the resolution area at the top of the cathodes. In addition to the difference in morphology, the surface of the deposits in the resolution area contained small foreign particles of approximately 2 to 4 micron size scattered throughout (Figure 15, top rt. and Figure 16, top).

Specimens taken at the demarcation line at the beginning of the resolution area show basal planes after various stages of dissolution (Figure 15, bottom lt. and Figure 16, bottom).

A piece of the cathode which was representative of the deposit outside the resolution area was allowed to corrode in cell solution for five minutes and then compared to the above. The attack appeared to be similar to that which took place during resolution, but the severity was greater (Figure 15, bottom rt.).

Cathodes that were produced at low temperatures (0°C and 15°C) with low current efficiency (∿80%), but in which current efficiency was independent of time, were examined for evidence of resolution. The upper part of the cathode, except for a diminution in crystallite size, appeared to maintain the same general structure of the part taken from a "good" area. There was no evidence of resolution or foreign particles on the surface of the zinc deposit at the top of the cathode in an area where resolution would have normally occurred (Figure 17).

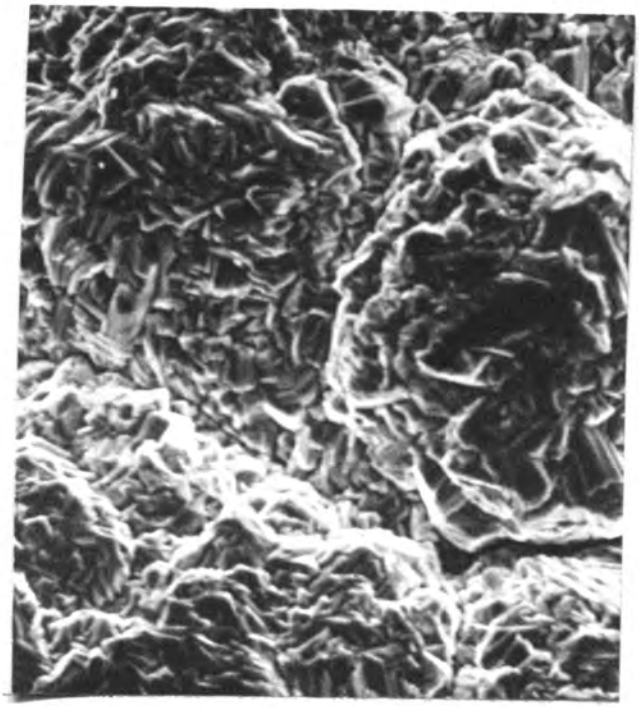

80 asf 0°C 500X
(middle)

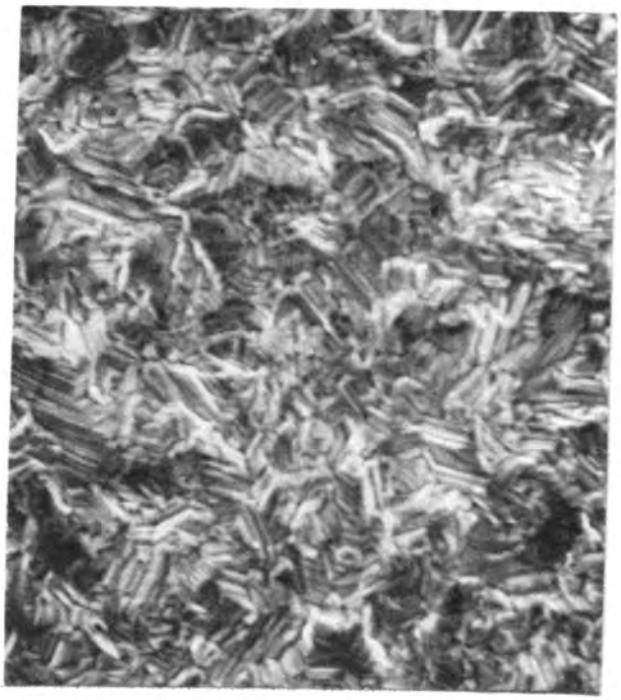

80 asf 0°C 500X
(top)

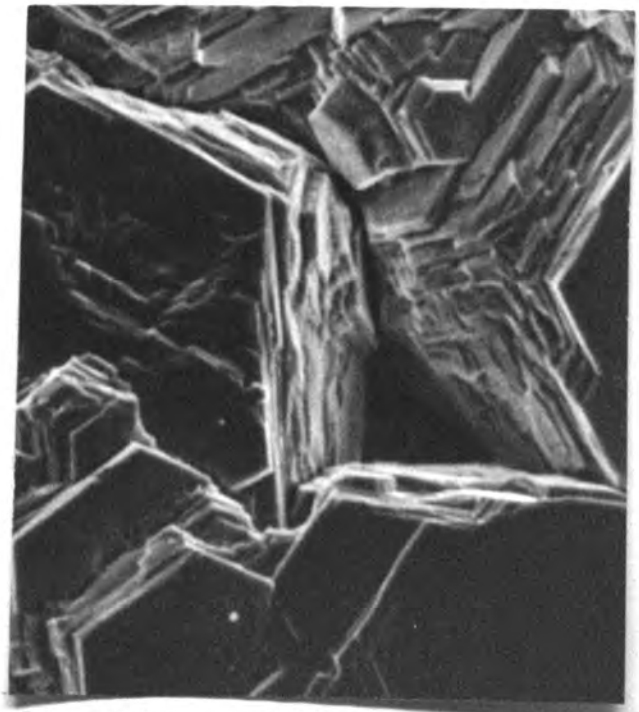

80 asf 15°C 500X
(middle)

80 asf 15°C 500X
(top)

FIGURE 17. SCANNING ELECTRON MICROGRAPHS OF DEPOSITS PRODUCED AT LOW TEMPERATURES WITH LOW CURRENT EFFICIENCIES.

The above would seem to indicate that resolution does not contribute to the lower current efficiencies at low temperatures where the current efficiency is independent of time.

The logical explanation for resolution, in light of the available data from the above work and from the work of others[11,17] is that impurities are responsible. Low overvoltage impurities depositing with the zinc on the cathode would have a two fold effect in that they would tend to lower the hydrogen overvoltage for zinc deposition and at the same time induce corrosion of the zinc through the action of local cells.

At certain critical combinations of current density and temperature (10 asf - 20°C, 20 asf - 30°C, 30 asf - 40°C and 80 asf - 50°C) the corrosion rate due to the local cells becomes greater than the deposition rate and resolution results.

Because the process seemed to be a function of time, it appeared that impurities were gradually building up in the cell rather than being present in the solution initially.

Since the anodes were under strong oxidizing conditions, and platinum oxide as well as platinum appeared to be insoluble at the pH and potentials involved in zinc electrolysis (Pourbaix diagram), the platinum and platinum coated titanium anodes were considered to be inert.

Further, no trace of platinum could be found in the electrolyte, even after a hundred hours of electrolysis. However, the cathode and the anodes seemed to be the only possible sources of internal contamination of the solution. As the above work indicated, aluminum was probably not detrimental, it remained to investigate the platinum anodes.

Many years ago (1907), Senter[30] found that platinum dissolved in H_2SO_4 solutions independent of current density. More recently, Thacker[31] has shown that platinum is also unstable in alkaline solutions. The platinum, of course, if it were not inert as was originally assumed, would serve as a source of impurities, due to its ability to drastically lower the hydrogen overvoltage and also to act as a local cathode on the zinc surface.

It was decided to check the effects of platinum indirectly by substituting different anode materials. Lead-silver anodes were tried first at 10 asf and 50°C where resolution could be expected to be severe. No resolution occurred, but the deposit had a very irregular, waffle type structure, which was probably due to lead from the anode that co-deposited with the zinc.

A pair of graphite anodes was tried next at 10 asf and 30°C and the deposit was good, uniform and crystalline and the current efficiency was 86% after nine hours. With platinum anodes it was impossible to get enough zinc

deposited at this current density and temperature to strip due to the rapidity with which resolution occurred. When the temperature was increased to 50°C and the current density to 80 asf, the anodes disintegrated and a great deal of graphite was deposited with the zinc resulting in a remarkably brittle deposit and a very unusual microstructure (Figure 18).

A new cell solution was prepared and a pair of vitreous carbon anodes was also tried at 10 asf and 30°C. Bubbles could be seen clinging to the surface of the cathode and the run was shut down after nine hours. Some small black pieces of the vitreous carbon were in the bottom of the cell and it appeared that the anodes were disintegrating.

Current efficiency was low (78%) which was probably due to resolution caused by impurities in the vitreous carbon binder depositing with the zinc and resulting in local cell action. In addition, the orientation of the deposit was primarily (101) and (100) which might also indicate adsorption of graphite, and this could contribute to the lower zinc yield.

A second run was made at higher current density (80 asf) and the anodes completely disintegrated after four hours. However, current efficiency of the deposit was 90% with a major crystal orientation of (101).

Photographs of two different areas of the same

80 asf 1000X

10 asf 1000X

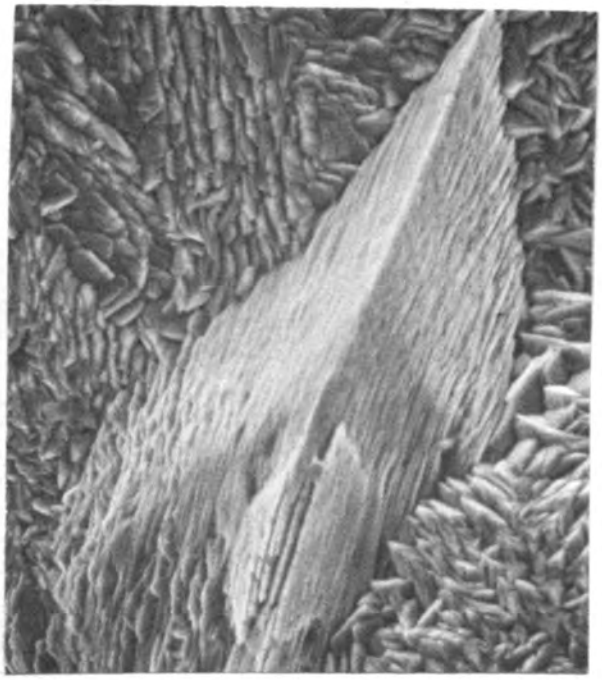

10 asf 300X

FIGURE 18. SCANNING ELECTRON MICROGRAPHS OF A DEPOSIT PRODUCED AT 50°C WITH GRAPHITE ANODES (upper) AND DEPOSITS PRODUCED AT 30°C WITH VITREOUS CARBON ANODES (lower).

deposit are included in Figure 18, partly for the unusual character, but also because they show the remarkable effect of carbon on orientation and structure of zinc deposits. Although the above results were not completely conclusive, it was indicated that platinum was contributing to resolution.

Near the end of this work an Ortec non-dispersive x-ray analysis system was added to the SEM. This system was utilized to investigate the foreign deposits seen on the zinc surface in the resolution area at the top of the cathode. An x-ray spectrum was obtained on the base metal (zinc) and also on the small, white, ~3.5μ salt like particle that can be seen in the center of the upper right photograph in Figure 16. Three extraneous peaks were identified (left to right) as aluminum, platinum and chlorine (Figure 19). This analysis was the first direct evidence that platinum was present in the solution and on the zinc deposit, although there was a great deal of indirect evidence to support this view.

Previously, the microprobe had been used in an attempt to detect platinum, but without success. On the strength of the above results, the same specimen was examined on the microprobe and again no platinum was detected on an element scan. The detector was then set for platinum and moved slowly over the surface. Platinum was found to be present in finely divided form throughout the resolution

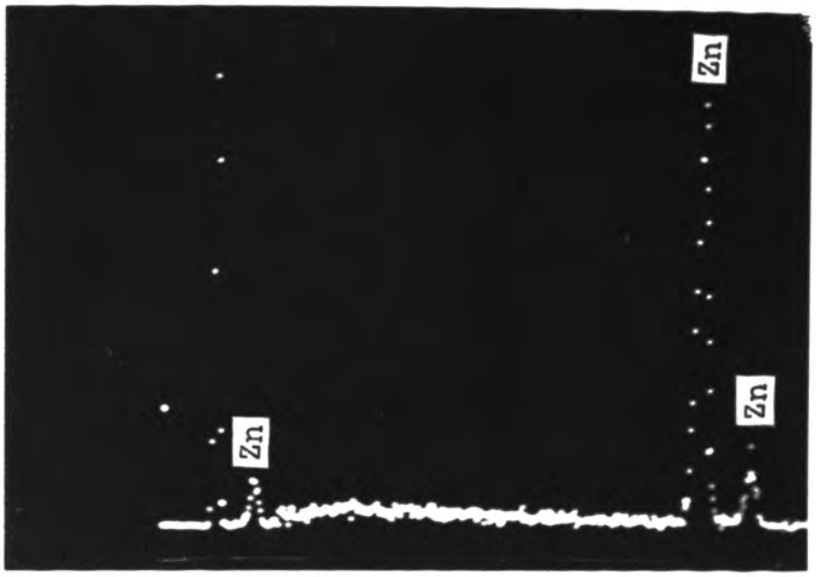

substrate

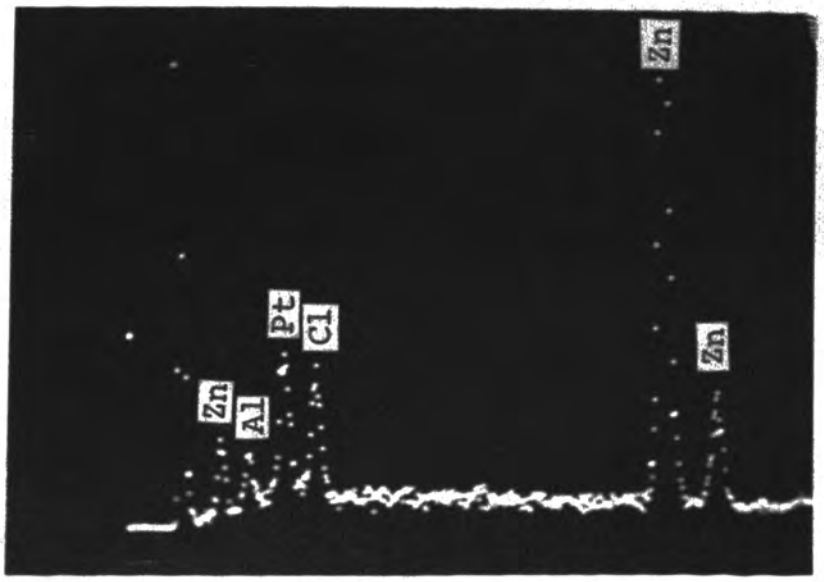

particle located on substrate

FIGURE 19. X-RAY SPECTRUM OBTAINED FROM SUBSTRATE AND FOREIGN PARTICLE IN RESOLUTION AREA.

area. The presence of chlorine was also confirmed and one can speculate that the platinum might have reached the cathode as a platinum-chlorine compound. Also, that chlorine might have contributed to the dissolution of the platinum anodes. Aluminum was not found during the microprobe examination and it appears that the presence of aluminum in the x-ray analysis spectrum was due to scatter from the specimen holder; a problem which had been encountered on other occasions.

The upper parts of deposits that were produced at low temperatures with low current efficiency and deposits made at high temperatures with good current efficiency were also checked by the x-ray energy analysis system but no trace of platinum or any other element except zinc was found.

The weight of the above evidence strongly suggests that platinum dissolves under the conditions of zinc electrolysis, co-deposits with zinc on the cathode and results in resolution as described herein. It appears that the mechanism is one of corrosion of the deposited zinc due to a galvanic couple of zinc to platinum as illustrated schematically in Figure 20 and described below.[32]

Since the hydrogen overvoltage is almost negligible on platinum as compared to zinc, the total rate of hydrogen evolution is effectively equal to the rate of evolution on the platinum surface. The mixed potential is shifted

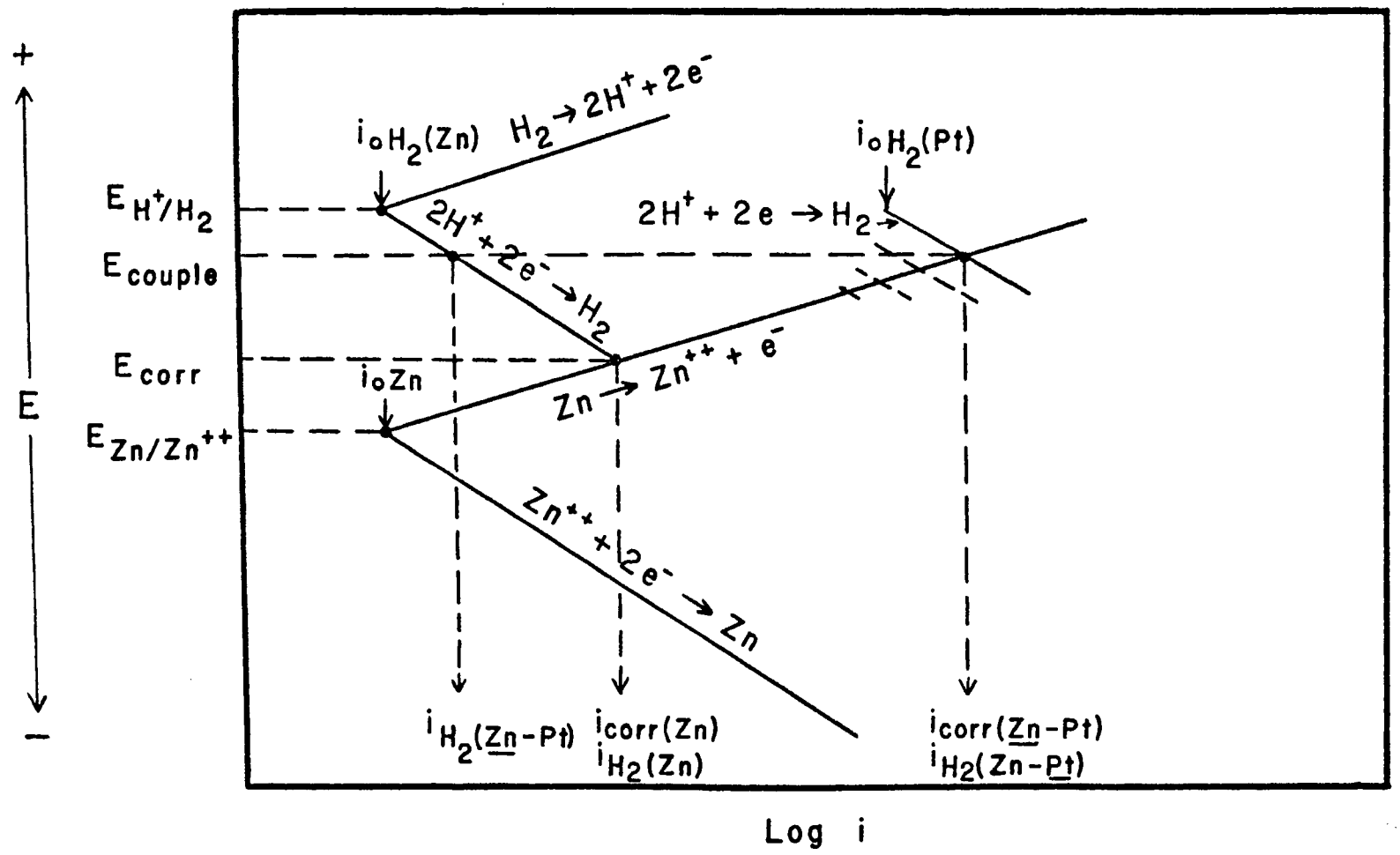

FIGURE 20. THE EFFECT OF GALVANICALLY COUPLING ZINC TO PLATINUM.

from E_{corr} to E_{couple} and the corrosion rate from $i_{corr(Zn)}$ to $i_{corr(\underline{Zn}\text{-}Pt)}$. Thus, platinum can accelerate the resolution of the zinc deposit to the point that the net reaction at the cathode is a loss of zinc.

The effect of increasing temperature is to increase the amount of platinum dissolved from the anodes and to increase the local corrosion of the cathode.

The effect of decreasing current density is to decrease the zinc deposition creating a greater imbalance between deposition and corrosion.

6. Orientation. As can be seen from the foregoing experiments, the orientation of the zinc deposits varied with the temperature and current density used for deposition. At 0°C and 10 asf the predominant orientation was equally mixed (101), (102) and (103) while at 0°C and 200 asf, it was mixed (101), (110). The tendency was for the orientation to change from mixed (101), (102), (103) to (002) at 10 asf and from (101), (110) to (101) to (002) at 200 asf with increasing temperature of the electrolyte. The orientation of the deposits produced at the intermediate current densities followed this same general trend, i.e., at 80 asf the orientation changed from (101) at 0°C to (002) at 40°C (Table I). The changes in orientation to the (002) direction were marked by corresponding increases in current efficiency.

The following attempt to correlate the morphology,

TABLE I

THE EFFECT OF TEMPERATURE AND CURRENT DENSITY ON ORIENTATION OF THE ZINC DEPOSITS*

C. D. (asf)	0°C	15°C	20°C	25°C	30°C	40°C
10	(101)-1 (102)-1 (103)-1	(101)-1	(002)-1 (101)-.3 (102)-.3 (103)-.3			
20					(002)-1	
30					(002)-1	(002)-1
80	(101)-1	(101)-1 (102)-.5 (103)-1		(101)-1		(002)-1
200	(101)-1 (110)-1		(101)-1 (102)-.5	(101)-1 (102)-.5		(002)-1 (101)-.5

*Random Orientation
(ASTM diffraction data card for zinc)

(101)-1
(002)-.5
(100)-.4
(102)-.3
(103)-.25

Note: The number after the notation for the plane represents relative intensity, i.e., (101)-1 means 100% intensity for 2θ values corresponding to the (101) plane.

orientation, current density and current efficiency is similar to the treatment of preferred orientation in nickel electro-deposits used by Reddy.[33]

There are several stages in the growth of electro-deposits. In the initial stage of growth the size, shape and orientation of the deposit crystals are influenced by the substrate. The initial stage is followed by a transition stage in which the substrate influence is gradually overcome. As deposition continues, the final stage develops and a preferred orientation of the deposit crystal can result.

In the ideal case of completely preferred orientation, the particular facets of all of the crystals are developed parallel to the substrate.

Sato[34] studied the crystal growth of electro-deposited zinc and interpreted the orientations of the flat, plate-like crystals "from the standpoint of development of crystallographic planes under various degrees of influence of hydrogen and/or organic colloids."

Whether or not a preferred orientation is produced depends on the conditions of electro-deposition, i.e., temperature, current density, etc.

Two important questions must be answered to explain the connection between deposition conditions and specific orientations developed under these conditions: a) how do the deposition conditions determine the particular type of

facets preferentially formed? b) what determines the inclination which the preferentially developed facets assume relative to the substrate?

a. Why certain facets are formed. All crystal faces do not grow at the same rate. The rate of growth of facets determines the probability of their survival. It can be proven by simple geometric arguments that fast-growing faces grow out of existence and slow-growing faces survive. The proof as first developed by Borgström[35] and later presented by Buckley[36] is given in Appendix C. For electro-deposits, the surviving faces will be those which have the greatest metallic overpotential and which therefore grow most slowly.

It is helpful to first consider free-growth of electro-deposits where free-growth is defined as deposition on a substrate-surface free of adsorbed hydrogen atoms and the adsorption of surface-active substances is excluded.

The Bravais law for free growth is adopted as the starting point. The Bravais law states that the velocity of growth of different crystal faces depends on the atomic population density (reticular density) of the faces, the greater the number of atoms per unit area of face, the lower the rate of growth in a direction normal to the face.

The velocity of growth (V_{hkl}) of a zinc crystal face and the population density P_{hkl} are as follows:[34]

$V_{(103)} > V_{(110)} > V_{(101)} > V_{(102)} > V_{(100)} > V_{(002)}$ and $P_{(002)} > P_{(100)} > P_{(102)} > P_{(101)} > P_{(110)} > P_{(103)}$. The differences in the velocity of growth are also manifestations of differences in the partial current densities on different faces. Therefore, $i_{(103)} > i_{(110)} > i_{(101)} > i_{(100)} > i_{(002)}$. Also the same results can be stated in terms of metallic overpotentials. That is, $Mn_{(002)} > Mn_{(100)} > Mn_{(102)} > Mn_{(101)} > Mn_{(110)} > Mn_{(103)}$. The above data indicate that during deposition from pure solutions and in the absence of additives (free-growth), zinc electrodeposits should tend to preferentially develop {002} basal plane facets.

Free-growth occurs only in the ideal case as some hydrogen evolution normally occurs simultaneously with zinc deposition. The formation of adsorbed hydrogen is an essential intermediate step in the evolution of hydrogen gas. The total metallic overpotential Mn_{hkl} for deposition on the face {hkl} can be considered to be the sum of two components; the free-growth contribution and the contribution due to adsorbed atomic hydrogen, i.e., $Mn_{hkl} = FGMn_{hkl} + HCMn_{hkl}$.

It seems very probable that hydrogen would influence the electro-deposition process. Bockris[37,38] and Gerischer[39] have shown that the reaction involving the transfer of the metal ion across the double-layer results in the formation of an adsorbed ion (adion) which undergoes

surface diffusion before lattice-incorporation at the crystal building site. The broadcast adsorbed hydrogen atoms can impede the surface diffusion process which is the rate-determining step at low current densities. At high current densities the transfer reaction becomes rate-determining. In this case, adsorbed hydrogen would increase the energy barrier because the transfer reaction would probably have to take place on to hydrogen which would at least partially screen the electron cloud in the metal. The reaction of adsorbed atomic hydrogen would be to increase the metallic overpotential above the free growth value. The question now arises as to whether hydrogen is adsorbed to the same extent on different facets of zinc crystals.

It has been shown[40,41] that the hydrogen overvoltage on zinc changes with orientation and is a direct function of planar packing density, i.e., $\eta_{(002)} > \eta_{(100)} \eta_{(102)} > \eta_{(101)} > \eta_{(110)} > \eta_{(103)}$.

This indicates that the greater the average interatomic spacing of adjacent zinc atoms on the lattice plane of zinc (the lower the reticular density), the more negative is the standard free energy of hydrogen adsorption, and hence, the greater the surface concentration of adsorbed hydrogen. Conditions occurring during electrodeposition that increase the amount of hydrogen evolved (lower the current efficiency) do not increase the hydrogen

adsorbed on the various crystal facets at the same rate. The maximum increase occurs on (103), and the minimum on (002). In contrast, since they are determined by crystallographic factors (and current density), the metallic overpotentials on all faces are equally affected by varying the conditions of electro-deposition. Thus, through the mechanism of hydrogen adsorption, the previously fast-growing faces can become the slowest-growing faces and will not grow out of existence.

b. <u>What determines the inclination which the preferentially developed facets assume relative to the substrate</u>? To answer this important question, it will first be necessary to consider the two main modes of growth, outward and lateral, that occur during electro-deposition.

One of the primary factors that influences the mode of growth adopted by electro-deposits is the metallic overpotential. Metals with a high metallic overpotential such as nickel, chromium, iron and cobalt[42] affect an outward growth mode. High metallic overpotentials increase the nucleation rate, the girth of the crystals is effectively reduced and consequently, acicular, needle like crystals are produced. Such crystals would be obtained when the outward velocity of growth in a direction normal to the substrate is greater than the lateral velocity in a direction parallel to the substrate. On the other hand,

metals such as zinc, copper, silver and gold with relatively low metallic overpotentials effect a lateral mode of growth. The low nucleation rate of low metallic overpotential metals results in lamellar, tabular plate-like crystals, whose lateral crystal growth velocity is greater than the velocity in a direction normal to the substrate.

The conditions of electro-deposition are largely responsible for determining which particular mode of growth is adopted by electro-deposits. In Reddy's opinion, the metallic overpotential and the non-uniformity of the deposit surface are the two factors mainly responsible for affecting the mode of growth in unadulterated baths. The metallic overpotential influences the nucleation rate and therefore affects the crystal size. The greater the nucleation rate, the less the girth of the crystals. On a non-uniform cathode surface, nonhomogeneity of the electric field exists. The field will be more intense near peaks than near recesses. Therefore, peaks will receive a greater supply of ions than recesses, giving rise to preferential deposition on peaks. The nonhomogeneity of the field is further accentuated and there is a cumulative tendency for deposition on to peaks and an outward growth is obtained.

Now, depending on the magnitude of adsorbed hydrogen, facets of a certain crystallographic type {hkl} should be

the slowest-growing facets and hence, they should be selectively formed. Further, the slowest growing of these facets would be developed, normal to the substrate if an outward mode of growth was effected. The term Wilman facets is used to describe facets which grow preferentially normal to the substrate. This hypothesis would be valid only for electro-deposits which adopt an outward mode of growth.

In attempting to explain the reasons for the preferred orientation developed by the zinc deposits produced during this work, the following must be compared:

i) the morphology of the zinc deposits as shown by the SEM photographs,

ii) the decrease in current efficiency with decreasing temperature and increasing current density (Figure 9) and,

iii) the variations in orientation with temperature and current density as described in the opening paragraph of this section and Table I.

In general, four distinct types of structures, which are delineated below, resulted from the different orientations of the zinc crystallites.

Type 1. Low temperature and low current densities produced the first type. This structure consists of asymmetrical hexagonal crystallites that have grown

together to produce what looks to be stacks of triangular shaped platelets. Approximately 60% of the facets exposed are (002) with the remainder being lesser reticular density facets of {101} or {100}. The principal orientation is equally mixed (101), (102) and (103) (Figure 11). The current efficiency of zinc deposition is approximately 90%.

Type 2. The second type is the result of low temperatures and high current densities. This structure appears to be fiberous, since only the thin edge of the hexagonal crystals are prominent. Greater than 90% of the facets exposed are of low reticular density. The primary orientation of these deposits is (101) and (110) (Figures 11 and 12 - lower). The current efficiency for zinc deposition is approximately 75%.

Type 3. The third structure is an intermediate structure between types 2 and 4, and it is produced as the temperature of deposition is increased. It consists of symmetrical hexagonal platelets which are inclined at an angle to the substrate. The faceting is approximately 30% (002) and 70% of the lesser reticular density planes. A good example of this structure can be seen in the 80 asf deposit at 15°C (Figure 12). Both the triangular and fiberous structure change to this type as the temperature of the electrolyte increases. The principal orientation is (101). The current efficiency for zinc deposition is

approximately 85%.

Type 4. This deposit morphology is the result of deposition at temperatures of 35°C or greater. It is composed of symmetrical hexagonal crystals which have grown parallel to the cathode surface to produce a strong (002) preferred orientation. The primary faceting is (002). However, a great deal of lower reticular density planes are exposed in the recesses produced by the growing pyramids (Figure 10). The current efficiency for zinc deposition is approximately 95%.

It appears from the preceding data that the tendency for (002) orientation leads to a greater exposure of (002) facets and to an increase in current efficiency.

Conversely, the greater the exposure of lesser reticular density planes, the lower the current efficiency. The maximum decrease in current efficiency is associated with a preferred orientation of (110), (101) and in this case only the thin plate edges are exposed with very little if any (002) facets showing.

X-ray diffraction patterns made from the back of every deposit indicated a strong (002) orientation, regardless of the temperature and current density used for deposition. This tendency for a (002) preferred orientation at the start of electrolysis is probably due to the influence of the aluminum substrate. When $Al_2(SO_4)_3$ was added to a zinc sulfate solution during zinc deposition, a basal plane orientation of the zinc deposit resulted.[43]

Since each deposit started with a basal plane orientation, it is obvious that changes occurring during electrolysis resulted in the growth of crystallites with a preferred orientation as outlined above.

Two possible explanations to explain the particular orientations and the resultant current efficiencies developed during zinc deposition are described below.

The first of these two theories assumes that zinc grows only by a lateral mode and the slowest growing facets grow parallel to the substrate.

It is evident from the current efficiencies listed above and from Figure 9 that more hydrogen is produced at low temperatures and high current densities. Since hydrogen adsorption is necessary for hydrogen evolution, it follows that more hydrogen is adsorbed at these low temperatures and high current densities. Further, it has been shown that the free energy for hydrogen adsorption is more negative on the less densely packed planes. Or stated another way, the hydrogen overvoltage is less on the less densely packed planes.

Considering the initial assumptions and the facts as presented above, it seems logical to assume that through the mechanism of hydrogen adsorption the lesser reticular density planes, that are initially the fastest growing and tend to grow out of existence, begin to grow more slowly and align themselves parallel to the substrate. This results in a preferred orientation of low density planes.

It must be understood that during the process of

shifting from (002) parallel to the substrate to (002) normal to the substrate, there is also probably a shift in the relative growth rates of the other planes.

This would result in a mixed morphology at intermediate temperatures and current densities. Finally when the growth was predominantly (002) the morphology should become more uniform and exhibit a preponderance of one or two specific facets. This does occur, as seen in Figures 11 and 12 - lower, where (100) seems to be the principle exposed facet.

It is seen in Table I that high current densities favor an orientation of lower reticular density planes. At low current densities, increases in temperature lead to (002) orientations much quicker than at high current densities. At 200 asf and 40°C there is still a tendency toward preferred orientation of lower density planes (Table I). This seems to be compatible with the observation that more hydrogen is produced at the higher current densities. However, the above implies that the hydrogen overvoltage decreases as current density increases which is contrary to general theory. However, the accepted theory that overpotential increases with increases in current density is valid only for random orientations. Thus, dependening on the relative overpotentials on the different faces, the amount of hydrogen evolved could possibly increase with increasedcurrent density, depending

on the orientation.

The second theory proposed to explain the results of the particular preferred orientations that result from deposition at the various current densities and temperatures requires no assumptions. However, it is implied (Figure 7) that the metallic overpotential increases as the temperature decreases and the current density increases. The increase in the metallic overpotential causes an increase in the nucleation rate. Also the growth mode of zinc is changed from lateral to outward. That is, for the two extremes, from (002) facets aligned parallel to the substrate (lateral) to (002) facets growing normal to the substrate (outward).

Once the switch to outward growth is initiated, the process is enhanced due to localizing of the electric field and an increase in zinc deposition at the crystal corners and edges.

The resulting orientation is simply due to the changes in the inclination of the zinc crystals as the growth mode is changed from outward to lateral.

The (002) faces would remain the slowest growing planes in all cases and they would simply change their preferred alignment from parallel to normal to the substrate. This behavior is exactly what is observed if one examines the SEM photographs of the four different types of morphologies as described before. The (002) facets

can be seen to change their alignment from parallel to the substrate (Figure 10 - Type 4) to normal to the substrate (Figure 12 - lower - Type 2).

Also, the apparent anomaly of the lowering of current efficiencies, at the low temperatures, with increases in current density is more readily explained. With the outward mode of growth and the (002) facets aligned normal to the substrate planes of lesser reticular density are exposed in the double layer. It was previously mentioned that the hydrogen overvoltage on a particular facet decreases as the planar packing density decreases. Hence, the lower current efficiencies are simply due to the lower hydrogen overvoltage on the exposed facets or the ratio, (i_{H2}/i_{Zn}), becomes greater.

Further evidence in support of this latter premise can be seen in Figure 18 which shows the effect of graphite on zinc deposition. Graphite apparently acts as a nucleating agent and produces acicular, needle-like crystals which is a characteristic of an outward mode of growth. The orientation of these deposits is mainly (101).

In summary, it might be said that zinc deposition occurs as follows. At normal operating conditions with temperatures of 35-40°C and a current density of 80 asf, zinc grows by a lateral mode in an unadulterated solution. The most densely packed (002) facets are aligned parallel to the substrate. The hydrogen overvoltage on the (002)

facets is greater than on any other facet and zinc deposition proceeds with relatively good current efficiencies. However, as the temperature is decreased and the current density increases, the metallic overpotential increases and the resulting increase in nucleation rate causes the growth mode to shift from lateral to outward. That is, the slow growing (002) facets change from being aligned parallel to the substrate toward orientation normal to the substrate. The orientation of the lesser reticular density facets also changes with more low density planes being exposed on the deposit surface. These lower reticular density planes having a lower hydrogen overvoltage result in less zinc being deposited and therefore, lower current efficiencies. Additives such as graphite, being good nucleating agents, cause the same effects at normal operating temperatures as they tend to shift the growth mode from lateral to outward which results in reduced current efficiencies.

B. Anode Reactions

1. H_2SO_4 Solutions. When it appeared that platinum anodes were contributing to solution contamination, attention was redirected to lead anodes and possible preconditioning treatments to produce a stable electrode for studying the zinc electrowinning process with a minimum of variables.

The work of Razina and Kiryakov[44] indicated that a PbO_2 anode was ten times more stable in H_2SO_4 solutions than an ordinary Pb-Ag anode under the same conditions.

Farmer[18] investigated the conditioning of lead-silver (1%) anodes in various solutions prior to electrolysis in Cominco's electrolytic cells and obtained good results using fluoride solutions.

It was decided to study the conditioning of lead anodes in sulfuric acid and fluoride solutions in an attempt to produce an anode that would be inert at the temperatures and current densities normally encountered in the zinc electrowinning process, i.e., 30-50°C, 50-100 asf.

The study in H_2SO_4 solutions was undertaken more as a means of establishing basic mechanisms and to serve as a comparison for subsequent investigations in fluoride solutions, than in any hope of producing a stable electrode.

Deposits were made at 0°, 30°, and 60°C for 2 and 12 hours at 10, 50, 100 and 200 asf in 1N and 4N H_2SO_4 solutions.

The electrolyte was prepared by mixing Fisher A300-C reagent grade sulfuric acid in distilled water.

Platanodes were used as cathodes for the 0°C runs and pure platinum foil was employed for the 30°C and 60°C experiments.

The lead-silver (1%) anodes were wire brushed on both sides and carefully weighed prior to electrolysis. At the end of each run the anodes were washed, blotted dry, re-weighed and x-rayed to determine the composition of the anode surface.

Using the peak of maximum intensity as an indication of the amount of each phase present on the anode, diffraction data were tabulate and are included in Table II.

Photographs of the various structures were obtained on the SEM after polarization, after depolarization and after depolarizing and repolarizing (Figures 21 and 23).

Selected 12 hour deposits at various current densities were allowed to remain in the cell after electrolysis and open circuit, decay potentials were recorded in 4N H_2SO_4 at 0°, 30° and 60°C. A typical set of decay curves is included in Figure 22.

The predominant x-ray pattern of the two hours deposits in both 1N and 4N H_2SO_4 and at each temperature and current density investigated was that of the lead-silver (1%) matrix. The 10 asf deposits, in addition to strong matrix lines, gave very weak $PbSO_4$ patterns at 0°C and/or 30°C in both 1N and 4N acid and very strong mixed α- and β- PbO_2 (N H_2SO_4) or just βPbO_2 (4N H_2SO_4) patterns at 60°C. The general trend for the remainder of the deposits was as time, temperature, acid concentration and current density increased, the lead-silver (1%) matrix lines

TABLE II

DIFFRACTION DATA FOR PHASES FORMED ON LEAD-SILVER (1%) ANODES IN H_2SO_4 SOLUTIONS

		$1NH_2SO_4$-2 hrs.			$1NH_2SO_4$-12 hrs.			$4NH_2SO_4$-2 hrs.			$4NH_2SO_4$-12 hrs.		
		0°C	30°C	60°C	0°C	30°C	60°C	0°C	30°C	60°C	0°C	30°C	60°C
10 asf	Pb-Ag(1%)	vs	vs	vs	vs	vs	m		vs		vs	vs	vvw
	$PbSO_4$	vw	vw						vvw		vw		
	αPbO_2			vw	vw	w	vs		vvw			vw	vw
	βPbO_2			vvw			vs						vs
100 asf	Pb-Ag(1%)	vs	vs	vs	vs	vs			vs		m	w	
	$PbSO_4$										vw		
	αPbO_2	vw	vw	vw	vs	vs	vs		vw		vs	vs	vs
	βPbO_2		vvw	vvw	vvw	vw	vvw		vvw		vvw	vvw	vvw
200 asf	Pb-Ag(1%)	vs	vs	vs	vw	vw			vs				
	$PbSO_4$												
	αPbO_2	vw	vw	w	vs	vs	vs		s			vs	vs
	βPbO_2	vvw	vvw	vvw	vvw	vvw	vvw		vvw			vvw	vvw

v=very, s=strong, m=medium, w=weak

vs=80-100%I; s=60-80%I; m=40-60°I; w=20-40%I; vw=5-20%I; vvw=0-5%I

decreased from very strong to zero and at the same time, αPbO_2 lines increased from very weak to very strong (Table II). Almost every pattern that had αPbO_2 lines also had a very weak indication of the highest intensity βPbO_2 peak at 3.5 Å .

Structures, as revealed by SEM, for each of the phases ($PbSO_4$, α and βPbO_2) identified above are included in Figure 21. The structure of the βPbO_2 deposit appears to consist of crystals of $PbSO_4$. Actually, these are hollow shells of $PbSO_4$ crystals, inside of which βPbO_2 has nucleated and grown until the predominant x-ray pattern is that of βPbO_2.[29] The structure of αPbO_2 is more fine grained and layer like than the $PbSO_4$ deposit and is very similar to the βPbO_2 structure without the sulfate crystals.

In general, three distinct voltage plateaus of -0.3, 0.2 to 0.4 and 1.6 to 1.7V (SHE) and an indication of a fourth at 1.0 to 1.2V were exhibited in the open circuit potential decay curves for the lead-silver anodes polarized in 4 N H_2SO_4 at the various current densities. One set of curves sufficed for all three temperatures investigated as only variations in the plateau length and insignificant changes in potential resulted from variations in electrolyte temperature. Consequently, only the open circuit decay curves obtained at 30°C are included in this work (Figure 22). A decay curve for a pure lead anode is included for comparison.

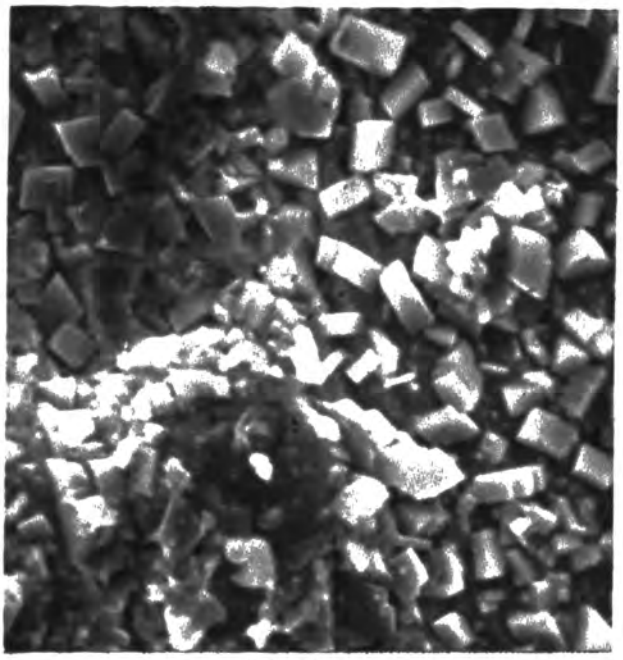

$PbSO_4$

10 asf 30°C 3000X

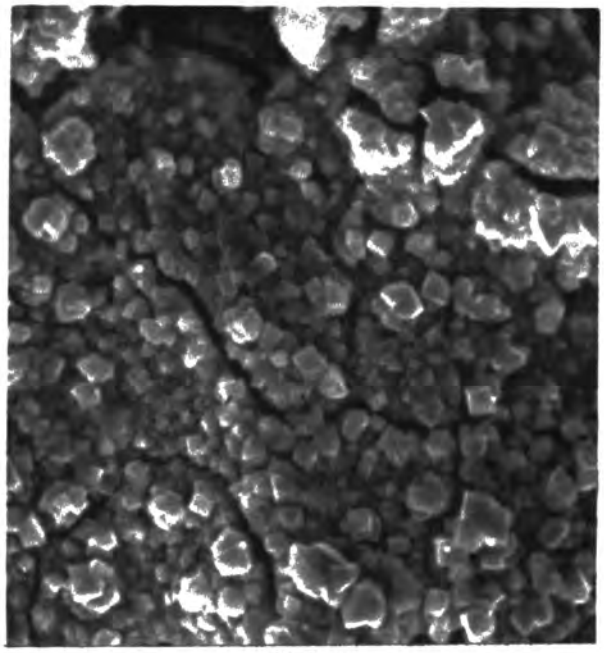

βPbO_2

10 asf 60°C 3000X

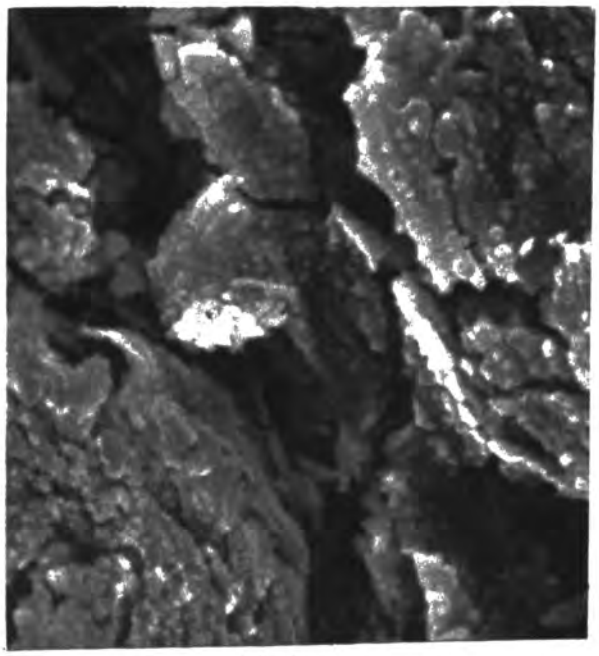

αPbO_2

100 asf 30°C 3000X

FIGURE 21. MORPHOLOGY OF Pb-Ag(1%) ANODES CONDITIONED IN 4N H_2SO_4 SOLUTIONS.

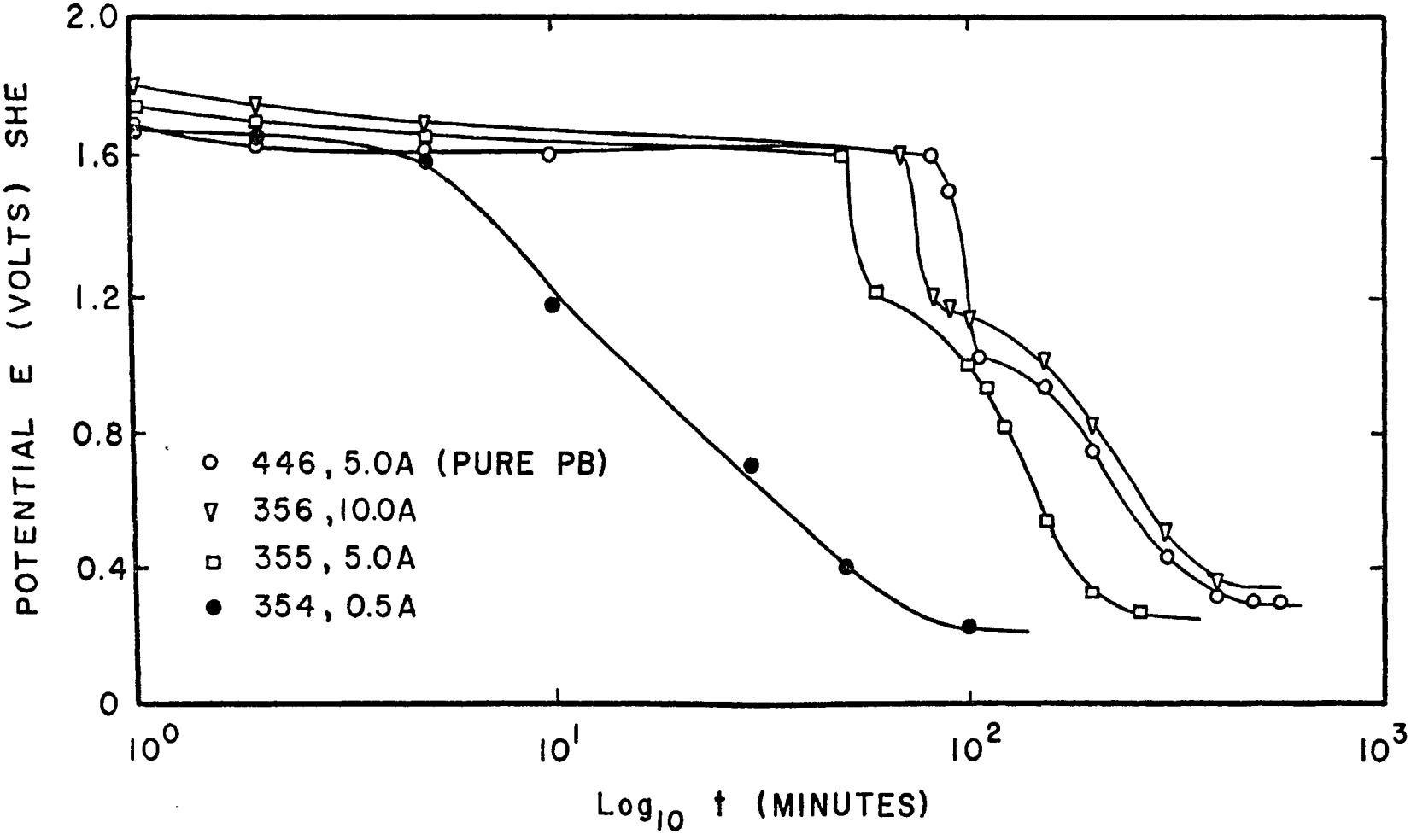

FIGURE 22. POTENTIAL DECAY CURVES FOR LEAD-SILVER (1%) AND PURE LEAD ANODES POLARIZED IN 4N H_2SO_4 SOLUTIONS AT 30°C AND AT VARIOUS CURRENT DENSITIES.

The following equilibrium reactions were suggested by the potential arrests listed above (see Appendix D).

1) $PbSO_4 + 2\bar{e} = Pb + SO_4^{=}$

$E = -0.359 - 0.0295 \log A_{SO_4^{=}}$

$E = -0.29V$

2) $PbO_t + 2H^+ + 2\bar{e} = Pb + H_2O$

$E = 0.249 - 0.0591\ pH$

$E = +0.23V$

3) $\alpha PbO_2 + 2H^+ + 2\bar{e} = PbO_t + H_2O$

$E = 1.075 - 0.0591\ pH$

$E = +1.06V$

4) $PbO_2 + SO_4^{=} + 4H^+ + 2\bar{e} = PbSO_4 + 2H_2O$

$E = 1.683 - 0.1182\ pH + 0.0295 \log A_{SO_4^{=}}$

$E = +1.58V$

Reactions 1, 2 and 4 were verified by x-ray diffraction and reaction 3 is suggested by the potential decay data, but not directly confirmed by x-ray analysis. However, the existence of αPbO_2 and PbO_t, which are normally only stable in alkaline solutions is consistent with the observations of previous researchers[19,24,26-28] and is added evidence that a pH gradient exists in the anodic layer.

As in other investigations,[25] the PbO/Pb couple was the most prominent and was maintained for several hours before dropping off to the sulfate potential at -0.29V.

To check further on the reaction taking place at the $PbO_2/PbSO_4$ plateau, a lead-silver anode was polarized for 12 hours at 100 asf, allowed to decay for ten minutes and then x-rayed and photographed on the scanning electron microscope. A part of this anode was then decayed for an additional 10 minutes and the remainder was repolarized for 30 minutes at 100 asf.

X-ray diffraction revealed the presence of $PbSO_4$ after a 10 minute decay and an additional 10 minute decay resulted in a substantial increase in the amount of the orthorhombic $PbSO_4$ crystals (Figure 23). The structure seen on SEM after repolarizing appeared to be the same as after decay, with large $PbSO_4$ crystals in a αPbO_2 matrix. However, x-ray diffraction indicated αPbO_2 was the predominant phase present. This observation, as was mentioned previously, is in keeping with the results of Simon, et. al.[29] that PbO_2 nucleates and grows inside the $PbSO_4$ crystals, and the outer morphology remains the same.

The hardness of the anodized coatings was difficult to assess since the surface layer, even for the 12 hour deposits at high current densities, was relatively thin and any values obtained were probably more an indication of the hardness of the lead-silver (1%) matrix than of the surface deposit.

The weight of the anodes was relatively constant in N H_2SO_4, at all temperatures and current densities

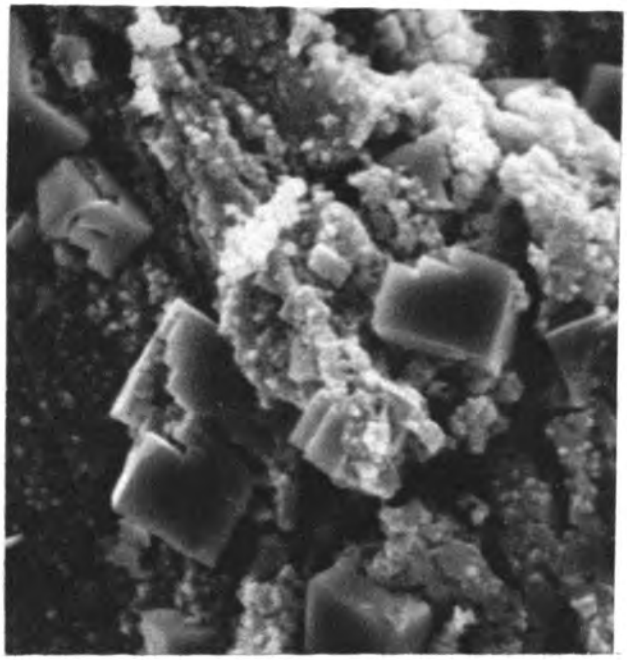

αPbO_2+PbSO_4 3000X

10 min. decay

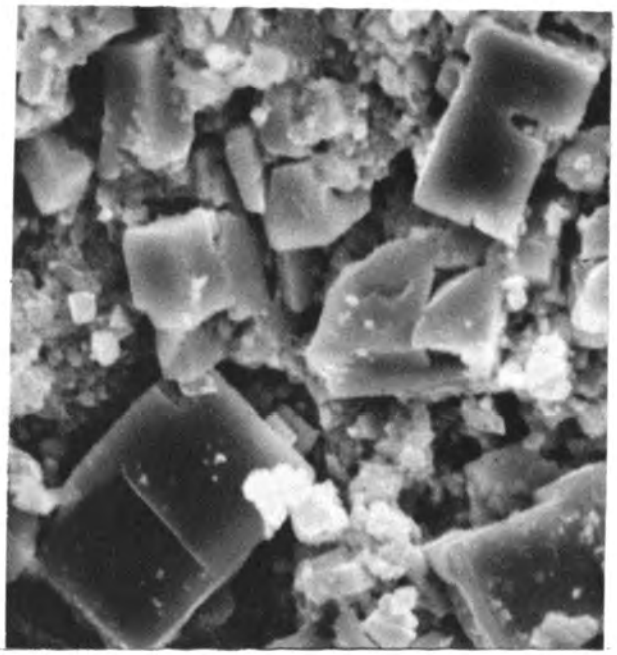

αPbO_2+PbSO_4 3000X

20 min. decay

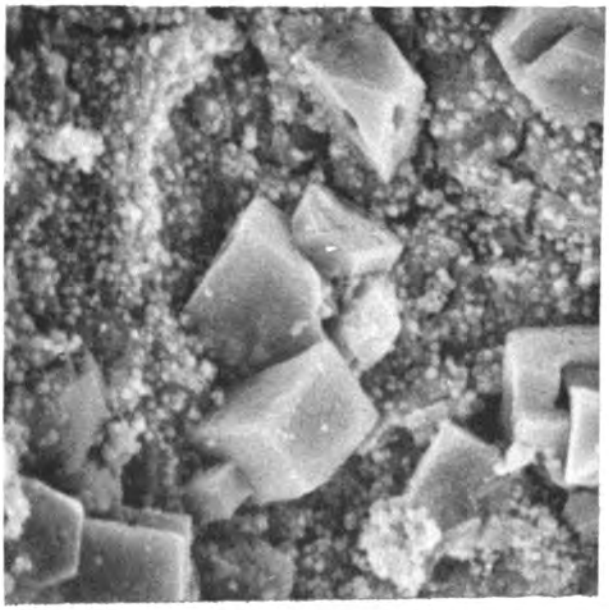

αPbO_2 3000X

10 min. decay + 30 min. repolarize

FIGURE 23. MORPHOLOGY OF Pb-Ag(1%) ANODES POLARIZED IN 4N H_2SO_4 SOLUTIONS AT 100 asf FOR 12 HOURS AT 30°C AFTER VARIOUS PERIODS OF DECAY, AND DECAY WITH REPOLARIZING.

investigated. The anode weight was also constant in 4N H_2SO_4 solutions at 0°C and each current density. However, at 30°C and 60°C the anodes electrolyzed at 10 asf showed increases in weight of a few tenths of a gram, while the anodes conditioned at 100 and 200 asf decreased in weight as much as 0.4 grams after 12 hours.

The products found in the residues from the bottom of the cells after electrolysis consisted of the same phases found on the anodes (Table II) that were conditioned in the cells, indicating the residues were stable in the H_2SO_4 solutions.

2. Na_2SO_4 Solutions. Due to the numerous amount of x-rays to be identified in this work, it was difficult to index accurately each pattern due to fluctuations in the alignment of the diffractometer. Instead, standards were prepared from reagent grade materials and experimental patterns were identified by comparing with these standards.

The above procedure worked very well for all the compounds involved except αPbO_2. The methods outlined by Fraunhofer[45] to produce exclusively αPbO_2, using 4N Na_2SO_4 solutions, pure lead anodes and a current density of 1.5ma/cm^2, were unsuccessful. The resulting x-ray pattern was predominantly αPbO_2 but the line of maximum intensity for βPbO_2 was also present. However, this pattern sufficed as a standard for the majority of the anodes that were examined during the course of this

research, where αPbO_2 was a dominant phase, also had an indication of βPbO_2 at 2θ values corresponding to the peak of maximum intensity.

3. NaF and KF Solutions. Lead-silver, pure lead and D.S. lead anodes were conditioned for 12 hours at 30° and 45°C, in various strength NaF-H_2SO_4 and KF-H_2SO_4 solutions, at current densities of 10, 50, 100 and 200 asf between two cathodes of like material. Both N and 2N sodium fluoride solutions were tried with H_2SO_4 concentrations varying from 4N to 1N. The concentration of all the KF solutions was 40 gpl F^- and sulfuric acid was added as necessary to adjust the solution to pH 5. Both x-ray diffraction and the scanning electron microscope were utilized to study the phases present on the conditioned anode surface. Polarization and potential decay curves were obtained with lead-silver(1%) and pure lead anodes in the NaF and KF solutions.

Anodes that appeared to be the most stable, from the standpoint of hardness, adherence and density of coating, were used to make zinc deposits as in the early part of this work.

The predominant phase present on the outer surface of the lead-silver anodes after anodization, regardless of current density, temperature or solution composition, was βPbO_2. The anodes conditioned in NaF-N H_2SO_4 and KF - H_2SO_4 solutions also had weak αPbO_2 lines at each current

density. Electrodes treated in the rest of the NaF solutions exhibited, along with strong βPbO_2 indications, increasing amounts of αPbO_2 with increases in current density. Also, one of the deposits made at 10 asf in KF solutions was very spotty, leaving the anode bare in some places. It gave a strong αPbF_2 pattern where the lead-silver matrix was exposed. Similarly, a deposit made in an NaF solution at 10 asf gave strong lines of βPbF_2 (see Table III). The x-ray pattern of a lead-silver anode left soaking in an NaF solution (pH = 5) for 40 hours consisted of αPbF_2.

The relative hardness of the anode surface, after conditioning, was determined with a Bierbaum Microcharacter.[46] A diamond stylus was mechanically drawn across the surface to be tested and the width of the cut produced was measured. An average of five independent measurements on each of the surface identified after the various conditioning processes along with the relative hardness of the lead-silver matrix are listed below.

	Width of Cut (microns)
Pb-Ag (1%) matrix	27.0
PbF_2	23.0
$PbSO_4$ (after decay)	45.0
βPbO_2	8.2
αPbO_2 (dark underlayer)	5.0

TABLE III

DIFFRACTION DATA FOR PHASES FORMED ON LEAD-SILVER (1%) ANODES IN FLUORIDE SOLUTIONS

		1N NaF 1N H_2SO_4 30°C	2N NaF 4N H_2SO_4 30°C	1N NaF pH = 5 30°C	1N NaF pH = 5 45°C	KF 40 gpl F^- 30°C	KF 40 gpl F^- 45°C
10 asf	βPbO_2	vvs	vvs	vvs	vvs	vvs	vvs
	αPbO_2	vvw		vvw			
	βPbF_2		m				
	αPbF_2						vs
50 asf	βPbO_2	vvs		vvs	vvs	vvs	vvs
	αPbO_2	vvw		m	m		vvw
100 asf	βPbO_2	vvs	vvs	vvs	vvs	vvs	vvs
	αPbO_2	vvw	m	vs	vs		
200 asf	βPbO_2	vvs	vvs			vvs	vvs
	αPbO_2	vvw	s			vvw	

v=very, s=strong, m=medium, w=weak

vvs=90-100%I; vs=80-90%I; s=60-80%I; m=40-60%I; w=20-40%I; vw=5-20%I; vvw=0-5%I

The values obtained can only be interpreted in a very general way. Due to the powdery nature of the anode surface, it was extremely difficult to get consistent and reliable results. For example, it was impossible to ascertain the effects of temperature, current density or even solution composition in producing a reliable anode coating merely by comparing hardness values. However, in a relative sense, the lead-silver anodes conditioned in fluoride solutions are approximately three times as hard as the same anodes conditioned in H_2SO_4, as the anodes conditioned in H_2SO_4 showed hardness values very nearly those obtained for the lead-silver (1%) matrix.

The anodes conditioned in NaF solutions at 30° and 45°C increased in weight from a low of 0.5 grams at 10 asf to a high of 1.0 grams at 50 asf and the 100 and 200 asf deposits had weight gains between these two values. Anodes conditioned in KF solutions at 30°C only had weight gains of 0.3 grams at 10 asf and 0.8 grams at 50 asf. The 100 and 200 asf deposits showed weight increases of less than 0.3 grams. No change of weight was noted for anodes conditioned in KF solutions at 45°C, regardless of current density.

As mentioned above, the deposits were harder after conditioning and appeared to be very adherent until an attempt was made to clip off a piece for x-ray analysis. The deposits made at 10 asf and 50 asf flaked off during cutting and revealed a light gray under layer, which was identified

by x-ray diffraction as βPbF_2.

The anodes conditioned in N NaF (pH = 5) solutions had in addition to PbF_2 next to the electrode surface, a much harder outer layer of PbO_2. The anodes conditioned in the rest of the solutions appeared to consist of three layers, a PbF_2 inner layer, PbO_2 outer layer and a dark purple middle layer which appeared to be either αPbO_2 or PbO_t.

Both D.S. and pure lead anodes were conditioned at 50 and 100 asf in the KF and NaF solutions. The phases produced in the anodic coating consisted of mainly βPbO_2 at 50 asf and a mixture of α and βPbO_2 at 100 asf. The pure lead anodes, like the lead-silver (1%) anodes, appeared to have the same three layers on the surface after conditioning but unlike the lead-silver anodes, the pure lead anodes lost weight during electrolysis, primarily due to severe attack at the solution line. The D.S. lead anodes were attacked very severely and lost as much as 20% of their original weight after conditioning.

Three distinct arrests at $\sim$1.3, 0.9 and 0.4V, respectively, are exhibited in the potential decay curves for lead-silver anodes that were polarized for 12 hours in 40 gpl F^- (KF) solutions at 100 asf and allowed to decay on open circuit (Figure 24). The potentials (SHE) of the voltage plateaus observed in Figure 24 correspond to the following equilibrium reactions in the KF solutions at a

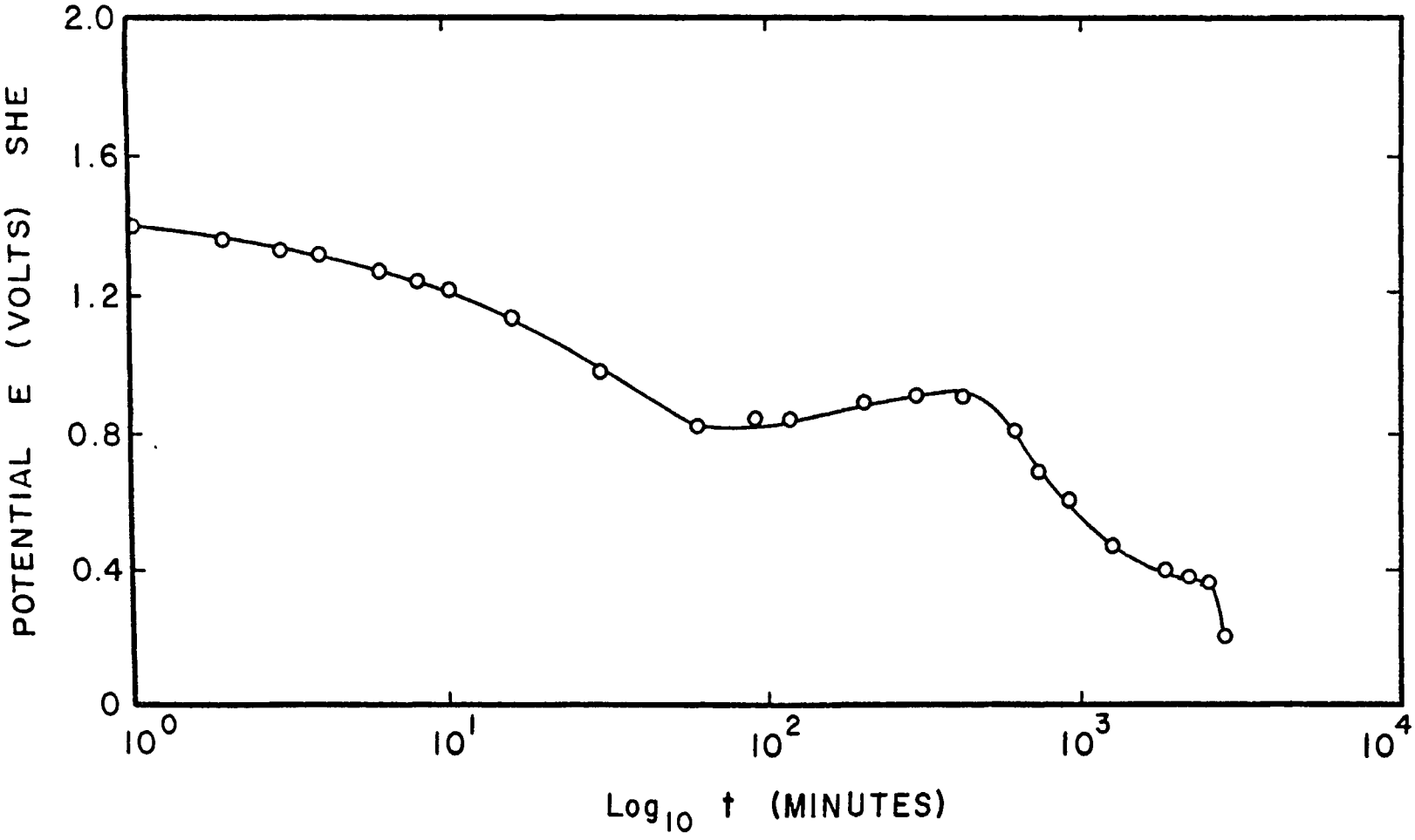

FIGURE 24. POTENTIAL DECAY CURVE FOR A LEAD-SILVER (1%) ANODE POLARIZED IN A 40 gpl F^- (KF) SOLUTION AT 30°C AND 100 asf.

pH of approximately 5 (see Appendix D).

1) $\beta PbO_2 + 2H^+ + 2HF + 2e^- = PbF_2 + 2H_2O$

$$E = 1.66V - 0.059\ pH$$

$$E = +1.37V$$

2) $\beta PbO_2 + SO_4^= + 4H^+ + 2e^- = PbSO_4 + 2H_2O$

$$E = 1.68V - 0.1182pH + 0.0295 \log A_{SO_4^=}$$

$$E = +0.935V$$

3) $\alpha PbO_2 + 4H^+ + 4e^- = Pb + 2H_2O$

$$E = 0.665 - 0.0591\ pH$$

$$E = +0.370V$$

Two further reactions would be observed at much longer times and can be represented as follows.

4) $PbSO_4 + 2e^- = Pb + SO_4^=$

$$E = -0.359 - 0.0295 \log A_{SO_4^=}$$

$$E = -0.2023V$$

5) $PbF_2 + 2e^- + 2H^+ = Pb = 2HF$

$$E = -0.6014 - 0.0591\ pH$$

$$E = -0.8969V$$

All of the various phases identified by the potential arrests were also confirmed by x-ray diffraction before and during anodic decay. The dark purple, underlying layer tentatively identified by x-ray analysis as PbO_t or αPbO_2

appeared to be mainly αPbO_2 as the arrest for PbO_t/Pb was not observed.

Pictures taken on the SEM are included in Figure 25 for anodes conditioned in both KF and NaF solutions. The surface of the anodes conditioned at 100 asf in both solutions is quite similar and consists of numerous cracks with a dense, uniform layer of small PbO_2 particles between the cracks. A photograph taken inside one of the cracks shows the dark colored second layer described above. The anode conditioned in KF solution at 10 asf is unique in that the surface is primarily covered with a layer of dendritic βPbO_2 crystals.

Lead-silver anodes polarized in 4N H_2SO_4 solutions for 12 hours reached a maximum potential of slightly greater than 2.0V (SHE) in the first few seconds after the current was turned on and then the potential stabilized at 2.0V. Lead-silver anodes polarized under similar conditions (100 asf - 12 hours) in 40 gpl F^-(KF) solution attained a maximum of 4.4V in 60 seconds and then leveled off at 1.7V.

The potential for pure lead anodes, polarized in 40 gpl F^-(KF) solutions for 12 hours at 100 asf, rose to a maximum value of 7.2V in slightly over a minute. The potential then dropped to a steady value of 3.6V for a short time after which it gradually increased as the anode slowly disintegrated. Pure lead anodes in

βPbO_2

100 asf 30°C 3000X

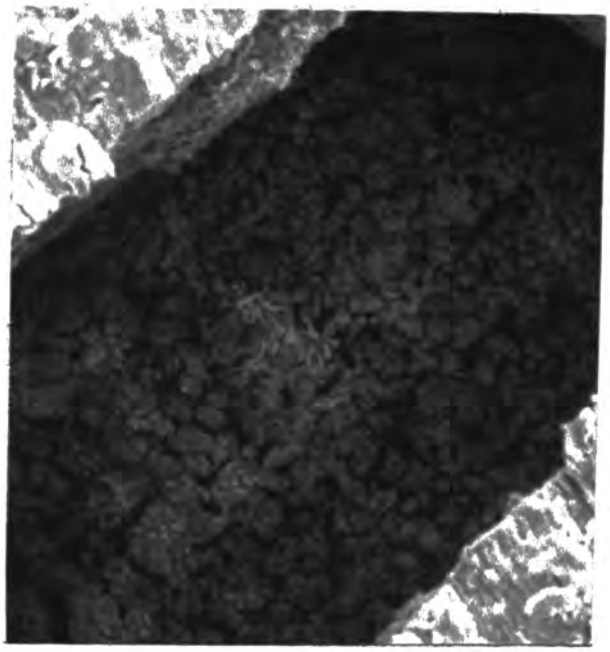

αPbO_2

10 asf 30°C 1000X

inside a crack

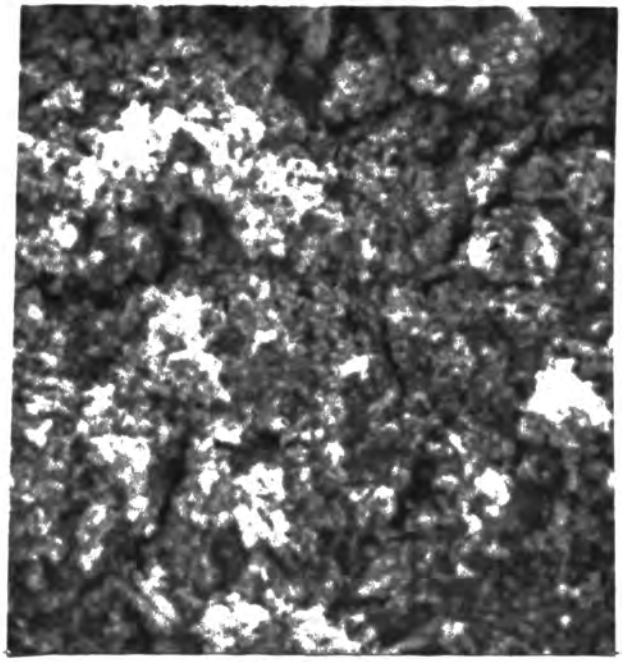

βPbO_2

100 asf 30°C 3000X

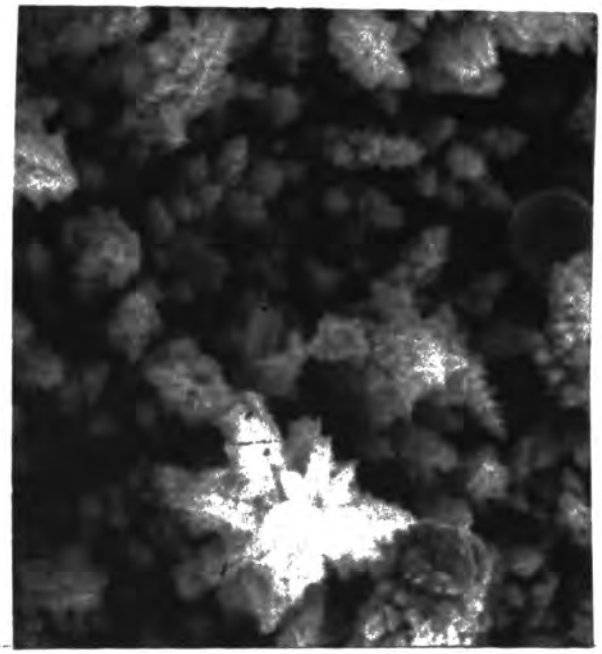

βPbO_2

10 asf 45°C 3000X

FIGURE 25. MORPHOLOGY OF Pb-Ag(1%) ANODES CONDITIONED IN NaF SOLUTIONS (upper) AND KF SOLUTIONS (lower) FOR 12 HOURS.

4N H_2SO_4 at 100 asf for 12 hours attained a maximum potential of 2.4V in a few seconds and then stabilized at approximately 2.2V for the remaining 12 hours.

The formation of a dielectric layer of PbF_2 next to the electrode surface of the anodes conditioned in the KF solutions is responsible for the high initial surge in the potential and is analogous to the formation of $PbSO_4$ in H_2SO_4 solutions.

Anodization of lead-silver anodes using platinum cathodes in NaCl, H_2O_2 - H_2SO_4 and $K_2Cr_2O_7$ solutions was initiated in the hope of getting better insight into why fluoride ions accelerate the reaction at the anode and produce such a marked increase in the amount of material deposited on the electrode surface.

A solution of 40 gpl Cl^- ion in H_2O, with the pH lowered to 4.5 by addition of H_2SO_4, resulted in such a drastic increase in the total cell voltage that the maximum voltage (40V) for the power supply was exceeded. When the Cl^- ion concentration was reduced to 10 gpl, the total cell voltage was only 6.5V and a ten hour deposit was made at 50 asf.

The anode gained approximately one gram in weight and the predominant phase on the surface was βPbO_2 which was comparable to anodes conditioned in fluoride solutions. Unlike anodes conditioned in fluoride solutions, the deposit was corrugated and large pieces fell off revealing

a gray under layer of lead sulfate and lead chloride hydroxide Pb(OH)Cl next to the electrode. It appeared that Cl^- accelerated the formation of the anodic layer, but much poorer adherence resulted compared to the coating obtained with fluoride ion. The effect of even lower chloride concentrations is open to speculation.

The presence of the strong oxidizing agents H_2O_2 and $K_2Cr_2O_7$ in 4N H_2SO_4 solution did not result in any increase in anode weight when the anodes were polarized at 50 asf for 12 hours. Also, the hardness of the deposit was only that of the lead-silver matrix. The predominant x-ray pattern for anodes conditioned in both solutions was αPbO_2 and in addition, strong lines from the lead-silver matrix were present.

The deposits made with 15 gpl $K_2Cr_2O_7$ in 4N H_2SO_4 solutions looked similar to deposits made in 4N H_2SO_4 at the same current density and temperature except for the presence of a few arrow-shaped, dendritic crystals. However, the deposits made in the H_2O_2 (125 ml's H_2O_2) solutions were quite different than any produced in sulfuric acid solutions (see Figure 26).

The contribution of the fluoride ion in producing the substantial anodic layer is still not clear. Fluoride ions appear to accelerate or catalyze the reaction at the anode surface in such a way as to produce a large increase in the amount of PbO_2 formed over the amount resulting from

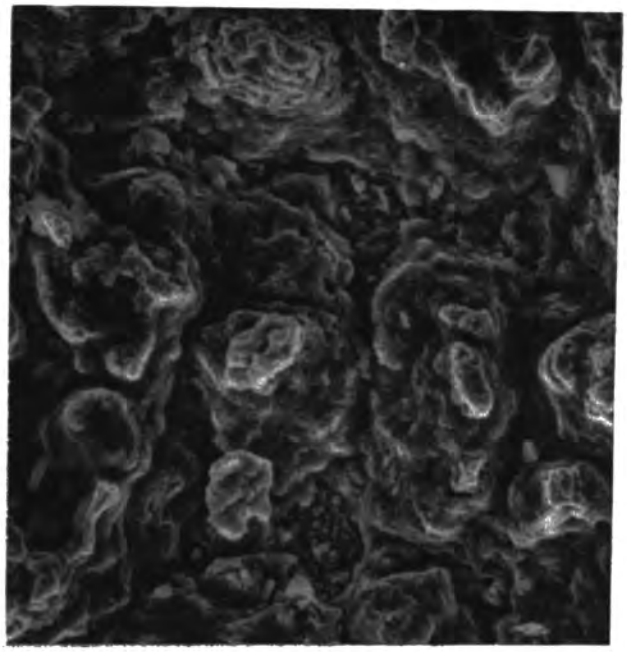

αPbO_2

50 asf 30°C 1000X

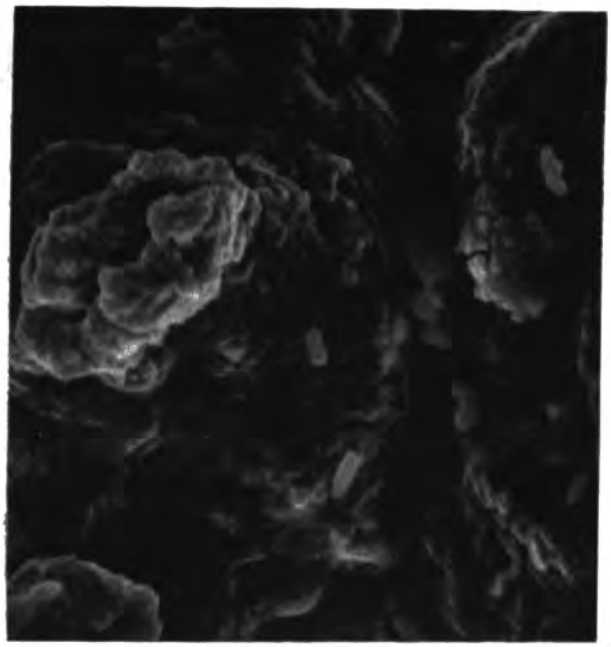

αPbO_2

50 asf 30°C 3000X
(same area as at left)

αPbO_2

50 asf 30°C 3000X

FIGURE 26. MORPHOLOGY OF Pb-Ag(1%) ANODES CONDITIONED IN H_2O_2-4N H_2SO_4 (upper) AND $K_2Cr_2O_7$-4N H_2SO_4 SOLUTIONS (lower) FOR 12 HOURS.

polarization in sulfuric acid solutions.

Preliminary experiments with anodes conditioned in both NaF and KF solutions, under actual conditions of zinc electrolysis, indicated that anodes conditioned in NaF solutions at 80-100 asf were superior to anodes conditioned in KF solutions. Electrodes treated in NaF solutions produced a good, crystalline zinc deposit in 65 gpl Zn^{++} - 200 gpl H_2SO_4 solutions with no manganese for the first 4 to 6 hours (depending on current density) of electrolysis. The multiple phases on the anode surface began to separate and pull away with time, due to stresses set up between the layers because of differences in lattice structure. Simultaneously with the break up of the anode surface, the amount of lead in the zinc deposit increased. Also, it became increasingly more difficult to strip the deposit due to increasing amounts of fluoride ion in the solution from decomposition of PbF_2 at the anode.

It appears that more extensive research will be necessary to develop a stable PbO_2 electrode that can be used without the presence of manganese in the solution to form a protective MnO_2 layer.

4. Aluminum Solutions. An attempt was made to condition a lead-silver anode using aluminum cathodes in 40 gpl F^- (KF) solutions. Also, lead-silver anodes were conditioned with platinum cathodes at different current densities and temperatures in both NaF and KF solutions

to which various amounts of $Al_2(SO_4)_3 \cdot 18\ H_2O$ had been added. X-ray diffraction was used to determine the various phases formed on the anode.

When pure aluminum (4 - 9's) cathodes were used to condition a lead-silver anode in a KF solution at 30°C for 12 hours at 50 asf, the anode was attacked very severely and the edges were eaten away, leaving a narrow band in the center with a thick white coating on the surface. The anode lost approximately one-third of its weight in the 12 hours. In addition, the aluminum cathodes were depply etched and the grain structure was revealed.

To determine the amount of aluminum necessary to cause the anode to lose weight, a series of runs was made, with gradually increasing current densities, using one aluminum cathode and one lead-silver cathode. The aluminum cathode was weighed, along with the anode, before and after each run to monitor the amount of aluminum in the solution. The weight of the aluminum cathode was still constant after 12 hours at 10 and at 30 asf. The anode deposits were the same as those made with the lead-silver cathodes.

Three consecutive runs were then made at 50 asf with a new lead-silver anode for each run. The aluminum cathode lost 0.5, 0.78 and 1.62g, respectively, for a total of 2.9 grams of aluminum in the solution. The anodes gained 0.43 grams during the first two runs and 1.58 grams for the third run.

The first two deposits appeared to be just βPbO_2, while the last conditioned anode had a dark brown under layer and a heavy white outer coating like the initial anode that disintegrated. X-ray analysis of the anode deposit showed a mixed pattern of βPbO_2 and $K_3Al\ F_6$. The white deposit taken from the initial anode that had almost disintegrated was in addition to $K_3Al\ F_6$, a compound tentatively identified as αK-Pb-F. It seems likely that in the presence of greater than 3 gpl aluminum in the solution, the anode became completely covered with a layer of $K_3\ Al\ F_6$ after which the production of a soluble compound of αK-Pb-F was promoted and the anode disintegrated.

In addition to the above experiments, reagent grade hydrated aluminum sulfate [$Al_2(SO_4)_3 \cdot 18\ H_2O$] was added to 20 gpl F^- (NaF) solutions and lead-silver anodes were electrolized for 12 hours at 35-40°C using platinum cathodes. With no aluminum, 0.5 gpl aluminum and 5 gpl aluminum in solution, the anode coating was βPbO_2, but with 1 gpl and 3 gpl aluminum in solution, the principal phase on the anode surface was βPbF_2.

When a lead-silver anode was anodized at 50 asf for 12 hours in 20 gpl F^- (NaF) solutions at 30°C with pure aluminum cathodes, similar results were obtained as when aluminum cathodes were used in KF solutions. Although the current density and temperature were the same, the

anode did not disintegrate like the anode conditioned in the KF solution, but the surface was covered with a white layer.

It appears that aluminum added to the solution as $Al_2(SO_4)_3 \cdot 18\ H_2O$ does not have the same effect as aluminum present from dissolution of an aluminum cathode. The different effects may be due to the different amounts of aluminum in the solution at any given time due to the different modes of introduction or the aluminum may be present in a different state.

The above results were quite interesting but since the amount of aluminum necessary to produce any deleterious effect on the anode far exceeded the amount that would normally be present in solutions (grams vs ppm) used for zinc electrolysis, this line of investigation was discontinued.

V. CONCLUSIONS

1. The growth mode, orientation and morphology of zinc electrowon from acid zinc sulfate solutions is directly dependent on the temperature, current density and type of electrode used for deposition.

2. At high temperatures and high current densities, the zinc appeared to adopt a lateral mode of growth with (002) facets aligned parallel to the substrate. The current efficiencies were approximately 95%.

3. At low temperatures and high current densities, the zinc appeared to adopt an outward mode of growth. The current efficiencies decreased as the current density increased.

4. The change in growth mode is possibly caused by an increase in the metallic overpotential or the presence of nucleating agents such as carbon.

5. The platinum anodes do not remain inert at certain combinations of temperature and current density. Traces of platinum were positively identified on the surface of cathodes which exhibited time dependent current efficiencies.

6. At each temperature investigated, a limiting current density existed below which a reasonable zinc deposit could not be obtained.

7. Aluminum in solution may influence the morphology of the zinc deposit.

8. Titanium does not appear to be a suitable cathode material for zinc deposition.

9. Graphite and vitreous carbon do not make suitable anodes as they tend to disintegrate at any appreciable current density.

10. The predominant phase formed on lead-silver anodes conditioned in H_2SO_4 solutions was αPbO_2.

11. The predominant phase formed on lead-silver anodes conditioned in fluoride solutions was βPbO_2.

12. The rate of formation of PbO_2 on the lead-silver anodes conditioned in fluoride solutions was considerably greater than the rate in H_2SO_4 solutions.

13. The relative hardness of the coating was much greater on anodes conditioned in fluoride solutions than on anodes conditioned in H_2SO_4 solutions.

14. Lead-silver anodes lost two-thirds of their initial weight when conditioned in fluoride solutions with aluminum cathodes.

VI. APPENDICES

APPENDIX A

PREPARATION OF NEUTRAL ZINC SULFATE ELECTROLYTE

(2 - Liter Batches)

A. CALCULATIONS

Basis 200 grams per liter (gpl) zinc

M.W. Zn = 65 M.W. H_2SO_4 = 98

M.W. ZnO = 81 Sp. Gr. H_2SO_4 = 1.84 g/cc

$$ZnO + H_2SO_4 = ZnSO_4 + H_2O$$

$$\frac{81 \text{ g ZnO}}{65 \text{ g Zn}} \text{ (400 g Zn/2-liters)} = 498.5 \frac{\text{g ZnO}}{\text{2-liters}}$$

98 g of (100%) H_2SO_4/mole (assay min. 95% - max. 98%)

assume minimum assay of 95%

$$\frac{98 \text{ g (100\%) } H_2SO_4\text{/mole}}{0.95} = 103 \text{ g of 95\% } H_2SO_4\text{/mole}$$

$$\frac{103 \text{ g } H_2SO_4\text{/mole}}{81 \text{ g ZnO/mole}} = 1.272 \text{ times more } H_2SO_4 \text{ than ZnO}$$

498.5 g ZnO x 1.272 = 634 g H_2SO_4/2-liters

$$\frac{634 \text{ g } H_2SO_4}{1.84 \text{ g } H_2SO_4\text{/ml}} = \frac{345 \text{ ml's } H_2SO_4}{\text{2-liters}}$$

B. Procedure

After carefully cleaning all glassware as described previously, photoconductive zinc oxide, Fisher A300-C concentrated sulfuric acid and distilled water were mixed and purified in two 3-liter beakers as follows:

1. Pour 250 ml's distilled H_2O into each beaker.
2. Add 345 ml's of conc. H_2SO_4 to each 3-liter beaker by pouring it slowly down the side and allow to cool to room temperature (approximately 4 minutes to add each 345 ml's).
3. Tare two 1-liter beakers and add 498.5 grams of French ZnO to each, add H_2O to 800 ml's, mix and add the slurry very slowly to each 3-liter beaker with mechanical stirring. A Talboys model 103 stirrer with teflon coated stirring rod was used to help dissipate the heat and control the temperature. Approximately 20 min. is required for each addition as the reaction is extremely exothermic and the mixture will sputter, boil and even explode if the slurry is added too fast. The temperature can be controlled by adding distilled water, but care must be taken not to make much over two liters of solution when the ZnO is all added, or a great deal of time is wasted boiling off the excess water.
4. Adjust the solution level to 2-liters and oxidize

by adding 0.1N $KMnO_4$ drop wise to maintain a faintly pink color for two hours. The total amount of $KMnO_4$ necessary is approximately 1 ml/ liter (17 drops) or 1.1 mg Mn/l.

5. After the two hour oxidation period the solution is placed on a Thermolyne 2200 hot plate at 700°F and brought to a hard boil for 20 minutes. The color is now pale yellow with tiny black flakes present among the small anount of undissolved white ZnO in the bottom of the beaker.
6. The pH is adjusted to approximately 5.5 by adding conc. H_2SO_4 drop wise to change Fisher Alkacid Test Ribbon (pH range 2-10 by increments of 2 pH) from orange to very slightly red.
7. The boiling solution at pH 5.5 is filtered into a 2-liter side arm flask using a No. 3 Buchner Funnel and two thicknesses of filter paper. Suction was supplied by running tap water through an aspirator type vacuum pump, connected through a trap to the filter flask with 0.25" I.D. vacuum hose. The funnel is prepared for filtering by placing a piece of 11 cm diameter Whatman No. 41 filter paper on the bottom and moistening it to hold it in place. Then a piece of 15 cm diameter paper is folded to fit the bottom and the edges are turned up and crimped to adhere to the sides of

the funnel when wet. The solution level during filtering was maintained just below the top of the turned up paper.

8. The filtrate is poured from the flask back into the 3-liter beakers; the beakers are then placed back on the hot plate. Blackwell zinc dust (2.5 gpl) is added with stirring and the solutions are brought to a hard boil for 20 minutes and filtered as before.
9. After cooling to room temperature, the solution is poured into a 2-liter volumetric flask, the volume is adjusted to 2-liters by adding distilled H_2O and the electrolyte is stored in 9-liter pyrex serum storage jugs.

NOTES:

a) Temperature of solution after adding 345 ml's of conc. H_2SO_4 to 250 ml's H_2O in 4 min., 110-120°C.
b) Sputtering begins to occur at 90°C when adding ZnO, with violent reactions commencing at higher temperatures.
c) Temperature of the solution at finish of ZnO addition (20 to 30 min. to add), 85°C.
d) Temperature of solution when placed on the hot plate, 55°C.
e) Temperature of solution at beginning of boiling (soft boil), 97°C.

f) Temperature of solution at hard boil (filter temp.), 102°C.

g) Temperature of solution in funnel while filtering, 90°C.

h) Temperature of solution with zinc dust (hard boil), 102°C.

APPENDIX B

PROCEDURE FOR PREPARING LEAD AND LEAD ALLOYS FOR PHOTOMICROGRAPHS

1. Belt Sander:

   a) 120 grit emery paper with H_2O (light touch) wash with soap and tap water after grinding

   b) 240 grit emery paper with H_2O (light touch) wash with soap and tap water after grinding

2. Circular Wheel:

   (Sand)

   600 grit paper with H_2O, wash with soap and tap water after grinding

   note: you have already picked up some grit at this point even using a very light touch

3. Hand Polish:

   4/0 paper with paraffin and kerosene lubricant* wash with soap and tap water, rinse with alcohol and vibrate in alcohol to aid in removing grit

4. Circular Wheel:

   (Polish)

   Buehler microcloth with 6 micron diamond paste, soak nap with kerosene (Fisher - odorless and refined), put bead of diamond paste in a complete circle around the center of the wheel and work in

---

*Paraffin and kerosene lubricant

2000 cc Fisher odorless and refined kerosene
86.3 g paraffin (kind bought in grocery store)

with fingers. Keep wheel wet with kerosene (squeeze bottle). Wash with soap and tap water, rinse with alcohol and vibrate in alcohol.

5. Etch:

Immerse 10 - 15 sec or more in H_2O_2-Acetic Acid etchant,* wash with tap water, rinse in alcohol and vibrate in alcohol, dry in warm air. This step will aid in removing grit.

6. Circular Wheel:
(Repolish)

Repeat step 4. Check surface at 250X for grit. Repeat this step until no grit is visible in the specimen at 250X (usually takes 5 - 10 min.).

7. Circular Wheel:
(Polish)

Buehler microcloth with 1 micron diamond paste. Prepare nap as in step 4. Polish with very light touch for approximately 2 min., wash with soap and tap water, rinse with alcohol, vibrate in alcohol and dry with warm air.

8. Circular Wheel:
(Polish)

Repeat step 7, except use 1/4 micron diamond paste. Polish with a very light touch for a maximum of 1 min.

---

*Etchant

10 ml's 30% H_2O_2
20 ml's distilled H_2O
50 ml's Glacial Acetic Acid (99.7% conc.)

9. Etch.

Immerse for approximately 5 sec in H_2O_2 - Acetic Acid etchant, wash with tap water, rinse with alcohol, vibrate in alcohol, dry with warm air.

Repeat steps 8 and 9 as necessary to reveal structure.

APPENDIX C

GEOMETRIC ARGUMENTS SHOWING THAT FAST GROWING FACES GROW OUT OF EXISTENCE AND SLOW GROWING FACES SURVIVE

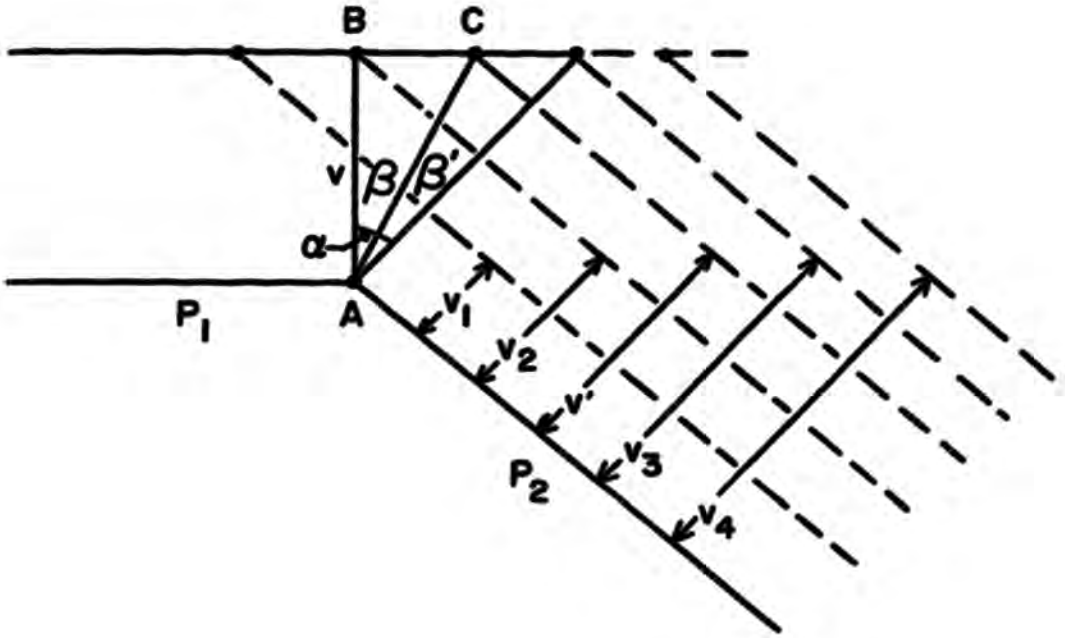

Two adjacent planes P_1 and P_2 intersecting at point A are growing outward at different velocities. The outward growth velocity of P_1 is taken as a constant and equal to v over a unit interval of time, while P_2 is allowed different growth rates expressed as v_1, v_2 --- v_n, etc. AC divides the angle α between the normals of the two planes into β and β'. If v' is taken to represent any velocity of outward growth of the type v_1, v_2 --- v_n, etc., it can be seen that $\frac{v'}{v} = \frac{\cos \beta'}{\cos \beta}$. If β increases, β' will decrease

($v' = v_4$), the ratio $\frac{v'}{v}$ becomes larger and the velocity of growth of P_2 increases. The plane P_2 will then decrease relative to P_1 during growth which, if sufficiently prolonged, will result in its extinction. When β' increases, β decreases ($v' = v_1$) and $\frac{v'}{v}$ decreases, the reverse is true and plane P_1 will tend to disappear.

APPENDIX D

CALCULATION OF EQUILIBRIUM POTENTIALS

The potential E corresponding to the equilibrium

$$x\ Ox + m\ H^+ + ne^- = y\ Rd + z\ H_2O$$

is calculated as follows:

Ox = oxidized species

Rd = reduced species

for oxidized species + ne^- = reduced species

$$\Delta G = -n\ FE \qquad \text{and} \qquad E = E^\circ - RT/nF \ln K_{eq}$$

$$E^\circ = -\frac{\Delta G^\circ}{nF}\ ; \qquad \Delta G^\circ = y\ \Delta G^\circ_{Rd} + z\ \Delta G^\circ_{H_2O} - x\ \Delta G^\circ_{O_x}$$

$$-\Delta G = x\Delta G^\circ_{O_x} - y\ \Delta G^\circ_{Rd} - z\ \Delta G^\circ_{H_2O}$$

$$K_{eq} = \frac{[Rd]^y [H_2O]^z}{[O_x]^x [H^+]^m}$$

$$\log K_{eq} = \log [Rd]^y [H_2O]^z - \log [O_x]^x [H^+]^m$$

but $\log AB = \log A + \log B$

$$\log K_{eq} = \log [Rd]^y + \log [H_2O]^z - \log [O_x]^x - \log [H^+]^m$$

$$\log K_{eq} = \log \frac{A_{Rd}^{y}}{A_{O_x}^{x}} - m \log [H^+] \quad ;$$

$$\log K_{eq} = \log \frac{A_{Rd}^{y}}{A_{O_x}^{x}} + m \, pH$$

assuming the concentration equals activity

$$E = E^\circ \frac{2.303 \, RT}{nF} \log K_{eq} \quad ;$$

$$E = -\frac{\Delta G^\circ}{nF} - \frac{2.303 \, RT}{nF} \log \frac{A_{Rd}^{y}}{A_{O_x}^{x}} + m \, pH$$

or, at 25°C (298°K)

$$E = \frac{x \, \Delta G^\circ_{O_x} - y \, \Delta G^\circ_{Rd} - z \, \Delta G^\circ_{H_2O}}{23{,}070 \text{ (cal) } n} - 0.0591 \frac{m}{n} pH + \log \frac{A_{O_x}^{x}}{A_{Rd}^{y}}$$

An example of the use of the above equation is given below:

$$PbO_2 + SO_4^{=} + 4H^+ + 2e^- = PbSO_4 + 2 \, H_2O$$

$$E = \frac{1}{23,070(2)} \{(\Delta G^\circ_{PbO_2}{}^{Ox} + \Delta G^\circ_{SO_4^=}) - \Delta G^\circ_{PbSO_4}{}^{Rd} - 2\Delta G^\circ_{H_2O}\}$$

$$- 0.0591 \cdot \frac{4}{2} pH + \frac{0.0591}{2} \log \frac{A_{SO_4^=} \; A_{PbO_2}}{A_{PbSO_4}}$$

$$E = \frac{1}{46,140 \text{ cal}} \{(-52.34-177.34) - (-193.89) - 2(-56.72)\}$$

$$- 0.1182 pH + 0.0295 \log A_{SO_4^=}$$

$$E = \frac{1}{46,140 \text{ cal}} (-229.68 + 307.33) - 0.1182 pH$$

$$+ 0.0295 \log A_{SO_4^=}$$

$$E = \frac{77,650 \text{ cal}}{46,140 \text{ cal}} - 0.1182 pH + 0.0295 \log A_{SO_4^=}$$

$$\underline{\underline{E = 1.683 - 0.1182 pH + 0.0295 \log A_{SO_4^=}}}$$

For 1N H_2SO_4, the pH = 0.3 and $\log A_{SO_4^=} = -2.27$ (Pavlov).[27]

$$\underline{\underline{E = +1.58V}}$$

The following thermodynamic data used to calculate the potentials are from the 50th (College) Edition "Handbook of Chemistry and Physics."

	ΔG° (Kcal)		ΔG° (Kcal)
$PbSO_4$	-193.89	PbF_2	-148.10
$SO_4^{=}$	-177.34	HF	- 64.70
PbO_2	- 52.34	H_2O	- 56.72
PbO_t	- 45.25	F^-	+ 66.08

APPENDIX E

TABULAR DATA FOR FIGURE 7

(Cathode Potentials)

	E (volts) SHE				
$\log_{10}$ C.D.	0°C	15°C	30°C	40°C	50°C
1.0	0.912	0.844			
1.3	0.942	0.892	0.846		
1.6	0.966	0.918	0.871	0.837	
1.9	0.972	0.939	0.898	0.860	0.831
2.08	0.974	0.950	0.908	0.869	0.844
2.20	0.982	0.953	0.913	0.877	0.848
2.30	0.982	0.956	0.916	0.878	0.848

APPENDIX F

TABULAR DATA FOR FIGURE 8

(Anode Potentials)

	E (volts) SHE				
$\log_{10}$ C.D.	0°C	15°C	30°C	40°C	50°C
1.0	2.042	1.972			
1.3	2.102	2.021	1.990		
1.6	2.152	2.086	2.040	2.020	2.002
1.9	2.192	2.142	2.100	2.078	2.052
2.08	2.222	2.172	2.122	2.125	2.075
2.20	2.232	2.185	2.138	2.122	2.096
2.30	2.242	2.200	2.152	2.132	2.112

APPENDIX G

TABULAR DATA FOR FIGURE 9

(Time Independent Current Efficiency)

	Current Efficiency - Percent					
C.D.(asf)	0°C	15°C	20°C	25°C	30°C	40°C
9	90	93				
18	88		95	94		
27					95	
37				92		96
73	78	83	91	92	95	96
110	76					
146	75					
183	74	82	86	88	92	96

APPENDIX H

TABULAR DATA FOR FIGURE 13

(Time Dependent Current Efficiency)

	Current Efficiency - Percent			
Time(hrs.)	20°C-10asf	30°C-20asf	40°C-30asf	50°C-80asf
2	93.8	94.5	95.7	98.0
4	86.0	89.0	92.0	
5	87.0			
6		69.0	77.0	80.0
8	80.0			
12	61.0			35.0

VII. BIBLIOGRAPHY

1. Tainton, U., Taylor, A., and Ehrlinger, H., "Lead Alloys for Anodes in Electrolytic Production of Zinc of High Purity," Am. Inst. Mining Met. Eng., Tech. Pub. No. 221, pp. 192-202, 1929.

2. Hanley, H. Clayton, C., and Walsh, D., "Investigation of Anodes for Production of Electrolytic Zinc," Ibid., Tech. Pub. 321, pp. 3 - 8, 1930.

3. Hanley, H., Clayton,C., and Walsh, D., "Investigation of Anodes for Production of Electrolytic Zinc, II," Ibid., General Vol., pp. 142 - 146, 1931.

4. Kiryakov, G., and Stender, V., "Stability of Anodes of Lead and its Alloys in the Electrolysis of Sulfate Solutions," J. Appl. Chem., U.S.S.R., Vol. 24, pp. 1429 - 1439, 1951.

5. Kiryakov, G., and Stender, V., "Anode Potentials of Lead and its Alloys," Ibid., Vol. 25, pp. 25 - 31, 1952.

6. Kiryakov, G., and Stender, V., "Binary Electro-Chemical Systems Composed of Lead and its Alloying Ingredients," Ibid., Vol. 25, pp. 33 - 40, 1952.

7. Koenig, A., MacEwan, J., and Larsen, E., "Investigation of Lead Anodes in the Electrolysis of Zinc Sulfate Solutions," Transactions of the Electrochemical Society, Vol. 79, pp. 331 - 345, 1941.

8. Koch, D., "The Effect of Cobalt on a Lead Anode in Sulfuric Acid," Electrochimica Acta, Vol. 1, No. 1, pp. 32 -38, April 1959.

9. Lander, J., "Silver, Cobalt, and Positive-Grid Corrosion in the Lead-Acid Battery," Journal of the Electrochemical Society, Vol. 105, No. 6, pp. 289-292, 1958.

10. Fink, C., and Dornblatt, A., "The Effect of Silver (0.05 to 0.15 per cent) On Some Properties and the Performance of Antimonial Lead Storage Battery Grids," Transactions of the Electrochemical Society, Vol. 79, pp. 269 - 305, 1941.

11. Wark, I., "Influence of Cobalt in the Electrodeposition of Zinc," Proc. Australian Conf. Electrochem., 1st, Sidney, Hobart, Australia 1963, pp. 889 - 900 (Pub. 1965).

12. Turomshina, U., and Stender, V., "Electrolysis of Acid Zinc Sulfate Solutions," J. Appl. Chem., U.S.S.R., Vol. 27, pp. 1019 - 1025, 1954.

13. Percherskaya, A., and Stender, V., "The Influence of Impurities in the Electrolytic Production of Zinc From Sulfate Solutions," Ibid., Vol. 23, pp. 975 - 989, 1950.

14. Turomshina, U., and Stender, V., "Current Efficiency and Cathode Potentials in the Electrolysis of Zinc Sulfate Solutions in the Presence of Ions of Metals More Electropositive than Zinc," Ibid., Vol. 28, pp. 347 - 361, 1955.

15. Turomshina, U., and Stender, V., "Current Efficiency and Cathode Potentials in the Electrolysis of Zinc Sulfate Solutions in the Presence of Ions of Metals More Electronegative than Zinc," Ibid., Vol. 28, pp. 151 - 158, 1955.

16. Salin, A., Volkova, V., Tokaev, Yu., Tulenkov, I., Kopytov, S., and Guzairov, R., "Electrodeposition of Zinc at Increased Electrolyte Temperatures," Tsvetn. Metal., Vol. 35, No. 12, pp. 13 - 18, 1962.

17. Tainton, U., "Hydrogen Overvoltage and Current Density in the Electrodeposition of Zinc," Transactions of the American Electrochemical Society, Vol. 41, pp. 389 - 410, 1922.

18. Farmer, R., "Electrometallurgy," Proceedings of the Extractive Metallurgy Division Symposium on Electrometallurgy, Cleveland, Ohio, pp. 242 - 250, Dec. 2 - 3, 1968.

19. Burbank, J., "Anodization of Lead in Sulfuric Acid," Journal of the Electrochemical Society, Vol. 103, No. 2, pp. 87 - 91, 1956.

20. Burbank, J., "Anodization of Lead and Lead Alloys in Sulfuric Acid," Ibid., Vol. 104, No. 12, pp. 693 - 701, 1957.

21. Burbank, J., "Morphology of PbO_2 in the Positive Plates of Lead Acid Cells," Ibid., Vol. III, No. 7, pp. 765 - 768, 1964.

22. Burbank, J., "Anodic Oxidation of the Basic Sulfates of Lead," Ibid., Vol. 113, No. 1, pp. 10 - 14, 1966.

23. Ruetschi, P., and Cahan, B., "Electrochemical Properties of PbO_2 and the Anodic Corrosion of Lead and Lead Alloys," Ibid., Vol. 105, No. 7, pp. 369 - 377, 1958.

24. Ruetschi, P., and Angstadt, R., "Anodic Oxidation of Lead at Constant Potential," Ibid., Vol. III, No. 12, pp. 1323 - 1330, 1964.

25. Abdul Azim, A., Anwar, M., "Anodic Passivation of Pb in Various Media," Corrosion Science, Vol. 9, pp. 245 - 260, 1969.

26. Pavlov, D., "Processes of Formation of Divalent Lead Oxide Compounds on Anodic Oxidation of Lead in Sulfuric Acid," Electrochimica Acta, Vol. 13, pp. 2051 - 2061, 1968.

27. Pavlov, D., "Mechanism of the Anodic Oxidation of Lead in Sulfuric Acid Solutions," Berichte der Bunsengesellschaft fur Physikalische Chemie, Band 71, Heft 4, Seite 398 - 404, 1967.

28. Pavlov, D., Poulieff, C., Klaja, E., and Lordanov, N., "Dependence of the Composition of the Anodic Layer on the Oxidation Potential of Lead in Sulfuric Acid," J. Electrochem. Soc., Vol. 116, No. 3, pp. 316 - 319, 1969.

29. Simon, A., Wales, C., and Caulder, S., "Morphological Changes in the Lead Dioxide Electrode During Its Reduction and Re-Oxidation," Ibid., Vol. 117, No. 8, pp. 987 - 992, 1970.

30. Senter, G., "Electrolysis of Dilute Solutions of Acids and Alkalis at Low Potentials; Dissolving of Platinum at the Anode by a Direct Current," Tran. Faraday Soc., Vol. 2, pp. 142 - 149, 1907.

31. Thacker, R., "Some Effects Resulting from the Use of a Platinum Catalyst in a Zinc-Oxygen Cell," Electrochimica Acta, Vol. 14, pp. 433 - 436, 1969.

32. Fontana, M.,and Greene, N., Corrosion Engineering, New York: McGraw-Hill Book Company, 1967.

33. Reddy, A.K.N., "Preferred Orientations in Nickel Electro-Deposits," J. Electroanal. Chem., Vol. 6, pp. 141 - 163, 1963.

34. Sato, R., "Crystal Growth of Electrodeposited Zinc," J. Electrochem. Soc., Vol. 106, No. 3, pp. 206-211, 1959.

35. Borgstrom, L., "Die Geometrische Bedingung Fur die Entstehung von Kombinationen," Zeitschrift fur Kristallographie, Vol. 62, pp. 1 - 12, 1925.

36. Buckley, H., Crystal Growth, New York: John Wiley & Sons, Inc., 1951.

37. Bockris, J., and Conway, B., "The Mechanism of Electrolytic Metal Deposition," Proc. Royal Soc. (London), Vol. A248, pp. 394 - 403, 1958.

38. Bockris, J., and Mehl, W., "On the Mechanism of Electrolytic Deposition and Dissolution of Silver," Can. J. Chem., Vol. 37, pp. 190 - 204, 1959.

39. Gerischer, H., "Mechanism of Electrolytic Deposition and Dissolution of Metals," Anal. Chem., Vol. 31, pp. 33 - 39, 1959.

40. Hamelin, A., "Evolution of Polarization Curves of Single-Crystal Electrodes of Zinc as a Function of Their Crystallographic Orientation," Compt. Rend., Vol. 248, pp. 1170 - 1173, 1959.

41. Hamelin, A., "The Discharge of Zinc Ions on a Single Crystal Zinc Cathode," J. Rech. Centre Natl. Rech. Sci., Lab. Bellevue (Paris), Vol. 57, pp. 321 - 351, 1961.

42. Raub, E., and Müller, K., Fundamentals of Metal Deposition, New York: Elsevier, 1967.

43. Abramson, D., "Electrodeposition of Zinc Crystals on the Surface of Some Metals," Bull. Acad. Sci. U.S.S.R., Ser. Chim., pp. 1197 - 1209, 1938.

44. Razina, N., and Kiryakov, G., "Lead Dioxide Electrodes," Izvest. Akad. Nauk Kazakh. S.S.R., Ser. Khim., pp. 26 - 31, 1959.

45. Von Fraunhofer, J., "Lead as an Anode - Part 1," Anti-Corrosion, Vol. 15, No. 11, pp. 9 - 14, 1968.

46. Conley, W.J., Conley, W.E., King, H., and Unger, L., "The Microcharacter as a Research Tool," ASM Transactions, Vol. 24, pp. 721 - 734, 1936.

III. VITA

Ernest Ray Cole, Jr., was born on June 29, 1932, in Webster Groves, Missouri. He received his primary and secondary diplomas from Dry Hill School (Valedictorian) 1945, Ellsinore, Missouri; Ventura Junior High School, 1947, Ventura, California, and Ellsinore High School (Salutatorian) 1949, Ellsinore, Missouri.

He enlisted in the United States Air Force, August, 1950, and was discharged in August, 1954, with the rank of Staff Sergeant.

He was employed by the Dow Chemical Company, Madison, Illinois, from February, 1955, to September, 1964, as a Metallurgical Lab Technician, Foreman and Junior Metallurgist and worked primarily with rolling, extruding and casting of magnesium and aluminum alloys.

From September, 1959, to May, 1964, he attended night school at Belleville Junior College, graduating as class Salutatorian with an Associate of Science Degree in 1964.

He received a Bachelor of Science Degree in Metallurgical Engineering - Nuclear Option from the University of Missouri-Rolla, Rolla, Missouri in May, 1966, and has been attending the Graduate School at the University of Missouri - Rolla since that time.

During his university tenure, he was the recipient of the Kennecott Copper Scholarship, NDEA Fellowship and is presently a Graduate Center for Materials Research Fellow.